UC Berkeley

SEMM Reports Series

Title

Stress Analysis in Non-Uniform Media By the Finite Element Method

Permalink

https://escholarship.org/uc/item/5x98334c

Authors

Clough, Ray

Raphael, Jerome

Publication Date

1963-03-01

STRESS ANALYSIS IN NON-UNIFORM MEDIA BY THE FINITE ELEMENT METHOD

WITH SPECIAL REFERENCE TO THE GROUT GALLERY FOR

OROVILLE DAM

BY

RAY W. CLOUGH

JEROME M. RAPHAEL

STRESS ANALYSIS IN NON-UNIFORM MEDIA
BY THE FINITE-ELEMENT METHOD
WITH SPECIAL REFERENCE TO THE
GROUT GALLERY FOR OROVILLE DAM

A Report of an Investigation

by

Ray W. Clough and Jerome M. Raphael
Professors of Civil Engineering

to

THE DEPARTMENT OF WATER RESOURCES
STATE OF CALIFORNIA
Under Standard Service Agreement
No. 351570

March, 1963

FOREWORD

In connection with the construction of Oroville Dam, a number of analyses were performed at the University of California utilizing a new analytical tool termed the method of finite elements. These design studies, ranging over a number of design elements, will be described in a series of reports, each report dealing with one class of structural elements. However, the method of finite elements itself will be described only in this, the first report of the projected series, with the particular application of the method to the stresses in the grout gallery given secondary emphasis.

STRESS ANALYSIS IN NON-UNIFORM MEDIA BY THE FINITE ELEMENT METHOD
WITH SPECIAL REFERENCE TO THE GROUT GALLERY FOR OROVILLE DAM

Ray W. Clough and Jerome M. Raphael
Professors of Civil Engineering
University of California
Berkeley, California

SUMMARY

Stresses in a number of configurations of a grout gallery to be embedded at the base of Oroville Dam are analyzed by the method of finite elements. The mathematical basis of the method is described, and the essential equations governing the deformation of the individual elements are derived. Three distinctive shapes of the grout gallery cross-section are analyzed: the gallery without gutter, the gallery with gutter, and a widened gallery used as an instrument chamber. In all, eleven distinct cases are analyzed. Statics checks show that computed stress resultants agree with imposed loads within an average of just over 2 percent. Magnitude and direction of principal stresses for all cases are shown on a series of drawings, together with a table of stress concentration factors.

TABLE OF CONTENTS

LIST OF ILLUSTRATIONS

LIST OF ILLUSTRATIONS (Cont'd)

LIST OF TABLES

STRESS ANALYSIS IN NON-UNIFORM MEDIA BY THE FINITE ELEMENT METHOD
WITH SPECIAL REFERENCE TO THE GROUT GALLERY FOR OROVILLE DAM

Ray W. Clough and Jerome M. Raphael
Professors of Civil Engineering
University of California
Berkeley, California

INTRODUCTION

The Physical Problem

Oroville Dam is designed as a 735 ft high by 5000 ft long embankment dam. Above the foundation, the water barrier consists of a variable-thickness sloping impermeable core, protected and strengthened up- and downstream by a more permeable gravel shell. Below the foundation line, a barrier against seepage of water through the foundation is formed by a grout curtain. Instead of the usual grout cap at the foundation line through which grout holes might be drilled and filled, a feature of Oroville Dam is a permanent grout gallery which furnishes a means to regrout the foundation, if necessary, as well as to permit the drilling of drainage holes to relieve pore pressures in the foundation. As shown on Fig. 1, the grout gallery runs practically the whole length of the dam with the exception of the top 100 ft of elevation, and a section in the center of the dam where the gallery runs into the concrete core wall. In general, it is a 5 ft by 7 ft opening set into a concrete-lined wedge-shaped trench. Loads on the gallery vary greatly depending on the height of the embankment above the foundation. Because of its great size and cost, it was desired to find the stress distribution in this irregularly shaped concrete structure as related to the thickness of the concrete around the opening.

PLAN

WATER SURFACE ELEV. = 900'   CREST ELEV. = 915'

ELEV. = 250'

ELEV. = 200'   CORE BLOCK   ELEV. = 150'
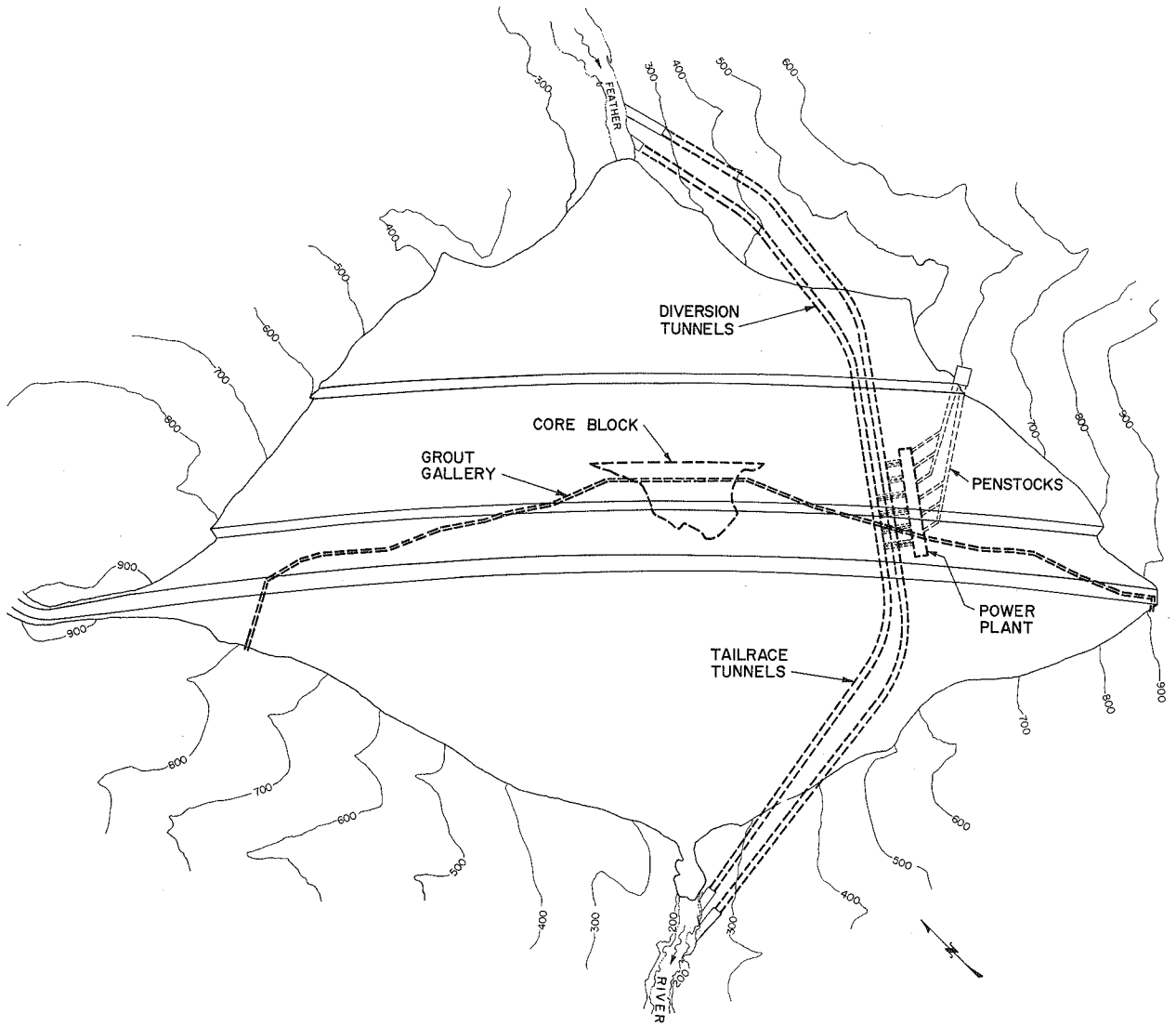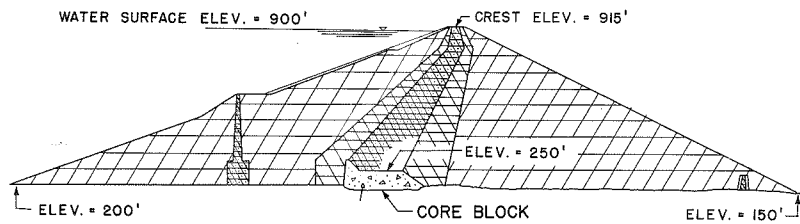
MAXIMUM   SECTION

FIG.I - GENERAL VIEW OF EMBANKMENT AND GALLERY

Choice of Method of Analysis

The grout gallery structure is essentially a hollow truncated wedge loaded on the top by the earth embankment and supported on the sides and bottom by the rock foundation. Internal stresses and reactions depend on the relative stiffness of the concrete and the foundation rock. Consideration had been given first to designs in which the grout gallery protruded to varying degrees into the fill. Study of the meagre existing records of concrete conduits embedded in earth fills showed that the loading depended greatly on the degree to which the conduit protruded into the fill, as well as on the general shape of the foundation in the immediate vicinity of the conduit. However, no general criteria were available to establish loadings for this case. It was finally decided to embed the grout gallery flush with the level of the foundation rock, as shown in Fig. 2, and to assume that for this condition, the load on top of the gallery, as well as on the foundation line, could be considered to be uniform. It was recognized that the reactions between the rock and the concrete would be determined by the geometry of the gallery and the relative stiffness of the concrete and rock. Accordingly, a method of analysis was sought which would take into account the interacting deformations of the two materials rather than to assume some arbitrary set of reactions at the outer boundary of the grout gallery. In general, two methods of analysis were considered: photoelastic analysis, and the finite element analysis[1,2] described here.

Photoelastic analysis, in addition to requiring a new model for every case considered, has the disadvantage that the photoelastic material has

(1) Clough, R. W., "The Finite Element Method in Plane Stress Analysis" Proceedings, 2nd ASCE Conference on Electronic Computation, Pittsburgh, Penn., Sept. 1960.

(2) Clough, R. W., "The Stress Distribution of Norfork Dam" Univ. of California Institute of Engineering Research Report Series 100, Issue 19, Aug. 1962.
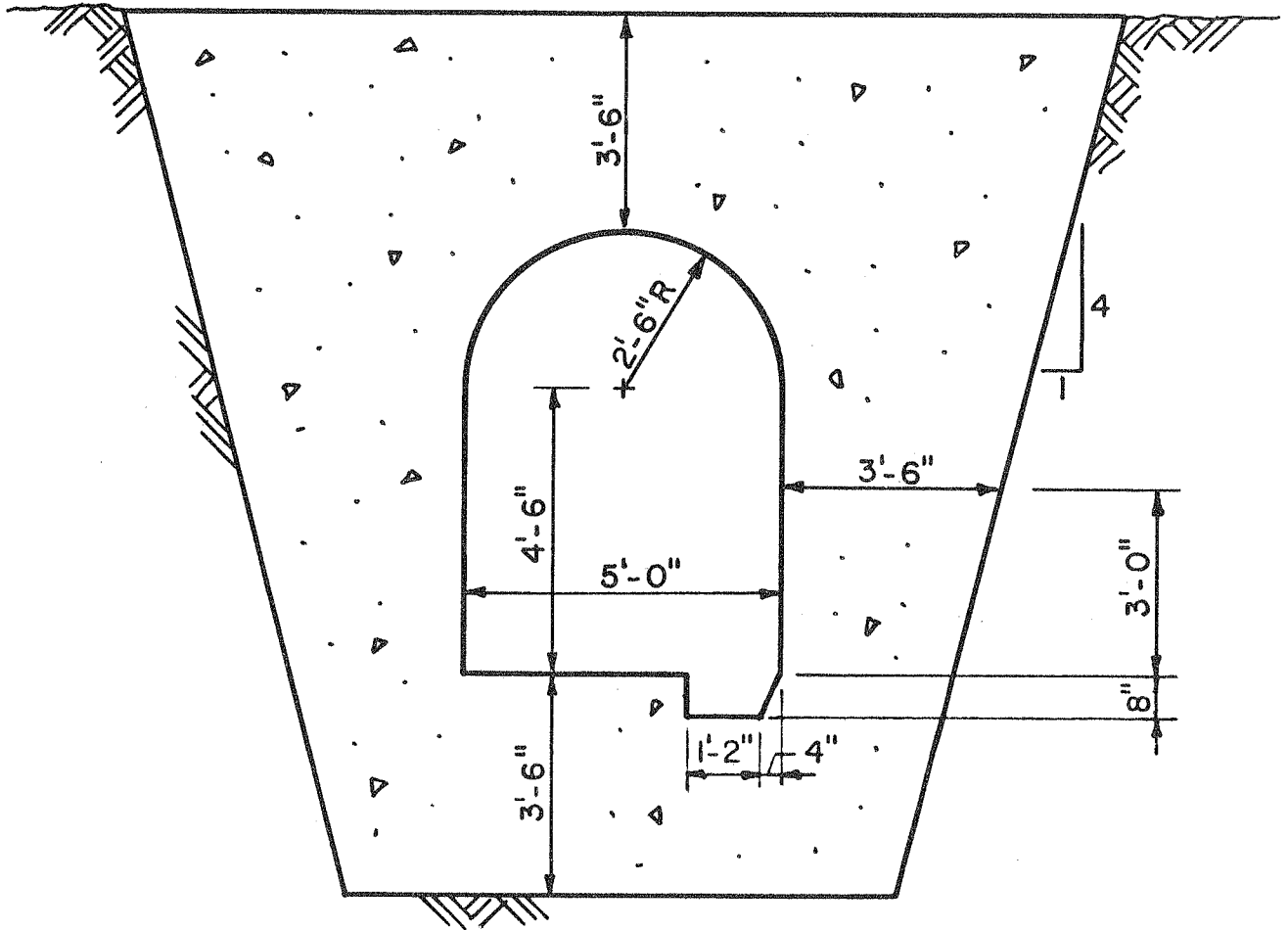
FIG. 2 – TYPICAL SECTION OF GROUT GALLERY

a fixed Poisson's ratio of 0.50. It was desired in this case to use
two Poisson's ratios close to those of the actual materials involved;
0.20 for concrete and 0.15 for rock. Furthermore, although photoelastic
analyses give the stresses at boundaries quite easily, they require addi-
tional numerical analyses for stresses remote from free surfaces. The
finite element method has none of these objections, and consequently it
was chosen for this study. A general description of the method is given
in the next chapter of this report.

Scope of the Analyses

Analyses discussed in this report were made for specific designs of
the grout gallery furnished by the State of California Department of Water
Resources. A variety of configurations was considered in order to arrive
at the optimum design for the assumed conditions of loading and support.
However, this report is concerned solely with evaluation of the stresses
in the given designs, and no attempt is made to indicate which design
should be used in specific instances.

METHOD OF ANALYSIS

The "finite element method" is a general method of structural analysis in which a continuous structure is replaced by a finite number of elements interconnected at a finite number of nodal points. (Such an idealization is inherent in the conventional analysis of frames and trusses.) In this investigation the finite element method is used to determine the stresses and displacements developed in two-dimensional elastic structures of arbitrary geometry and material properties. An assemblage of triangular plate elements is used to represent the continuous structure. Forces acting on the actual structure are replaced by statically equivalent concentrated forces acting at the nodal points of the finite element system. Figure 3 illustrates a very coarse-mesh idealization of the cross-section of a gravity dam.

Basic Assumptions

Continuity between elements of the system is maintained by requiring that within each element "lines initially straight remain straight in their displaced position." This is similar to the assumption made in classical beam theory that "transverse sections, originally plane, remain plane and normal to the longitudinal fibers of the beam after bending". The requirement for continuity is satisfied if the strains ε_x, ε_y, and γ_{xy} are assumed to be constant within each element. Therefore, the stresses σ_x, σ_y, and τ_{xy} which act on the edges of each element are also constant. These stresses are replaced by stress resultants which act on the corners of the element. Based on these assumptions, it is possible to determine the stiffness of a typical element, which is an expression for the corner forces resulting from unit corner displacements. After this
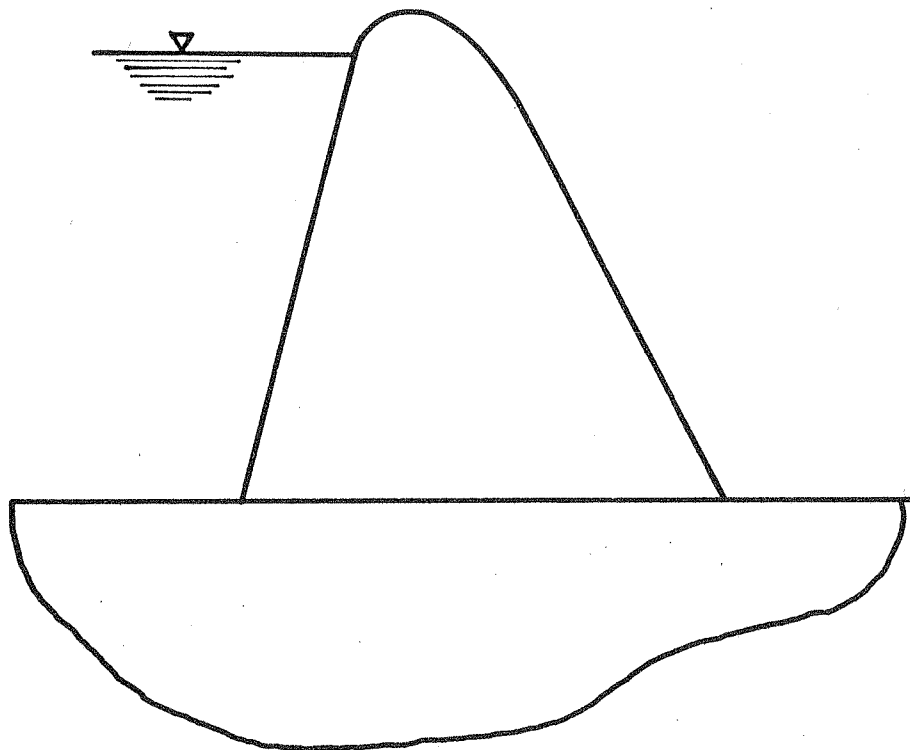
a. ACTUAL DAM SECTION
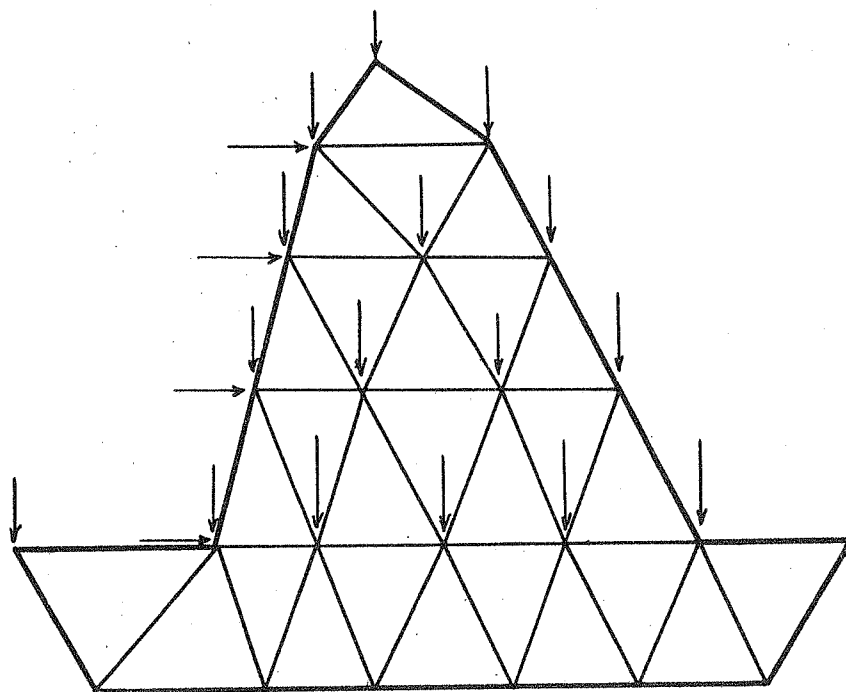
b. ELEMENT AND LOAD APPROXIMATION

FIG. 3 - THE TRIANGULAR FINITE ELEMENT IDEALIZATION

relationship is developed standard methods of structural analysis are employed to solve the complete system of elements.

Behavior of a Typical Element

Strain-Displacement Relationship - The first step in the development of the stiffness of a typical element is to express the three components of strain within each element in terms of the six corner displacements. The geometry of a typical element is defined in Fig. 4. The assumed displacement pattern is illustrated in Fig. 5. This linear displacement field is defined in terms of $u(x,y)$ and $v(x,y)$ by equations of the following form:

$$u_{(x,y)} = u_i + C_1 x + C_2 y$$
$$v_{(x,y)} = v_i + C_3 x + C_4 y$$

(1)

The constants C_1, C_2, C_3 and C_4 can be expressed readily in terms of the corner displacements and the geometry of the element:

$$C_1 = \left\{ b_k(u_j - u_i) - b_j(u_k - u_i) \right\} / (a_j b_k - a_k b_j)$$
$$C_2 = \left\{ -a_k(u_j - u_i) + a_j(u_k - u_i) \right\} / (a_j b_k - a_k b_j)$$
$$C_3 = \left\{ b_k(v_j - v_i) - b_j(v_k - v_i) \right\} / (a_j b_k - a_k a_j)$$
$$C_4 = \left\{ -a_k(v_j - v_i) + a_j(v_k - v_i) \right\} / (a_j b_k - a_k a_j)$$

(2)

The strains within the element can be obtained from the assumed displacement field, Equation 1, by considering the basic definitions of strain:

$$\epsilon_x \equiv \frac{\partial u}{\partial x} + C_1$$
$$\epsilon_y \equiv \frac{\partial v}{\partial y} + C_4$$
$$\gamma \equiv \frac{\partial u}{\partial y} + \frac{\partial v}{\partial x} = C_2 + C_3$$

(3)
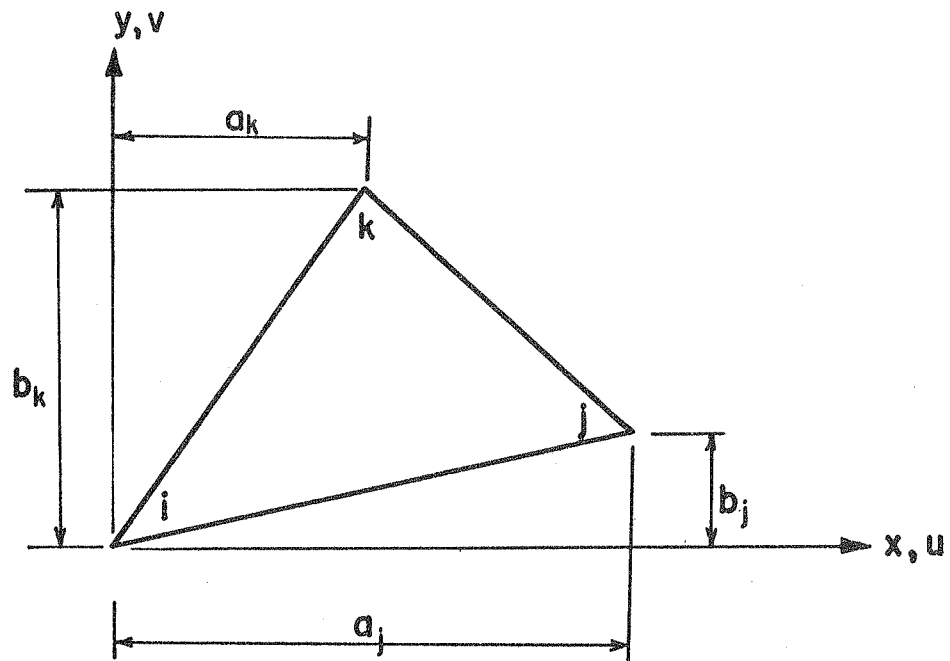
FIG. 4 - TRIANGULAR PLATE ELEMENT DIMENSIONS
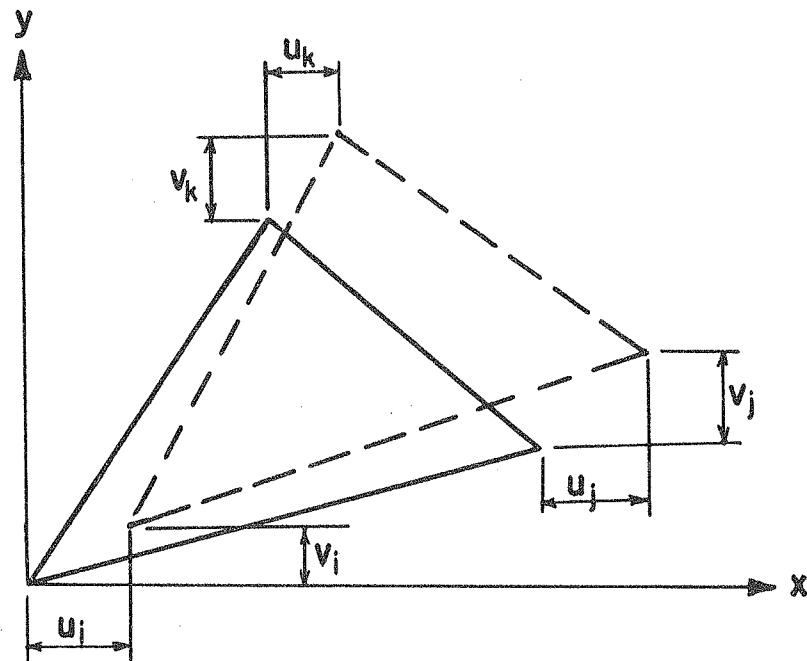
FIG. 5 - ASSUMED DISPLACEMENT PATTERN

If Equations 2 and 3 are combined, the element strains in terms of corner displacements are expressed by the following equations:

$$\varepsilon_x = \frac{1}{a_j b_k - a_k b_j}\left[(b_j - b_k)u_i + b_k u_j - b_j u_k\right]$$

$$\varepsilon_y = \frac{1}{a_j b_k - a_k b_j}\left[(a_k - a_j)v_i - a_k v_j + a_j v_k\right] \tag{4}$$

$$\gamma = \frac{1}{a_j b_k - a_k b_j}\left[(a_k - a_j)u_i + (b_j - b_k)v_i - a_k u_j + b_k v_j + a_j u_k - b_j v_k\right]$$

Equations 4 can be expressed in matrix form as:

$$\begin{bmatrix} \varepsilon_x \\ \varepsilon_y \\ \gamma \end{bmatrix} = \frac{1}{a_j b_k - a_k b_j}\begin{bmatrix} b_j - b_k & 0 & b_k & 0 & -b_j & 0 \\ 0 & a_k - a_j & 0 & -a_k & 0 & a_j \\ a_k - a_j & b_j - b_k & -a_k & b_k & a_j & -b_j \end{bmatrix}\begin{bmatrix} u_i \\ v_i \\ u_j \\ v_j \\ u_k \\ v_k \end{bmatrix} \tag{4a}$$

or in symbolic form

$$\left[\varepsilon\right] = \left[A\right]\left[r\right] \tag{4b}$$

Stress-Strain Relationship - One important advantage of the finite element method in two-dimensional elasticity is that structures with any form of

material properties can be considered. In general, the stress-strain relationship is of the form

$$\sigma_x = C_{11} \varepsilon_x + C_{12} \varepsilon_y + C_{13} \gamma$$
$$\sigma_y = C_{21} \varepsilon_x + C_{22} \varepsilon_y + C_{23} \gamma \qquad (5)$$
$$\tau_{xy} = C_{31} \varepsilon_x + C_{32} \varepsilon_y + C_{33} \gamma$$

which, in matrix notation, may be written as

$$
\begin{bmatrix} \sigma_x \\ \sigma_y \\ \tau_{xy} \end{bmatrix} =
\begin{bmatrix} C_{11} & C_{12} & C_{13} \\ C_{21} & C_{22} & C_{23} \\ C_{31} & C_{32} & C_{33} \end{bmatrix}
\begin{bmatrix} \varepsilon_x \\ \varepsilon_y \\ \gamma \end{bmatrix} \qquad (5a)
$$

or in symbolic form

$$\begin{bmatrix} \sigma \end{bmatrix} = \begin{bmatrix} C \end{bmatrix} \begin{bmatrix} \varepsilon \end{bmatrix} \qquad (5b)$$

For all structures considered in this investigation, the stress-strain relationship was assumed to be that of an isotropic material in the state of plane strain:

$$\sigma_x = \frac{E}{(1+\nu)(1-2\nu)} \left[(1-\nu)\varepsilon_x + \nu \varepsilon_y \right]$$
$$\sigma_y = \frac{E}{(1+\nu)(1-2\nu)} \left[\nu \varepsilon_x + (1-\nu)\varepsilon_y \right]$$
$$\tau_{xy} = \frac{E}{(1+\nu)(1-2\nu)} \left[\frac{1-2\nu}{2} \gamma \right] = \frac{E}{2(1+\nu)} \gamma \qquad (6)$$

In matrix notation, Equations 6 reduce to the following:

$$
\begin{bmatrix} \sigma_x \\ \sigma_y \\ \tau_{xy} \end{bmatrix} = \frac{E}{(1+\nu)(1-2\nu)} \begin{bmatrix} 1-\nu & \nu & 0 \\ \nu & 1-\nu & 0 \\ 0 & 0 & \frac{1-2\nu}{2} \end{bmatrix} \begin{bmatrix} \varepsilon_x \\ \varepsilon_y \\ \gamma \end{bmatrix} \tag{6a}
$$

Stress-Resultants - The next step in the development of the stiffness of a typical element is to replace the uniform stresses acting on the edges of the element with stress-resultants acting at the corners of the element. Fig. 6 illustrates a set of statically equivalent corner forces for each component of stress. The corner forces expressed in terms of the three components of stress are

$$
S_{xi} = \frac{1}{2}\left[(b_j - b_k)\sigma_x + (a_k - a_j)\tau_{xy}\right]
$$

$$
S_{yi} = \frac{1}{2}\left[(a_k - a_j)\sigma_y + (b_j - b_k)\tau_{xy}\right]
$$

$$
S_{xj} = \frac{1}{2}\left[b_k\sigma_x - a_k\tau_{xy}\right]
$$

$$
S_{yj} = \frac{1}{2}\left[-a_k\sigma_y + b_k\tau_{xy}\right] \tag{7}
$$

$$
S_{xk} = \frac{1}{2}\left[-b_j\sigma_x + a_j\tau_{xy}\right]
$$

$$
S_{yk} = \frac{1}{2}\left[a_j\sigma_y - b_j\tau_{xy}\right]
$$
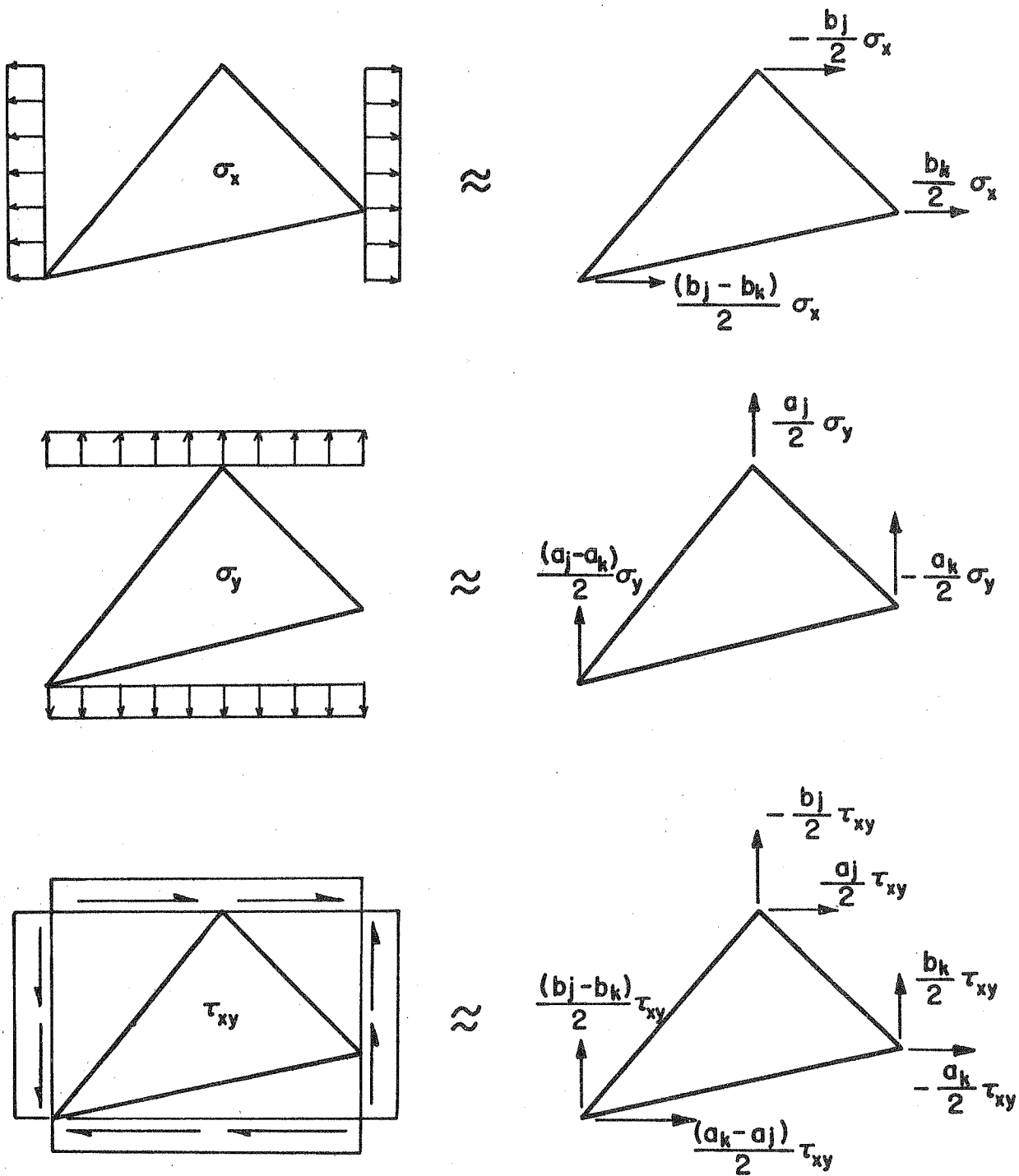
FIG. 6 – STRESS RESULTANTS

These may be expressed in matrix form as

$$
\begin{bmatrix} S_{x_i} \\ S_{y_i} \\ S_{x_j} \\ S_{y_j} \\ S_{x_k} \\ S_{y_k} \end{bmatrix} = \frac{1}{2} \begin{bmatrix} b_j - b_k & 0 & a_k - a_j \\ 0 & a_k - a_j & b_j - b_k \\ b_k & 0 & -a_k \\ 0 & -a_k & b_k \\ -b_j & 0 & a_j \\ 0 & a_j & -b_j \end{bmatrix} \begin{bmatrix} \sigma_x \\ \sigma_y \\ \tau_{xy} \end{bmatrix}
\tag{7a}
$$

or in symbolic form as

$$
[S] = [B][\sigma]
\tag{7b}
$$

Element Stiffness - Element stresses can be expressed in terms of corner displacements by substituting Eq. 4b into Eq. 5b. Or

$$
[\sigma] = [C][A][r]
\tag{8}
$$

The substitution of Eq. 8 into Eq. 7b yields

$$
[S] = [B][C][A][r]
\tag{9}
$$

Eq. 9, which is an expression for corner forces in terms of corner displacements, can be rewritten in the following form:

$$
[S] = [k][r]
\tag{10}
$$

where $[k]$ is the 6x6 stiffness matrix for the element and is given by

$$[k] = [B][C][A]$$

(11)

It should be pointed out that the algebraic manipulation necessary to establish the individual terms of this stiffness matrix for a typical element is not required, since within the computer program the stiffness matrices are numerically formed by standard matrix subroutines.

Equilibrium Equations For Complete Structure

The equilibrium of the complete system of elements, which is an expression for nodal point loads in terms of nodal point displacements, can be expressed by the following matrix equation:

$$[R] = [K][r]$$

(12)

where the stiffness of the complete structure $[K]$ can be found by a direct addition of the stiffnesses of all elements in the system. This addition can best be illustrated if Eq. 10 is rewritten in terms of a typical element q

$$
\begin{bmatrix} S_i^{(q)} \\ S_j^{(q)} \\ S_k^{(q)} \end{bmatrix} = \begin{bmatrix} k_{ii}^{(q)} & k_{ij}^{(q)} & k_{ik}^{(q)} \\ k_{ji}^{(q)} & k_{jj}^{(q)} & k_{jk}^{(q)} \\ k_{ki}^{(q)} & k_{kj}^{(q)} & k_{kk}^{(q)} \end{bmatrix} \begin{bmatrix} r_i \\ r_j \\ r_k \end{bmatrix}
$$

(13)

where, in terms of arbitrary nodal points ℓ and m, $S_\ell^{(q)}$ and r_m are vectors of the form

$$S_\ell^{(q)} = \begin{bmatrix} S_x^{(q)} \\ S_y^{(q)} \end{bmatrix}_\ell \qquad (13a)$$

$$r_m = \begin{bmatrix} u \\ v \end{bmatrix}_m$$

and the stiffness coefficient $k_{\ell m}^{(q)}$ is a 2x2 submatrix of the form

$$k_{\ell m}^{(q)} = \begin{bmatrix} k_{xx}^{(q)} & k_{xy}^{(q)} \\ k_{yx}^{(q)} & k_{yy}^{(q)} \end{bmatrix}_{\ell m} \qquad (14)$$

The term $k_{\ell m}^{(q)}$ represents the forces developed on element q at nodal point ℓ due to unit displacements at nodal point m. Therefore, the general stiffness term, $K_{\ell m}$, for the complete structure, which is the sum of the forces acting on all elements at nodal point ℓ due to unit displacements at nodal point m, is given by

$$K_{\ell m} = \sum_{q} k_{\ell m}^{(q)} \qquad (15)$$

It should be pointed out that $K_{\ell m}$ exists only if ℓ equals m, or if ℓ and m are adjacent nodal points in the physical system.

Solution of Equilibrium Equations

For structures considered in this investigation, Eq. 12 represents a system of several hundred equations. Three major difficulties are encountered in a direct solution of such a large set of equations.

First, the storage required by the complete stiffness matrix is equal to N^2, where N is the number of equations. Second, the time required for solution is proportional to N^3. Third, accuracy of solution can be a serious problem. Even on a large computer, such as the IBM 7090, these problems still exist; however, these difficulties can be minimized by the use of iterative methods.

Iteration Procedure - The specific iterative method used is a modification of the well-known Gauss-Seidel iteration procedure which, when applied to Eq. 12, involves the repeated calculation of new displacements from the equation

$$r_n^{(s+1)} = k_{nn}^{-1} \left[R_n - \sum_{i=1,n-1} k_{ni} r_i^{(s+1)} - \sum_{i=n+1,N} k_{ni} r_i^{(s)} \right] \tag{16}$$

where n is the number of the unknown and s is the cycle of iteration.

The only modification of the procedure introduced in this analysis is the application of Eq. 16 simultaneously to both components of displacement at each nodal point. Therefore, r_n and R_n become vectors with x and y components, and the stiffness coefficients may be expressed in the 2x2 submatrix form of Eq. 14.

Over-Relaxation Factor - The rate of convergence of the Gauss-Seidel procedure can be greatly increased by the use of an over-relaxation factor. However, in order to apply this factor it is first necessary to calculate the change in the displacement of nodal point n between cycles of iteration:

$$\Delta r_n^{(s)} = r_n^{(s+1)} - r_n^{(s)} \tag{17}$$

The substitution of Equation 16 into Equation 17 yields for the change in displacement

$$\Delta r_n^{(s)} = k_{nn}^{-1} \left[R_n - \sum_{i=1,n-1} k_{ni} \, r_i^{(s+1)} - \sum_{i=n,N} k_{ni} \, r_i^{(s)} \right]$$

(18)

The new displacement of nodal point n is then determined from the following equation

$$r_n^{(s+1)} = r_n^{(s)} + \beta \, \Delta r_n^{(s)}$$

(19)

where β is the over-relaxation factor. For the structure considered in this report it was found that values of β between 1.8 and 1.9 gave the most rapid convergence.

Physical Interpretation of Method - There is important physical significance in the terms of Equation 18. The term k_{nn}^{-1} is the flexibility of nodal point n. This represents the nodal point displacements resulting from unit nodal point forces, and can be written in the form of a submatrix

$$k_{nn}^{-1} = \begin{bmatrix} f_{xx} & f_{xy} \\ f_{yx} & f_{yy} \end{bmatrix}$$

(20)

The summation terms in Equation 18 represent the elastic forces acting at nodal point n due to the deformations of the plate elements:

$$Q_n^{(s+1)} = \sum_{i=1,n} k_{ni} \, r_i^{(s+1)} + \sum_{i=n+1,N} k_{ni} \, r_i^{(s)}$$

(21)

The difference between these elastic forces and the applied loads is the total unbalanced force which in sub-matrix form may be written:

$$\begin{Bmatrix} X \\ Y \end{Bmatrix}_n^{(s+1)} = \begin{Bmatrix} R_x \\ R_y \end{Bmatrix}_n - \begin{Bmatrix} Q_x \\ Q_y \end{Bmatrix}^{(s+1)} \tag{22}$$

Equation 19, which gives the new displacement of nodal point n, may now be rewritten in the following sub-matrix form:

$$\begin{Bmatrix} r_x \\ r_y \end{Bmatrix}_n^{(s+1)} = \begin{Bmatrix} r_x \\ r_y \end{Bmatrix}_n^{(s)} + \beta \begin{bmatrix} f_{xx} & f_{xy} \\ f_{yx} & f_{yy} \end{bmatrix}_n \begin{Bmatrix} X \\ Y \end{Bmatrix}^{(s+1)} \tag{23}$$

It is important to note that any desired nodal point displacement $r_n^{(o)}$ may be assumed for the first cycle of iteration. A good choice of these displacements will greatly speed the convergence of the solution. In fact, if all displacements were assumed correctly, the unbalanced forces given by Equation 22 would be zero and no iteration would be necessary. However, in a practical case there always will be unbalanced forces in the system at first, and the iteration process continually reduces them toward zero.

Boundary Condition - Equation 23 is valid for all nodal points within the structure; however, in order for it to be applied to boundary nodal points the flexibility coefficients must be modified to account for the specific types of restraint which may exist. Since these flexibility coefficients are independent of the cycle of iteration, this modification is performed before the start of iteration. There are three possible types of boundary nodal points whose flexibility coefficients must be modified as follows:

(1) For points fixed in both x and y directions, $\Delta r_x = \Delta r_y = 0$:

$$f_{xx}^* = f_{xy}^* = f_{yx}^* = f_{yy}^* = 0 \tag{24a}$$

(2) For points fixed in the x direction only, $\Delta r_x = 0$:

$$\left. \begin{array}{l} f_{xx}^* = f_{xy}^* = f_{yx}^* = 0 \\[2mm] f_{yy}^* = f_{yy} - \dfrac{f_{yx} \, f_{xy}}{f_{xx}} \end{array} \right\} \tag{24b}$$

(3) For points fixed in y direction only, $\Delta r_y = 0$:

$$\left. \begin{array}{l} f_{xy}^* = f_{yx}^* = f_{yy}^* = 0 \\[2mm] f_{xx}^* = f_{xx} - \dfrac{f_{yx} \, f_{xy}}{f_{yy}} \end{array} \right\} \tag{24c}$$

Nodal Point Loads

Three types of loadings will be discussed here: dead loads, live loads, and thermal loads. However, for the structures considered in this investigation only live loads were applied.

Dead Loads - The dead weight of each plate element is given, of course, by the product of its area, its thickness (which was taken as one foot) and its unit weight, γ. One third of the total element weight is applied at each of the three nodal points to which it is attached. Thus the total dead load at any nodal point is taken as one-third of the weights of all elements attached at that point, applied in a downward, or negative "y", direction.

Live Loads - Forces acting on the boundary of the structure are replaced by statically equivalent concentrated forces acting at the nodal points

of the finite element system.

Thermal Loads - The thermal loads may be calculated by first calculating the stresses which would exist in the elements if strains due to temperature changes were fully constrained. In a plane strain system these stresses are given by

$$\tilde{\sigma}_x = \tilde{\sigma}_y = \tilde{\sigma} = \frac{E\alpha}{(1+\nu)(1-2\nu)} \Delta T \qquad (25)$$

in which α is the thermal coefficient of expansion, and ΔT is the change of temperature. The nodal forces required to maintain these internal stresses in each element may then be found by simple statics. While these constraining forces are applied, no displacements or deformations of the structure may occur, and the stresses are given directly by Equation 25. However, the constraints are not really present, so their effect must be eliminated by applying equal and opposite nodal forces. These reversed constraining forces are the thermal loads for which the structure is analyzed. For the element shown in Fig. 4, they would be expressed by

$$\begin{bmatrix} R_{xi} \\ R_{yi} \\ R_{xj} \\ R_{yj} \\ R_{xk} \\ R_{yk} \end{bmatrix} = \frac{1}{2} \begin{bmatrix} b_k - b_j \\ a_j - a_k \\ -b_k \\ a_k \\ b_j \\ -a_j \end{bmatrix} \tilde{\sigma} \qquad (26)$$

in which $\tilde{\sigma}$ is given by Equation 25.

The displacements resulting from these thermal loads are the true thermal displacements in the system. However, the stresses resulting

from these loads are only the part of the thermal stress associated with the nodal displacements. The total thermal stress is the sum of the deformation stress resulting from the thermal loads, _plus_ the constrained stress given by Equation 25.

Element Stresses

Equation 8 expresses the three components of stress σx, σy, and τxy within a typical element in terms of the six corner displacements of the element. Therefore, after Equation 12 is solved for the nodal point displacements of the finite element system, the stresses within each element are determined by the direct application of Equation 8 to all elements of the system.

Although the normal and shear stresses (σx, σy, and τxy) completely define the state of stress in the elements, it frequently is of interest to know the principal stresses σ_1 and σ_2 and their directions θ. In this investigation these principal stress values were determined from the stress values related to the x, y coordinate axes by the standard transformation formulas of elementary mechanics.

COMPUTER PROGRAM

The digital computer program performs three major tasks in the complete analysis of a plane stress system. First, the equilibrium equations for the system are formed from a basic numerical description of the system. Second, this set of equations is solved for the displacements of the nodal points by an iteration procedure. Third, the internal element stresses are determined from these displacements.

The program is coded in the FORTRAN language and has been used with both the IBM 704 and IBM 7090 computers. The maximum size of system that can be analyzed is governed by the availability of computer storage. For computers with 32K (32768) storage the maximum number of elements is 450 and the maximum number of nodal points is 350. Only the main sequence of operations of the computer program will be described; the details of coding will be omitted.

Sequence of Operations

Input Data - For the purpose of numerically defining a structure, all nodal points and elements are numbered as illustrated in Fig. 7. The numerical description is read into the machine, in the form of punched cards, by the following four arrays:

A. Parameter Array (6 numbers)

   1. Numbered elements
   2. Number of nodal points
   3. Number of boundary points
   4. Over-relaxation factor
   5. Convergence limit
   6. Cycle limit

B. Element Array (8 numbers per element)

   1. Element number
   2. Number of nodal point i
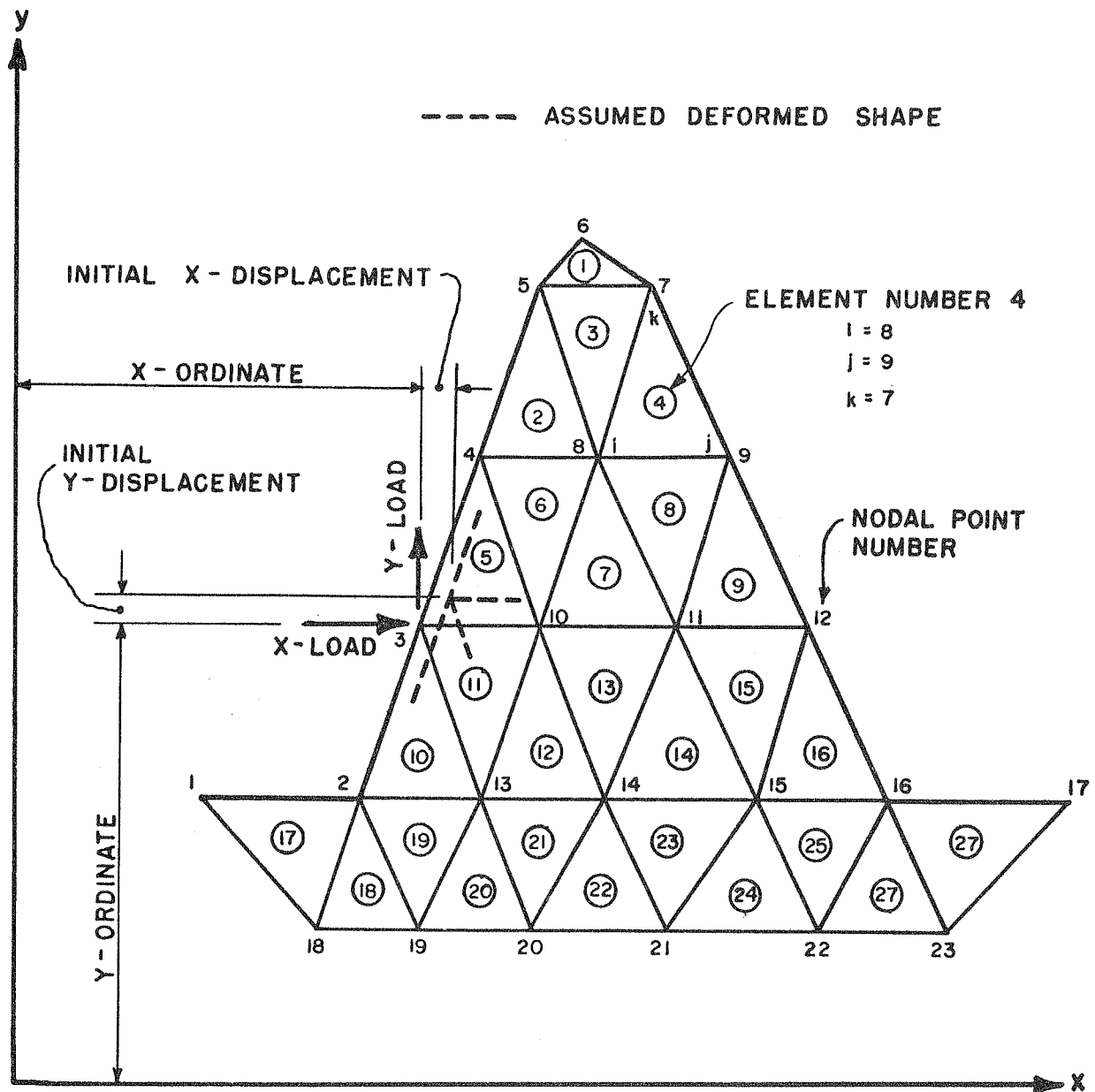   3. Number of nodal point j

FIG.7 - NUMBERING SYSTEM FOR NODAL POINTS AND PLATE ELEMENTS

4. Number of nodal point k
5. Modulus of elasticity E
6. Poisson's ratio ν
7. Unit weight of element γ
8. Temperature change within element ΔT

C. Nodal Point Array (7 numbers per nodal point)

1. Nodal point number
2. x-ordinate
3. y-ordinate
4. X-load
5. Y-load
6. Initial x-displacement
7. Initial y-displacement

D. Boundary Condition Array (2 numbers per boundary point)

1. Nodal point number
2. This number indicates the type of restraint; "0" for fixed in both directions; "1" for fixed in x-direction; and "2" for fixed in y-direction.

It should be noted that for a fixed boundary point, the initial displacement is the final displacement of the point, since it is not altered by the iteration procedure.

<u>Formation of Element Stiffness Matrices</u> - The stiffness matrix for each element is determined from Equation 11. The basic element dimensions are calculated from the coordinates of the connecting nodal points:

$$a_j = x_j - x_i$$
$$b_j = y_j - y_i$$
$$a_k = x_k - x_i$$
$$b_k = y_k - y_i$$

where i, j, and k are the nodal point numbers of the three connecting points and are given in the element array.

<u>Formation of Complete Stiffness of System</u> - Because of the large matrices that are developed in a plane stress system, the stiffness matrix used in Equation 12 is not formed directly. Since the complete stiffness matrix contains many zero elements, only the non-zero elements are developed

and retained by the program; thus, it is possible to treat large plane stress systems without exceeding the storage capacity of the computer.

Formation of Nodal Point Loads - The loads acting on the nodal points are composed of live loads, dead loads, and temperature loads. The equations which are used to determine these loads have been presented in the preceding section of this report.

Formation of Nodal Flexibilities - The nodal point flexibilities are determined from the previously developed stiffness coefficients. The flexibilities associated with the boundary nodal points are modified by the application of Equations 24, as required.

Iterative Solution - The repeated application of Equation 23 at all nodal points constitutes the iterative procedure. The sum of the absolute magnitude of the unbalanced forces at all nodal points (given by Equation 22) is also computed for each cycle; this sum, when compared to the convergence limit, serves as a check on the convergence of the procedure. In all analyses presented in this report, this sum was reduced to less than 1/1000 of the value obtained in the first cycle of iteration.

Calculation of Element Stresses - From the nodal point displacements, with the aid of Equation 8, the element stresses σ_x, σ_y, and τ_{xy} are calculated. As added information, the principal stresses σ_1 and σ_2 and directions θ are also calculated.

Output Information - At desired points in the iteration procedure, nodal displacements and element stresses are printed. Fig. 8 illustrates the form of the computer output, in a typical case.

Timing

The computational time required by the program is approximately equal to 0.012 n.m seconds, where n equals the number of nodal points and

ELEMENT	(PSI) X-STRESS	(PSI) Y-STRESS	(PSI) XY-STRESS	(PSI) MAX-STRESS	(PSI) MIN-STRESS	(DEGREES) DIRECTION
1	-99.6921	0.0186	-0.0974	0.02	-99.69	89.94
2	-99.9554	0.0105	-0.0512	0.01	-99.96	89.97
3	-99.9371	0.0280	-0.0400	0.03	-99.94	89.98
4	-100.0289	-0.0000	-0.0169	-0.00	-100.03	89.99
5	-99.9901	0.0112	-0.0088	0.01	-99.99	89.99
6	-99.9925	-0.0020	-0.0006	-0.00	-99.99	90.00
7	-99.9921	0.0045	0.0023	0.00	-99.99	-90.00
8	-100.0305	-0.0030	0.0157	-0.00	-100.03	-89.99
9	-99.9961	-0.0073	0.0058	-0.01	-100.00	-90.00
10	-100.0482	0.0468	0.0019	0.05	-100.05	-90.00
11	-100.0145	0.1012	-0.0303	0.10	-100.01	89.98
12	-100.1797	0.0563	-0.0510	0.06	-100.18	89.97
13	-99.9705	0.1140	-0.1128	0.11	-99.97	89.94
14	-100.1096	0.0647	-0.1479	0.06	-100.11	89.92
15	-99.8664	0.0348	-0.1551	0.04	-99.87	89.91
16	-99.9072	0.0253	-0.1543	0.03	-99.91	89.91
17	-99.4996	-0.0280	-0.1610	-0.03	-99.50	89.91
18	-99.7589	-0.0274	-0.0974	-0.03	-99.76	89.94
19	-99.2481	-0.0901	-0.0813	-0.09	-99.25	89.95
20	-99.7122	-0.0850	-0.0468	-0.08	-99.71	89.97
21	-99.7697	-0.3149	-0.0488	-0.31	-99.77	89.97
22	-100.0460	-0.2267	-0.1458	-0.23	-100.05	89.92
23	-99.8480	-0.2588	-0.2282	-0.26	-99.85	89.87
24	-100.2020	-0.0660	-0.3132	-0.06	-100.20	89.82
25	-99.9842	-0.0121	-0.2962	-0.01	-99.99	89.83
26	-100.4016	0.0933	-0.2982	0.09	-100.40	89.83
27	-100.1288	0.1882	-0.2053	0.19	-100.13	89.88
28	-100.4712	0.1988	-0.1238	0.20	-100.47	89.93
29	-100.1492	0.2832	-0.0399	0.28	-100.15	89.98
30	-100.3834	0.1170	0.0851	0.12	-100.38	-89.95

NODAL POINT	(INCHES) X-DISPLACEMENT	(INCHES) Y-DISPLACEMENT
1	-0.953211E-04	-0.353071E-02
2	-0.703761E-04	-0.346492E-02
3	-0.300471E-04	-0.342716E-02
4	-0.	-0.342106E-02
5	-0.	-0.294565E-02
6	-0.	-0.225796E-02
7	-0.123175E-04	-0.257252E-02
8	-0.283953E-04	-0.287127E-02
9	-0.503175E-04	-0.303056E-02
10	-0.687064E-04	-0.323746E-02
11	-0.871273E-04	-0.360655E-02
12	-0.549489E-04	-0.366905E-02
13	-0.	-0.369579E-02
14	-0.	-0.311026E-02
15	-0.146676E-04	-0.309955E-02
16	-0.377689E-04	-0.300372E-02
17	-0.443050E-04	-0.284266E-02
18	-0.368561E-04	-0.262266E-02
19	-0.206652E-04	-0.235286E-02
20	-0.196906E-05	-0.190746E-02
21	-0.	-0.154633E-02
22	-0.	-0.722961E-03
23	0.182143E-04	-0.114807E-02
24	0.173381E-04	-0.142471E-02
25	0.445808E-05	-0.166782E-02
26	-0.14935CE-04	-0.197367E-02
27	-0.311768E-04	-0.219988E-02

FIG. 8 - COMPUTER OUTPUT

m equals the number of cycles of iteration, and using an IBM 704 computer for calculations. If the IBM 7090 is used computational time is only one-sixth this time. The number of cycles required depends on the accuracy of the initially assumed displacements and on the desired degree of convergence. For the structure considered in this report, the computer time per solution was approximately 1 1/2 minutes for the coarse mesh and 2 1/2 minutes for the fine mesh idealization. Between 70 and 100 cycles of iteration were used in typical cases.

SCHEDULE OF ANALYSES

The Structural System

Figure 9 shows the typical cross-section of the grout gallery as designed by the Department of Water Resources, together with three idealized sections used in the analyses. From these three basic configurations, representing a gallery without gutter, an enlarged gallery section used as an instrument chamber, and a gallery with gutter, eleven basic cases were analyzed as shown in Table 1. Case 1 was a coarse mesh system spread over a wide area which was used to find the deformations at an inner surface used subsequently as the outer boundary for all the fine mesh cases. Cases 2 through 7 represented basic variations of the gallery without gutter. Cases 8 and 9 represented a thick-walled and thin-walled instrument chamber. Cases 10 and 11 represented a thick-walled and thin-walled gallery with gutter.

For each case, symmetry was used wherever possible to reduce the number of elements included in the analysis as well as to reduce the number of operations necessary for convergence of the solution.

The elastic modulus of rock and concrete was assumed equal to 3.0×10^6 psi. Poisson's ratio for concrete was taken as 0.20 and for the rock 0.15, except for Cases 1 and 2 where it was taken as 0.20 for both materials. While tests showed a fairly high modulus of elasticity for both concrete and rock cores, the low values used in the analysis reflect creep for the concrete, and cracks and other defects in the rock, which act to reduce their effective moduli and Poisson's ratio.
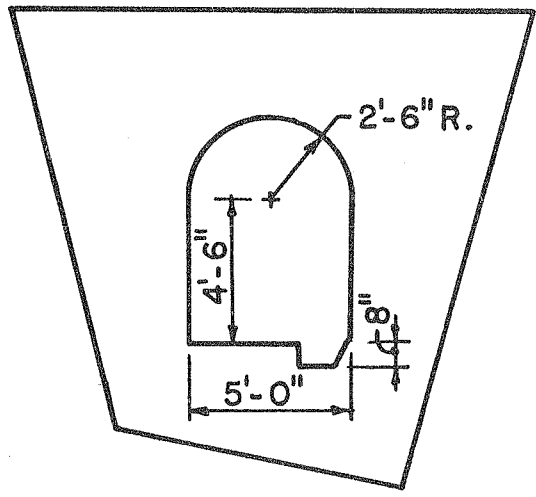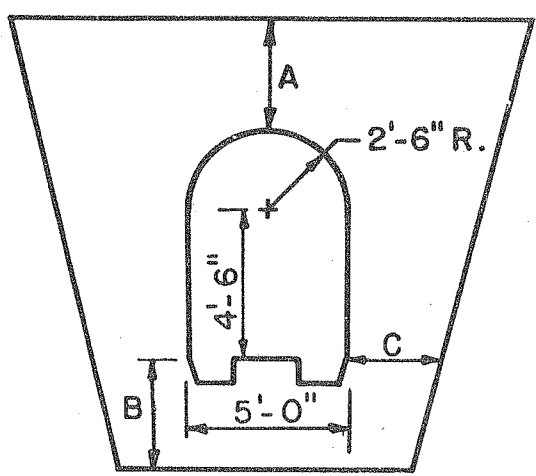
I

PROTOTYPE GALLERY
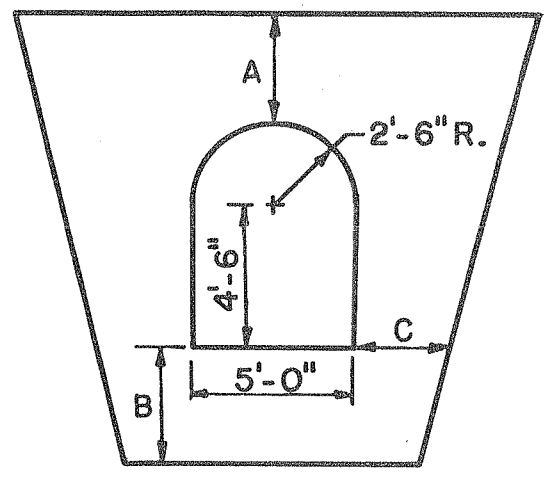
II

GALLERY WITHOUT GUTTER
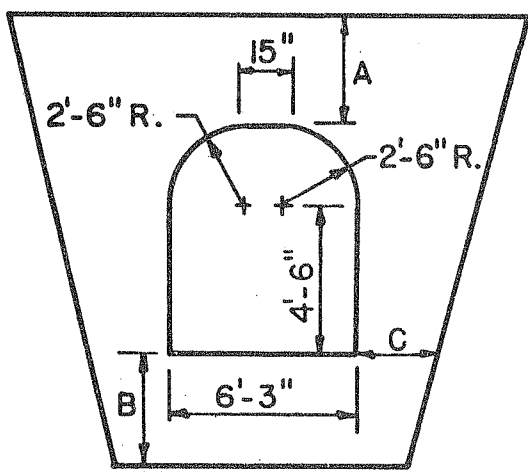
III

INSTRUMENT CHAMBER

IV

GALLERY WITH OPENING

FIG. 9 — GROUT GALLERY SECTIONS FOR ANALYSIS

TABLE 1 - Schedule of Cases Analyzed

Case	Figure[a]	Dimensions: Ft-in.		
		Crown A	Invert B	Side C
1	II	3-5	4-0	2-10
2	II	3-5	4-0	2-10
3	II	3-5	4-0	2-10
4	II	3-0	4-0	2-10
5	II	3-5	3-6	2-10
6	II	3-0	3-6	2-0
7	II	1-6	2-0	1-6
8	III	3-0	4-0	2-0
9	III	1-6	2-0	1-6
10	IV	1-6	2-0	1-6
11	IV	3-0	3-6	2-0

[a] Illustrated in Figure 9.

Loading

In constructing the grout gallery, a trench is first excavated, next the invert of the gallery is poured, and finally the arch is poured bringing the concrete up flush with the level of the rock. At a later time, the grout gallery receives the weight of from 100 to 600 ft of backfill from the dam above. Hence, in this analysis, it was considered that the gallery was essentially unloaded upon the completion of concrete construction, and that all load came from vertical distributed loads bearing directly on the concrete grout gallery and also on the surface of the adjacent rock. Since these loads vary greatly from place to place in the dam, it was decided to make all analyses for a unit load of 1000 psi so that the Department of Water Resources could apply whatever actual load was appropriate to the location being considered, and determine the appropriate stresses by direct proportion.

Scheme of Analysis

Figure 10 shows the general scheme used in the analysis. The grout gallery is essentially 5' x 7' in dimension. At a distance of 4 diameters in all directions from the grout gallery, it was assumed that stress and strain concentrations due to the opening would have disappeared, and the boundaries for the analysis were set here. The analysis was split in two on a vertical plane of symmetry through the centerline of the gallery. The bottom boundary AB was considered to be fixed. The vertical side boundary BC was considered to be a boundary across which there could be no horizontal movement under loading and along which there could be no vertical shear force, but which would permit vertical deformation.

Within boundary ABC, a course network of finite elements was drawn in the rock and in the concrete of the grout gallery as shown in Fig. 10.
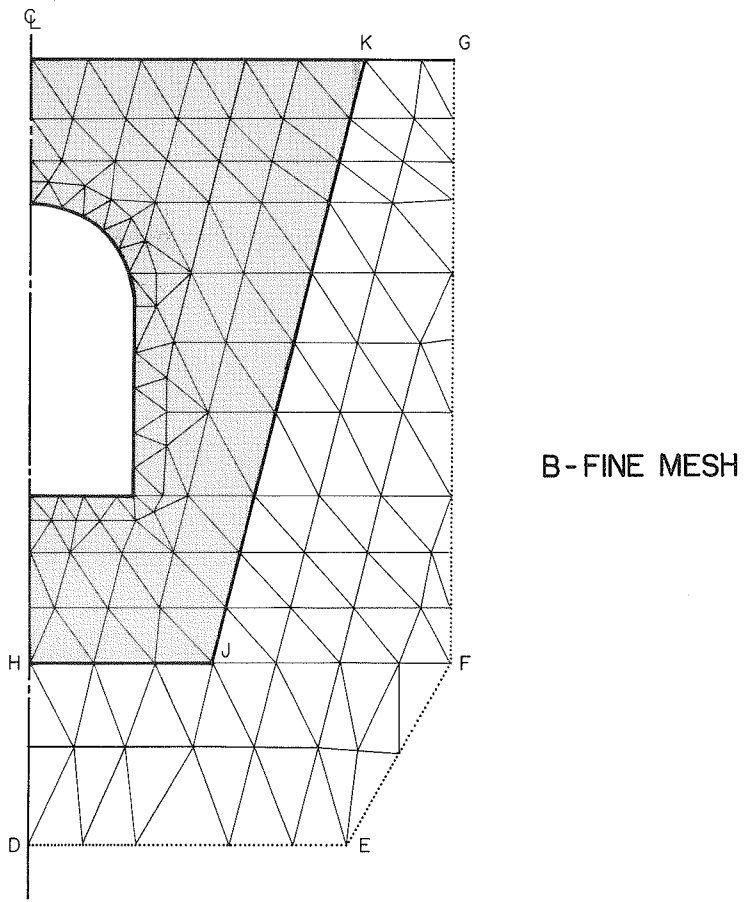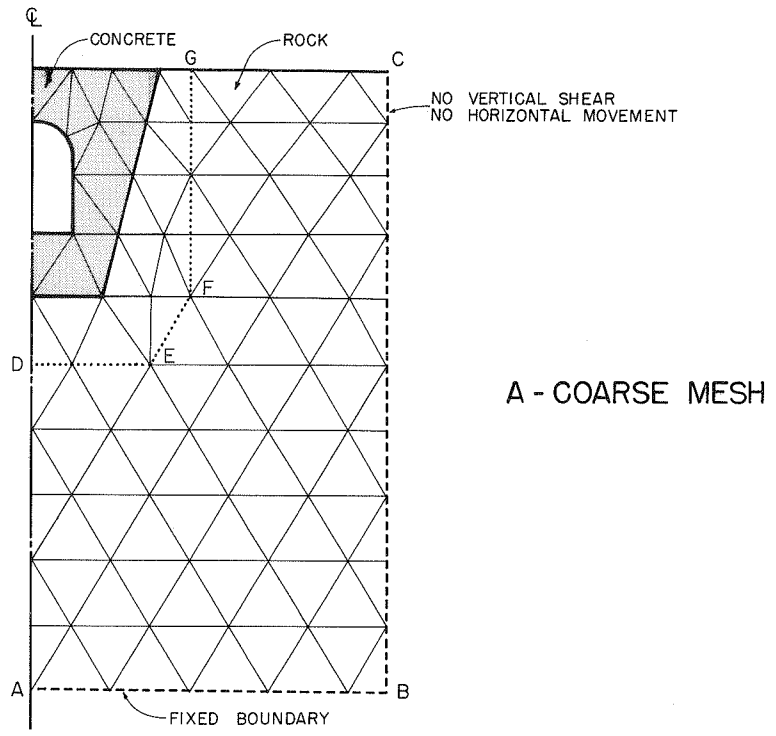
A - COARSE MESH

B - FINE MESH

FIG. 10 - TYPICAL FINITE ELEMENT LAYOUTS
FOR GROUT GALLERY

With a load of 1000 psi applied to the top surface of the figure, displacements were found at all nodal points of the figure. The translations along the surfaces DEFG were noted particularly, since these deflections become the boundary conditions for the mesh of finite elements shown in Figure 10B. There are about ten times as many elements within the concrete structure in the fine network as there are in the coarse network shown in Figure 10A. It will be noted that various element sizes were employed in the fine mesh system, with smaller elements being used near the gallery opening so that greater detail on the stress distribution could be obtained in this critical area.

Boundary DEFG shown in Figure 10B remained fixed in dimension for all subsequent studies. However, the concrete boundary HJK changed in position as dictated by the dimensions used in the several analyses. It was considered that these minor changes had negligible effect on the translations at boundary DEFG, and the boundary displacements determined in Case 1 were used throughout the analyses that followed.

RESULTS OF ANALYSES

Form of the Results

The direct results of the machine analyses were a series of tabu-lations giving the displacements of each nodal point, the vertical and horizontal normal stresses, vertical and horizontal shear stresses, and the maximum and minimum principal stresses together with their inclina-tion. However, these tabulated data did not permit ready visualization of the effect of load on the structures, hence a series of drawing has been prepared to show the variation of stress throughout the structure for the loadings and configurations considered.

Stress Contours

The magnitude of the principal stresses for each configuration studied has been shown on two drawings for each case. The maximum compressive stresses are defined on one drawing by means of contours connecting points having equal magnitudes of compressive principal stresses. On the second drawing only the tensile principal stresses are shown, for the reason that any compressive principal stresses on this figure will be smaller in magnitude than those shown on the previous drawing. By examining the two drawings, regions of high compressive stress concentration and regions of potential cracking requiring reinforcement are easily identified.

For three typical configurations, representing thick, intermediate and thin sections, three drawings showing the directions of principal stress have been given. These are so similar for all cases studied that it was not considered necessary to present them for every case.

Another drawing shows the distribution of shear stress on a line drawn vertically downward from the corner of the gallery, this being the region of the greatest variation in shear stress. All these results will be discussed in detail for each case studied in the sections that follow.

Coarse Mesh - Case 1

Case 1 is the coarse-mesh analysis covering a wide and deep area of the foundation rock which was used to establish the boundary conditions on the inner boundary used on all subsequent fine-mesh analyses. Figure 11 has been included to show the magnitude of the maximum compressive principal stresses throughout the grout gallery and the surrounding rocky mass. It can be seen that at not too remote a distance from the concrete grout gallery, the stresses are everywhere compressive and of the order of 1,000 psi, which is the same as the applied load. Hence, the inner boundary defined as the outer boundary of the fine network is fairly uniformly stressed. Little attention should be paid to the stresses shown in Figure 11 for the grout gallery itself, as these necessarily represent only average stresses for the cross section. Better detail for these stresses will be shown in the fine network analyses that follow.

Thick-Walled Grout Gallery - Case 2 (POISSON RATIO = 0.2)

Figures 12 and 13 are typical of the stress results obtained for all the fine mesh cases. Figure 12 shows contours of the compressive principal stresses. It can be seen that there are two regions of maximum stress concentration: the springing of the arch, and the lower corner of the gallery. Everywhere else, stresses are smaller in magnitude. Similarly, in Figure 13, it can be seen that there are three regions of tensile stress: the crown of the arch (which in this particular case has so little stress that only the zero stress line is plotted), the center of the invert
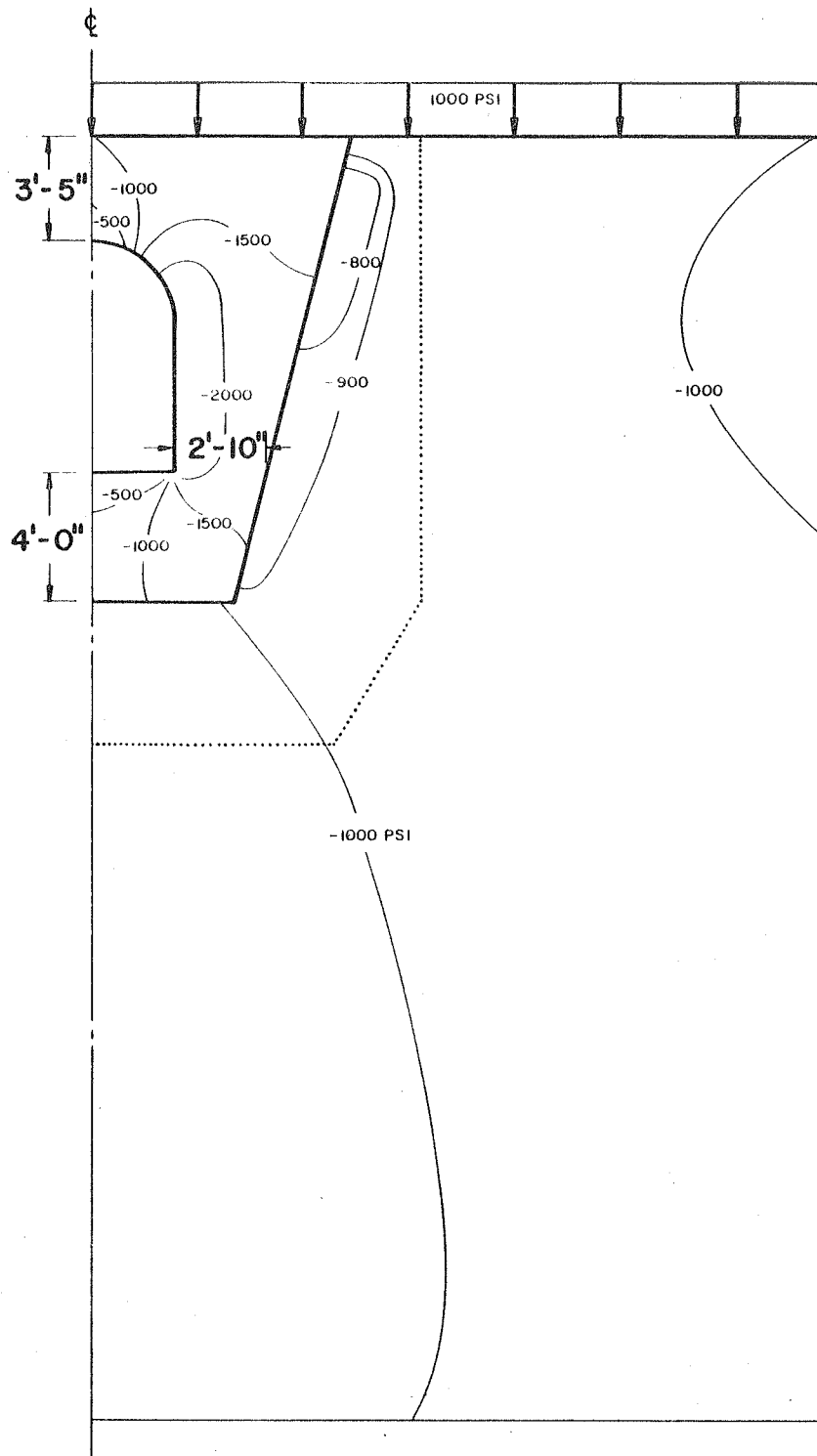
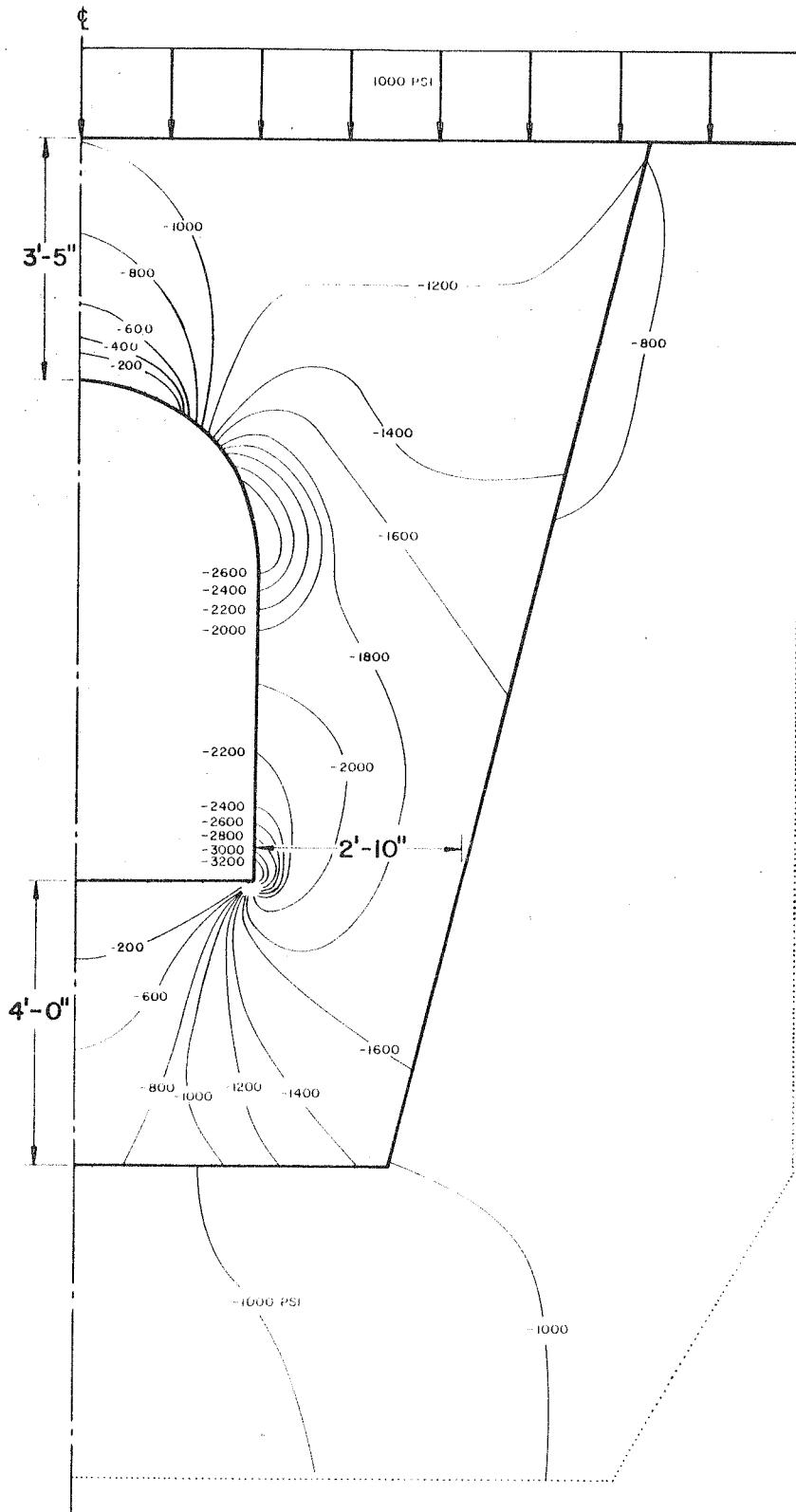FIGURE II - CASE I
COMPRESSIVE PRINCIPAL STRESSES

FIGURE 12 - CASE 2
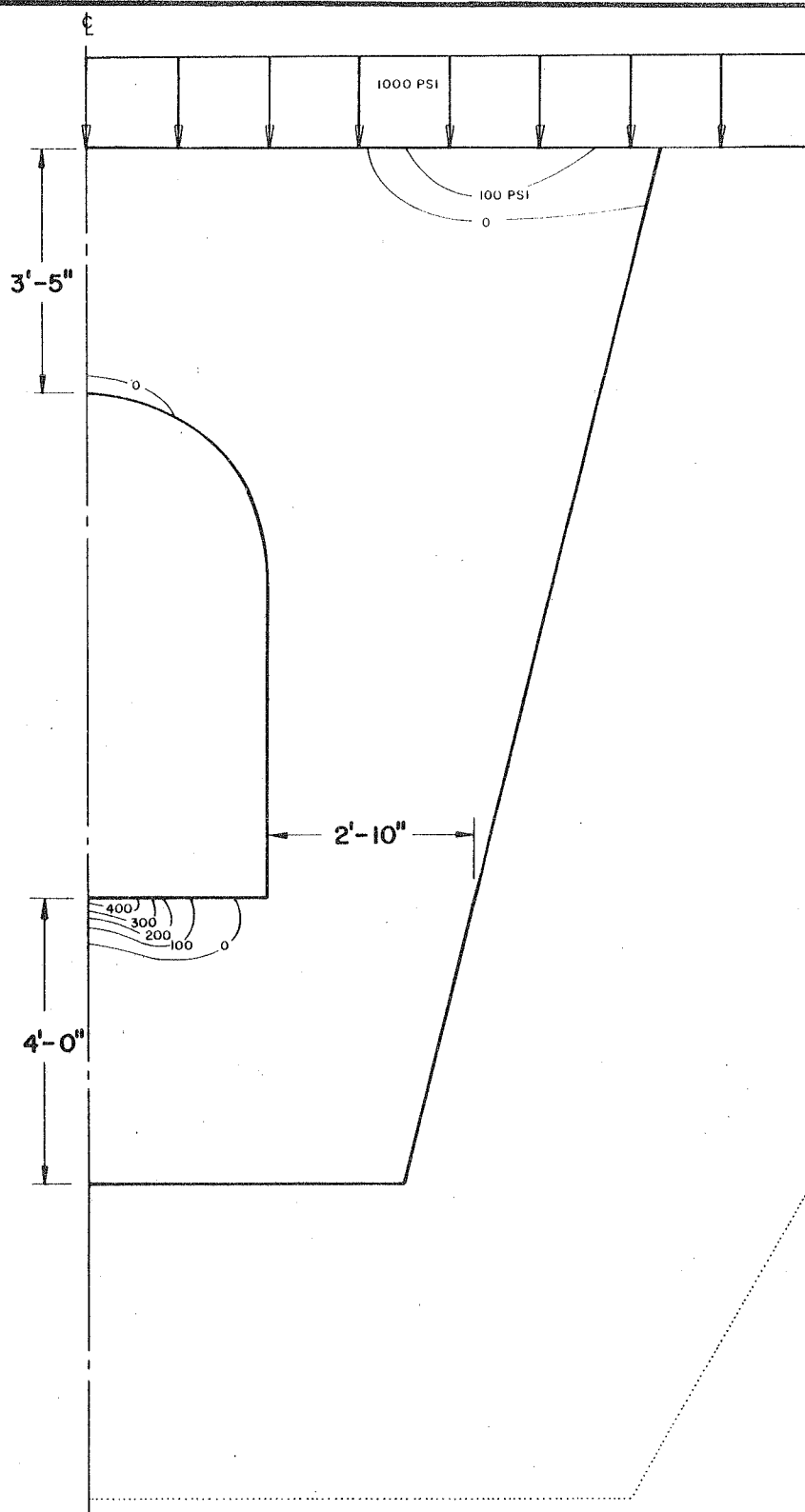COMPRESSIVE PRINCIPAL STRESSES

FIGURE 13 - CASE 2
TENSILE PRINCIPAL STRESSES

or floor of the gallery (which has a concentration factor of 0.4), and the upper outside corner of the concrete. Because the latter region could be extensively cracked without affecting the structural action of the grout gallery, the existence of tensile stresses here has not been considered important.

In interpreting the stress results shown in the figures, it should be remembered that the 1,000 psi load placed on top of the grout gallery is almost double the maximum load expected in the dam; it was adopted merely as a convenient reference quantity. Thus for a typical maximum load of 600 psi applied to the top of the gallery the maximum compressive stresses in the gallery for Case 2 might be of the order of 2,000 psi, a load that is easily handled with 4,000 psi concrete. Similarly, by examining Figure 13, it can be seen that the structural tensile stresses are quite moderate, that the tensile stress region is small, and these two facts together dictate the use of quite light reinforcement, with the probability that nominal or temperature reinforcement might suffice all around the opening for this configuration.

Another factor to be kept in mind is that it is impossible to determine, whether by mathematical analysis, structural model, or by any analogy, what the stresses are at a sharp corner such as at the lower corner of the gallery opening. Hence, the stress concentration factor at this point must be interpreted with caution. It is also quite likely that in constructing the gallery in two steps (by concreting up to the level of the invert or gallery floor first and then concreting the remainder of the grout gallery in a subsequent operation) that a horizontal shrinkage crack probably would be formed at the lower corner of the gallery opening. This would transfer the compressive stress further into the

concrete mass, away from the inner boundary of the opening, and would reduce greatly the stress concentration factor found here.

Figure 14 presents information on the shear stress distribution determined for Case 2. The curve shows the variation of shear stress on the vertical section y-y extending downward from the lower corner of the grout gallery. The computed stresses increase from less than 200 psi at the rock line to a theoretical value of infinity at the corner. However, 6 inches below the surface, at the level where the steel is likely to be found, the stresses have reached a maximum concentration factor of only 0.7. All along this line, shear stress has the same sign indicating that the side wall is tending to be forced downward past the invert. The high shear stresses in this region should not cause alarm, however, because concrete does not actually fail in shear, but rather in tension. Referring back to the contours of principal stress (Figure 16), it is seen that no tension exists along the line y-y, and hence, it should be concluded that no more than nominal reinforcement is needed in this region.

Case 3

Results for Case 3 which concerns the same grout gallery configuration as Case 2, are shown in Figures 15 to 18. The only difference between the two cases is that for Case 3 (and all subsequent cases) Poisson's ratio for the rock was assumed to be 0.15, while in Case 2 a ratio of 0.2 was assumed. Despite the change in rock properties, stress results are essentially the same as those found for Case 2, showing that weakening the rock support by reducing Poisson's ratio by 25 per cent makes very little difference. Concentration factors, stress contours, and shear stresses are practically unchanged from those found for Case 2.
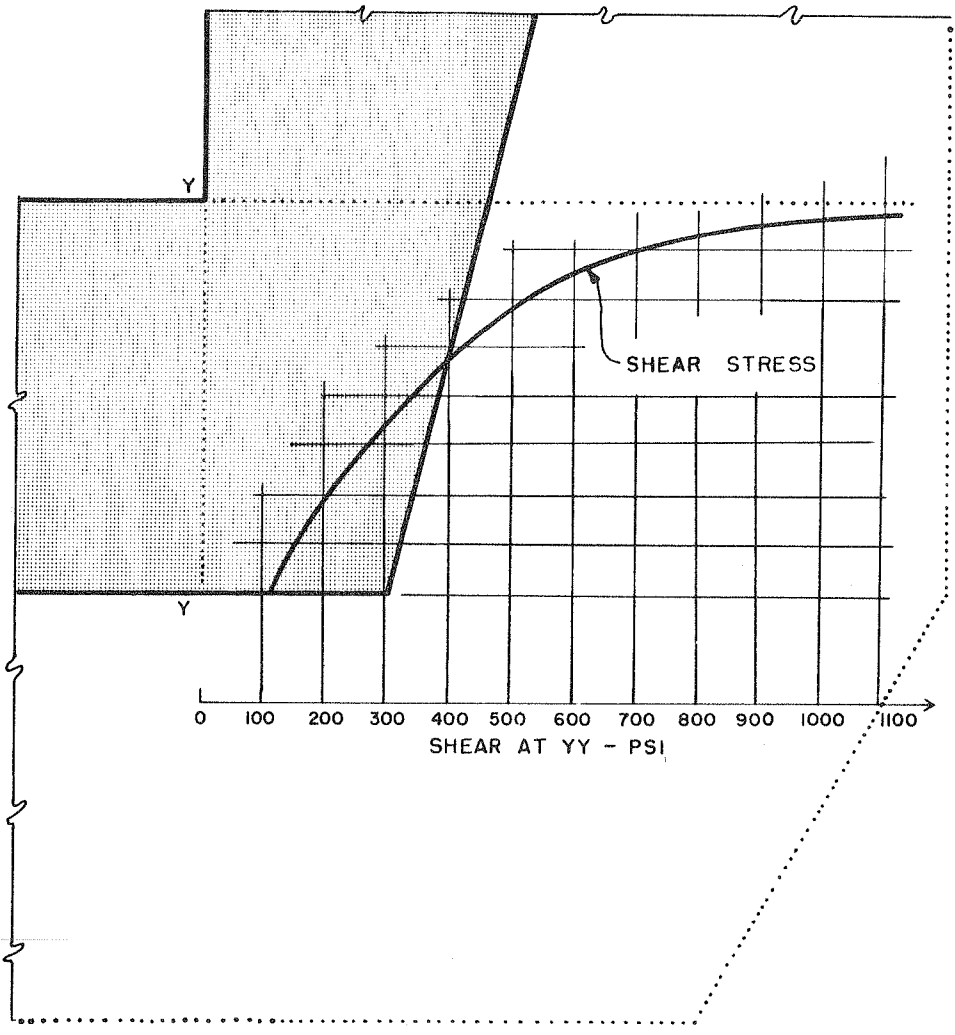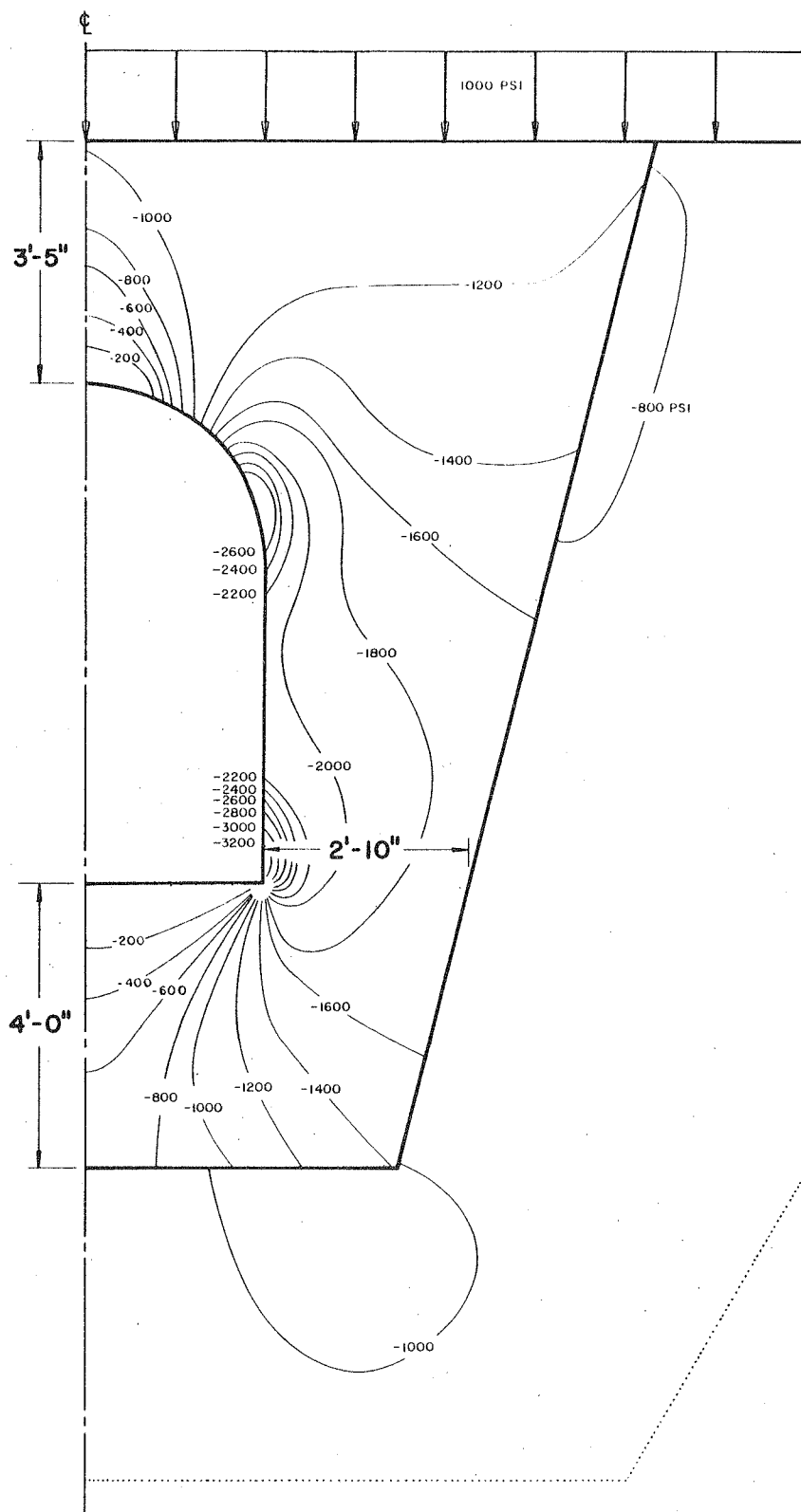
FIGURE 14 - CASE 2 - SHEAR STRESS AT BASE

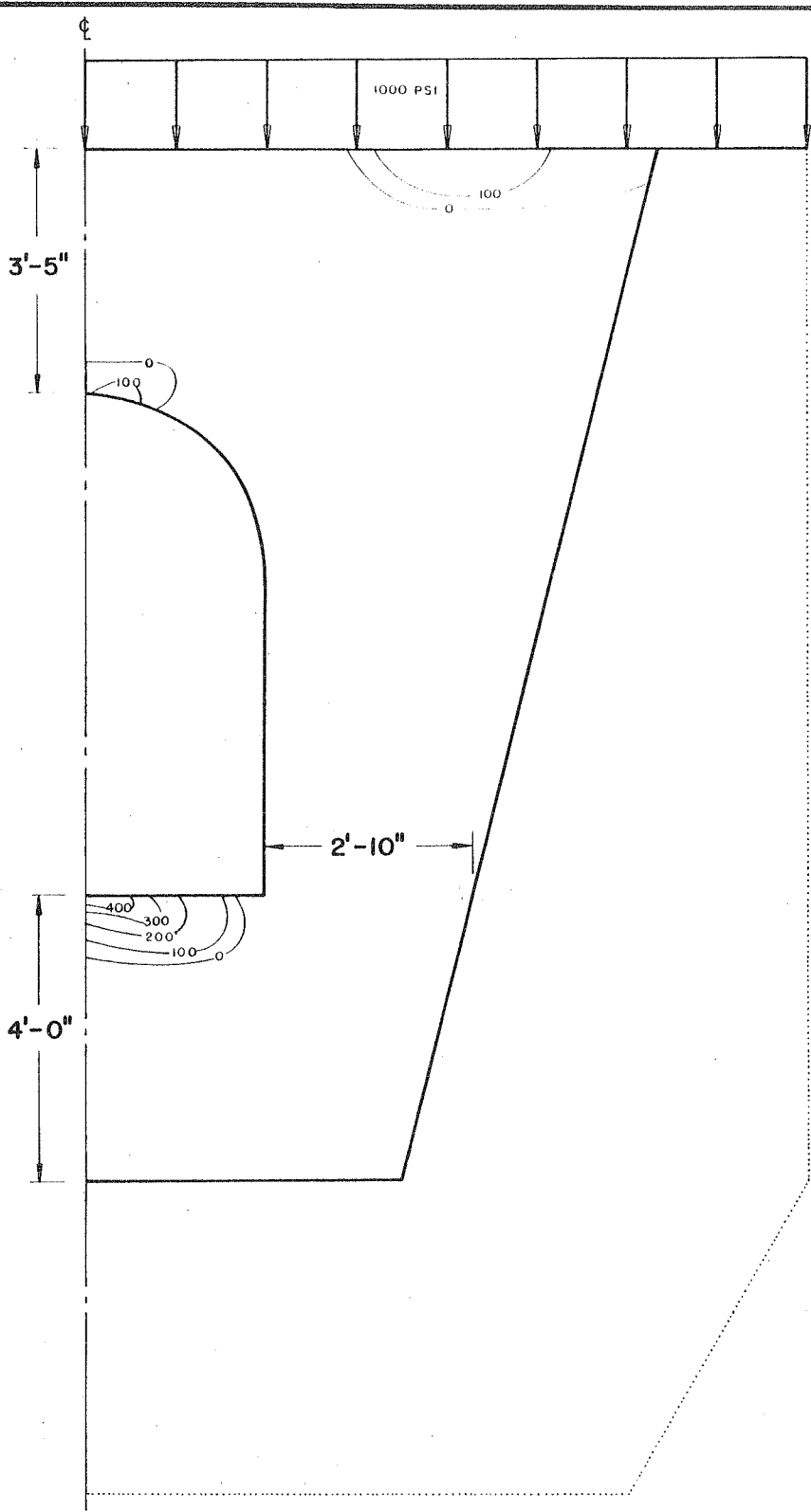FIGURE 15 - CASE 3
COMPRESSIVE PRINCIPAL STRESSES

FIGURE 16 - CASE 3
TENSILE PRINCIPAL STRESSES

SHEAR STRESS

0   100 200 300 400 500 600 700 800 900 1000 1100
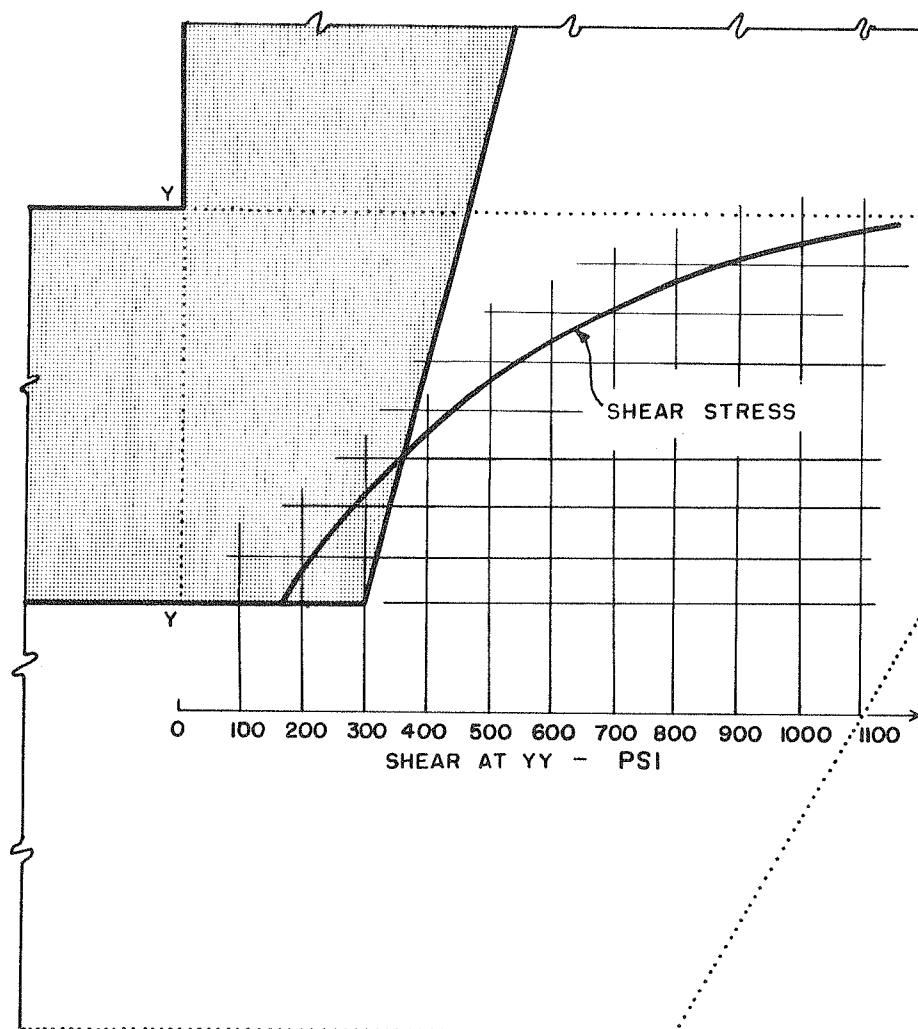SHEAR AT YY — PSI
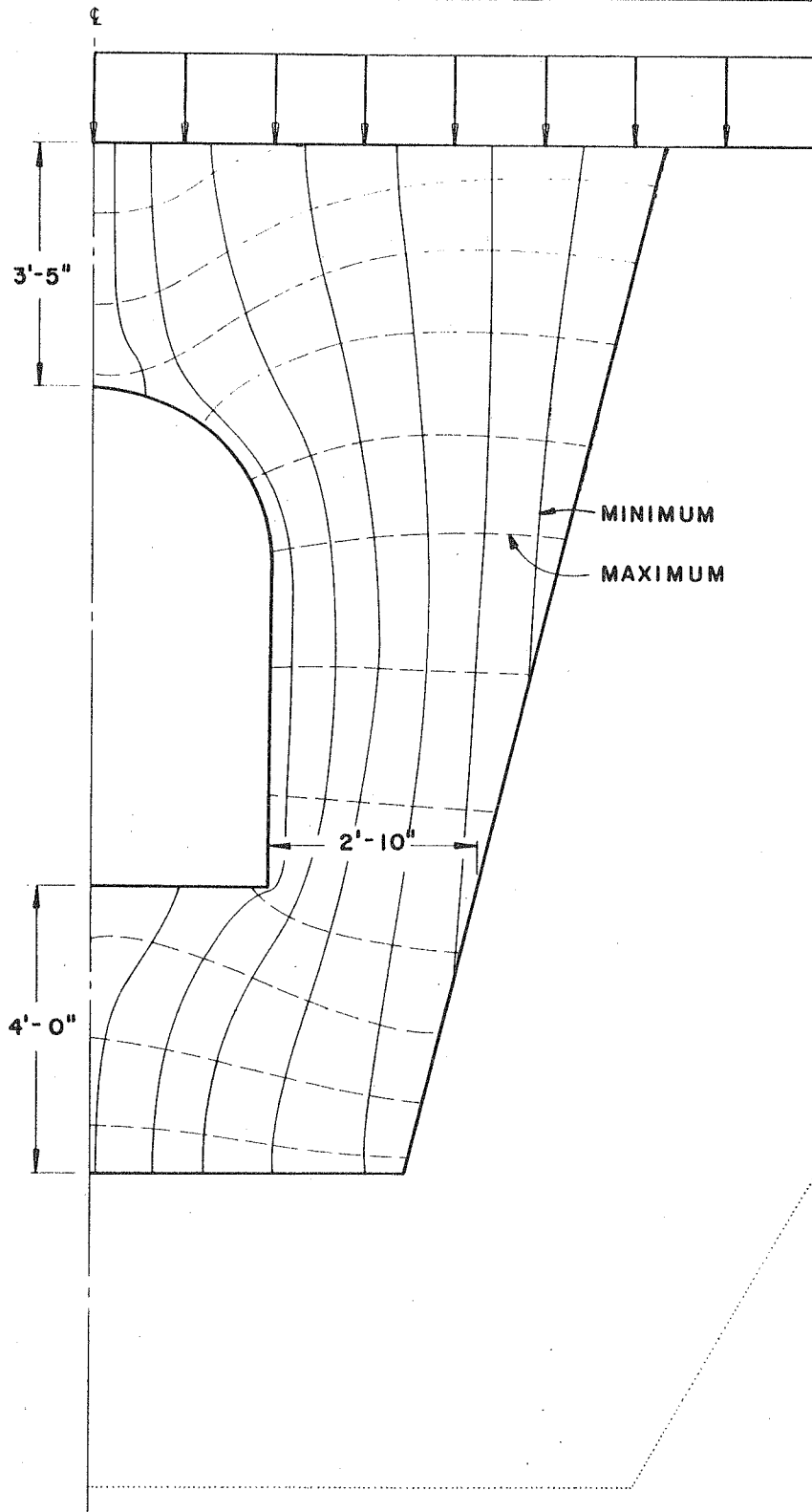
FIGURE 17 - CASE 3 - SHEAR STRESS AT BASE

FIGURE 18 - CASE 3
DIRECTION OF PRINCIPAL STRESSES

It is interesting to note the distribution of stress at the boundary between rock and concrete. Most elementary analyses of structures of this type assume uniform or linearly varying stress along these boundaries. The finite element approach however, indicates a definitely non-linear boundary stress distribution. These results, in fact, confirm the stresses found by observation of the stress meters at several field installations.

Figure 18 shows the directions of principal stresses determined for Case 3, and can be used as a guide in the layout of reinforcement. The solid lines show the directions of the maximum compressive stresses, and the dashed lines refer to the minimum compressive stresses (or maximum tensile stresses). The solid lines clearly show the stress flow paths carrying the applied load around the gallery opening.

Case 4

Cases 4, 5, and 6 are of variations of Case 3. In each case, one
dimension is made slightly smaller than that for Case 3 to gage its
effect separately. For Case 4, the thickness at the crown is reduced
from 3'-5" to 3'-0". This produced no noticable change in the maximum
compressive stresses, as may be seen in Figure 19. However, the tensile
stress at the crown, the region which was made thinner, has been doubled
to a maximum tensile principal stress concentration factor of 0.2 as
shown in Figure 20. No significant change resulted in the tensile
stresses near the base, but shear stresses near the base, shown in
Figure 21, are found to be slightly higher near the rock base and slightly
lower near the floor of the opening.

Case 5

In Case 5, the invert thickness is reduced from 4'-0" to 3'-6" (with
the crown thickness again returned to 3'-5"). The maximum compressive
stresses, shown in Figure 22, are still unchanged. Interestingly enough,
maximum tensile stresses, shown in Figure 23, are of the same order of
magnitude as those for Case 3, shown in Figure 16. However, the region
of tensile stress in the invert has increased in size slightly, and now
begins to reach into the region of shear shown on line y-y. Shear stresses,
shown in Figure 24, are roughly of the same order as those shown for Case 4,
but are increased slightly near the rock base.

Case 6

Case 6 differs from Case 3 in that all dimensions were reduced simul-
taneously to the slimmer configuration shown in Figure 25. Despite this
reduction in volume, stress concentration factors are only slightly in-
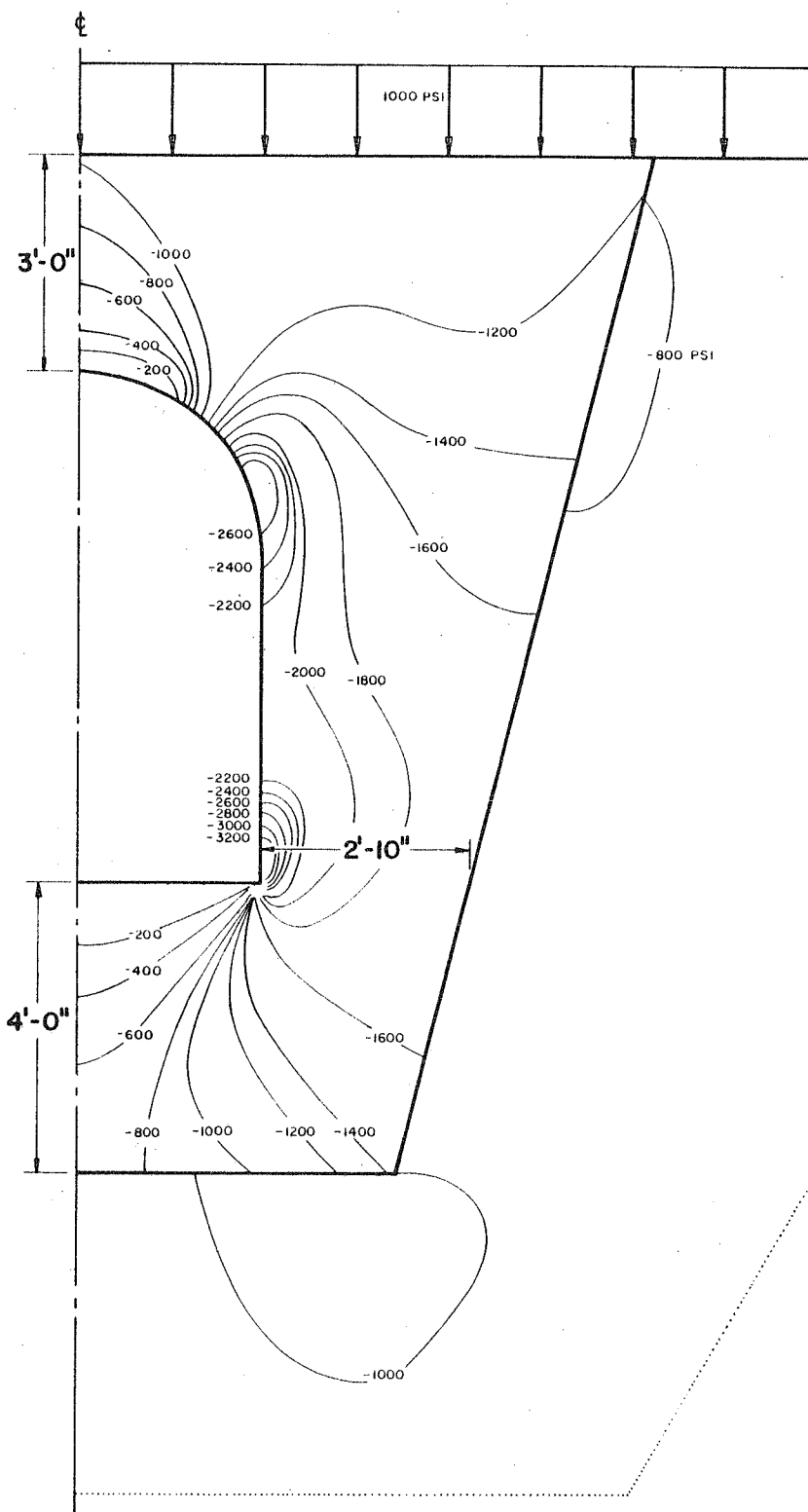creased. The maximum compressive stress concentration factor increases

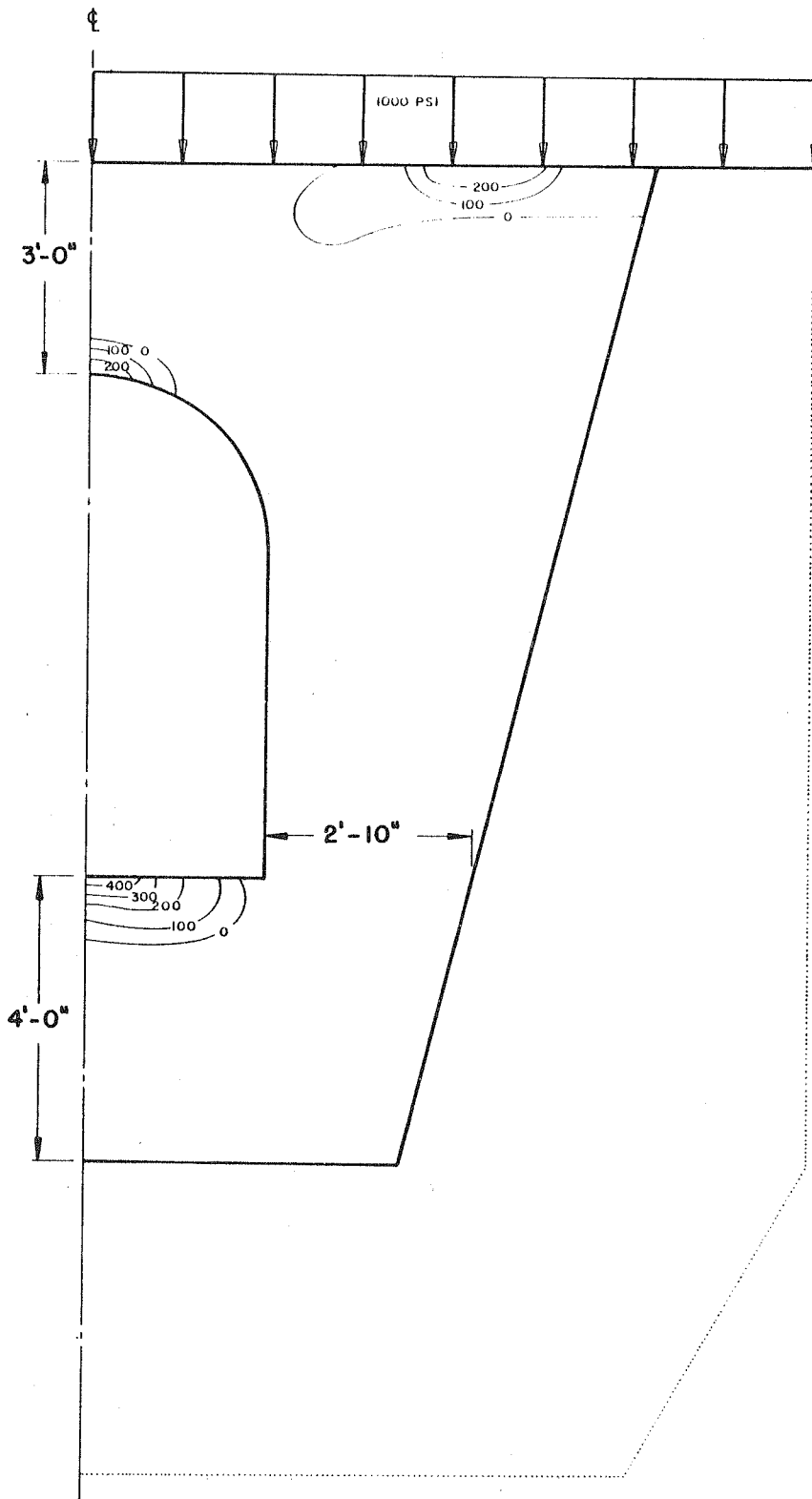FIGURE 19 - CASE 4
COMPRESSIVE PRINCIPAL STRESSES

FIGURE 20- CASE 4
TENSILE PRINCIPAL STRESSES

Y

Y

SHEAR STRESS

0   100   200   300   400   500   600   700   800   900   1000
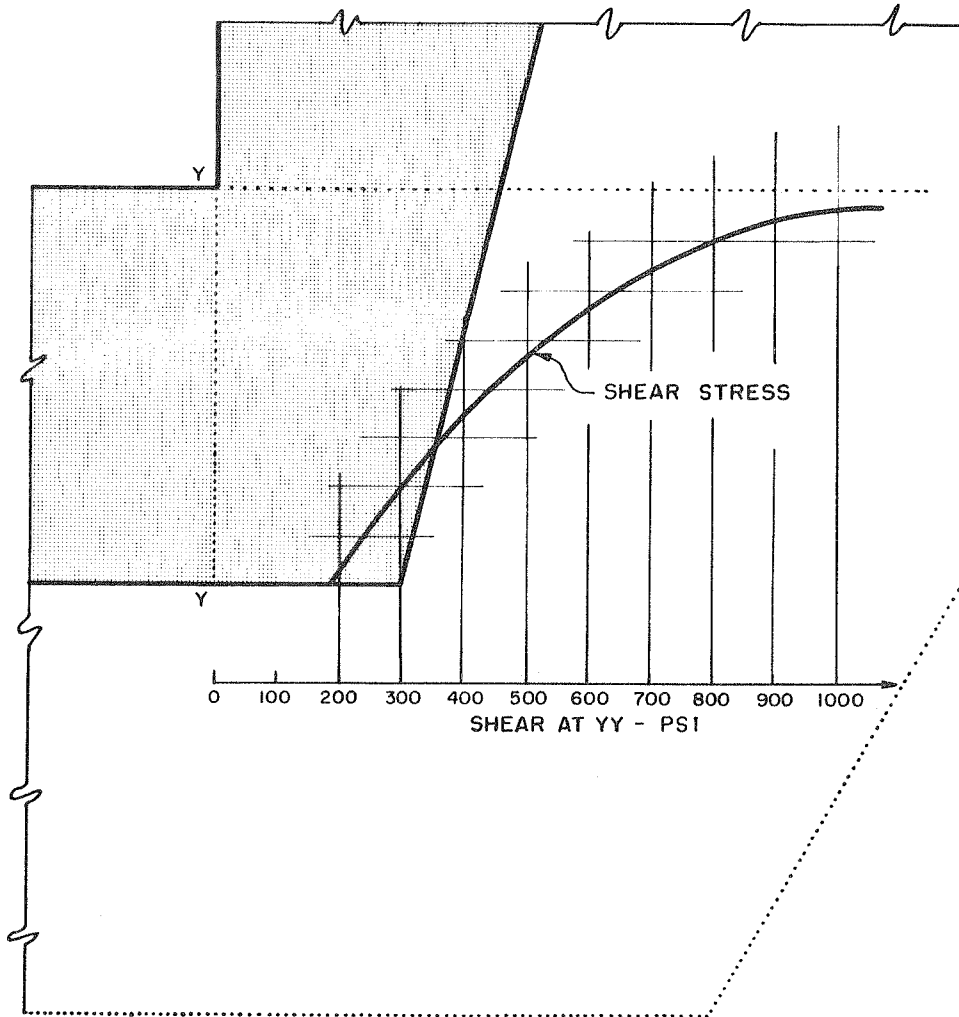
SHEAR AT YY - PSI

FIGURE 21 - CASE 4 - SHEAR STRESS AT BASE
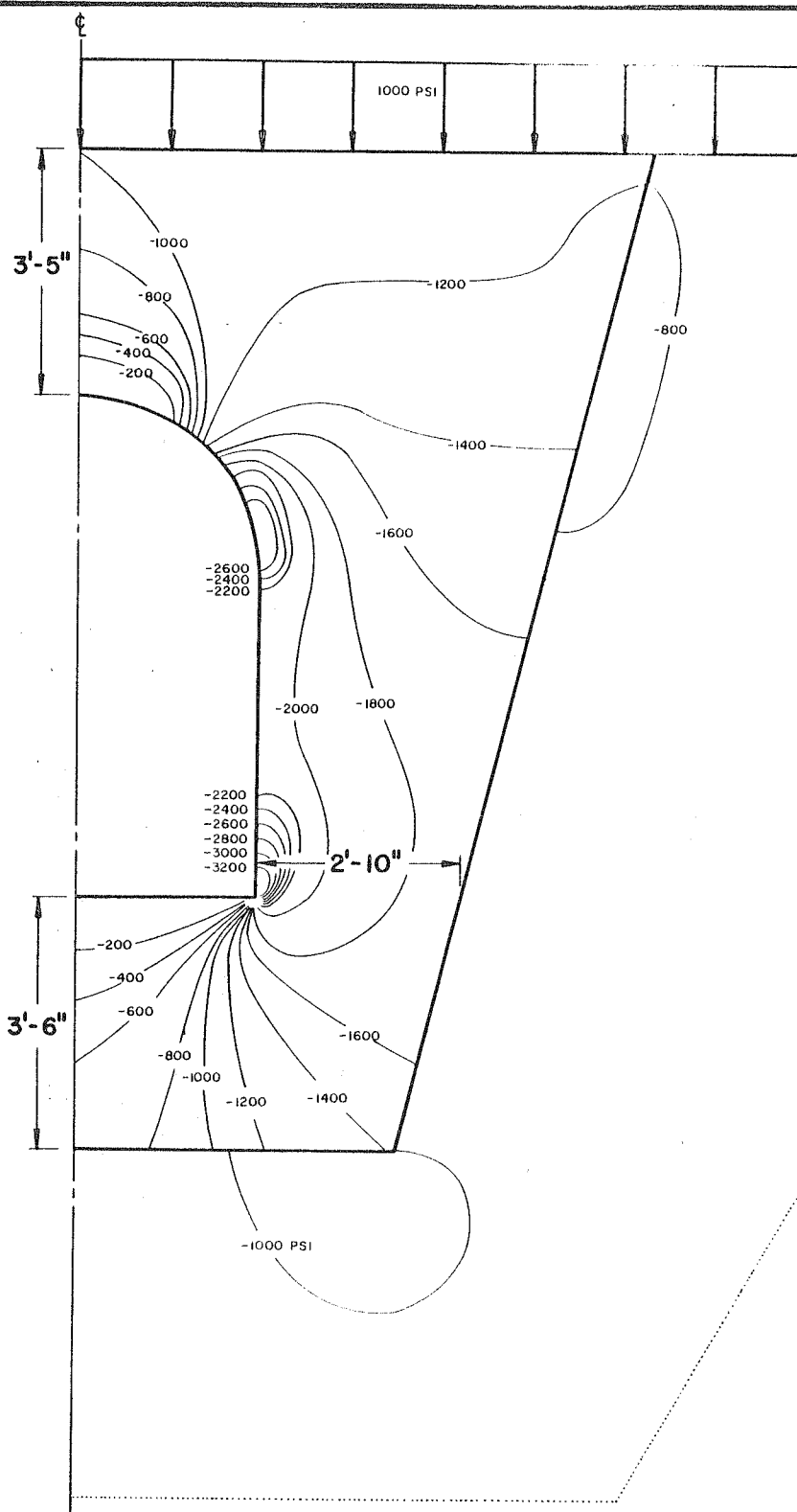
FIGURE 22 - CASE 5
COMPRESSIVE PRINCIPAL STRESSES
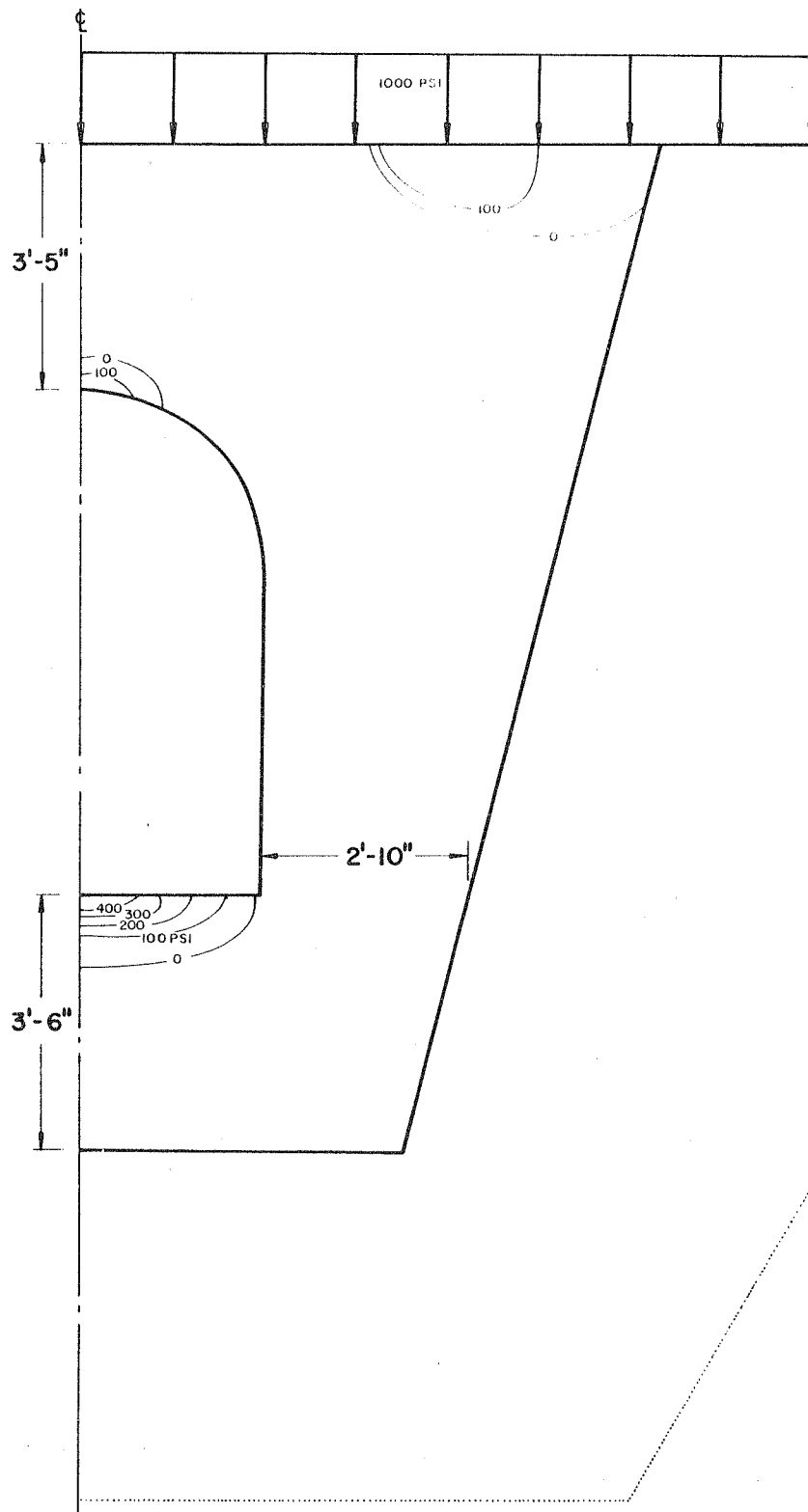
FIGURE 23 - CASE 5
TENSILE PRINCIPAL STRESSES
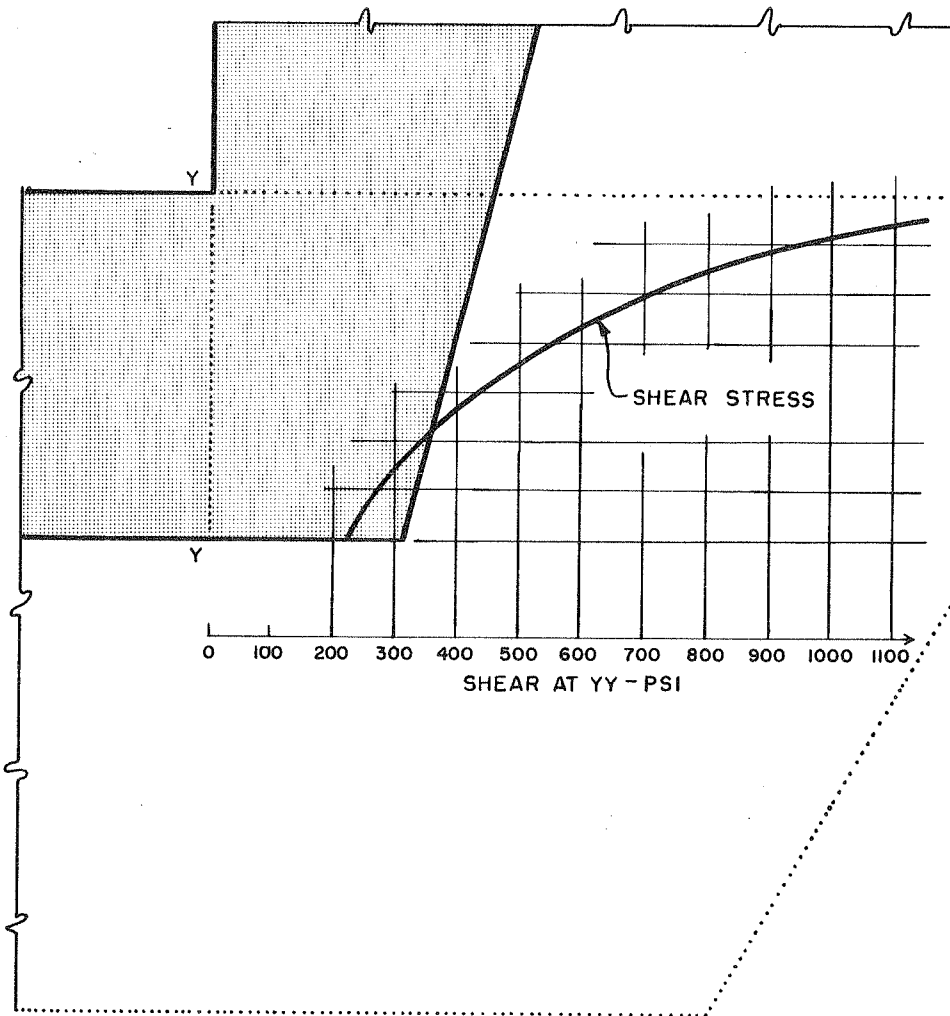
SHEAR STRESS

SHEAR AT YY – PSI

0   100   200   300   400   500   600   700   800   900   1000   1100

FIGURE 24 - CASE 5 - SHEAR STRESS AT BASE

by only 0.2, as shown on Figure 25. The maximum tensile stress concentration factor, shown on Figure 26, is increased by only 0.1. It is evident that a considerable volume of concrete can be saved with this thinner configuration without affecting the stresses measurably. Shear stresses, shown on Figure 27, do not differ greatly from those shown previously. In general, the directions of principal stresses shown on Figure 28 resemble those drawn previously for the larger-volume Case 3 with only slight differences in detail at the crown. These differences result from the fact that the horizontal compressive stresses at the top, due to beam action, now exceed the vertical stresses due directly to the applied load. Thus the principal stress directions are reversed.

Thin-Walled Grout Gallery - Case 7

For Case 7 all important dimensions were roughly half those used previously in Case 3. This structure is intended to be used where the loading will be considerably less than maximum, as at the upper levels of the dam. Hence, although the stress concentration factors shown in Figures 29 and 30 are increased appreciably, the superposed loads will be much smaller and the actual magnitudes of stresses in the structure may be of the same magnitude as those found previously. Despite the radical change in dimensions of the section, stress concentration factors are only slightly increased. This case demonstrates, therefore, that a minimum dimensioned gallery, constructed of strong concrete, can safely withstand all superimposed loads.

Instrument Chamber - Case 8

Case 8 corresponds most closely to Case 6, with the exception that the gallery has been widened by 15 inches so that it can be used as an instrument chamber. In general, as shown in Figures 32 to 34, this has
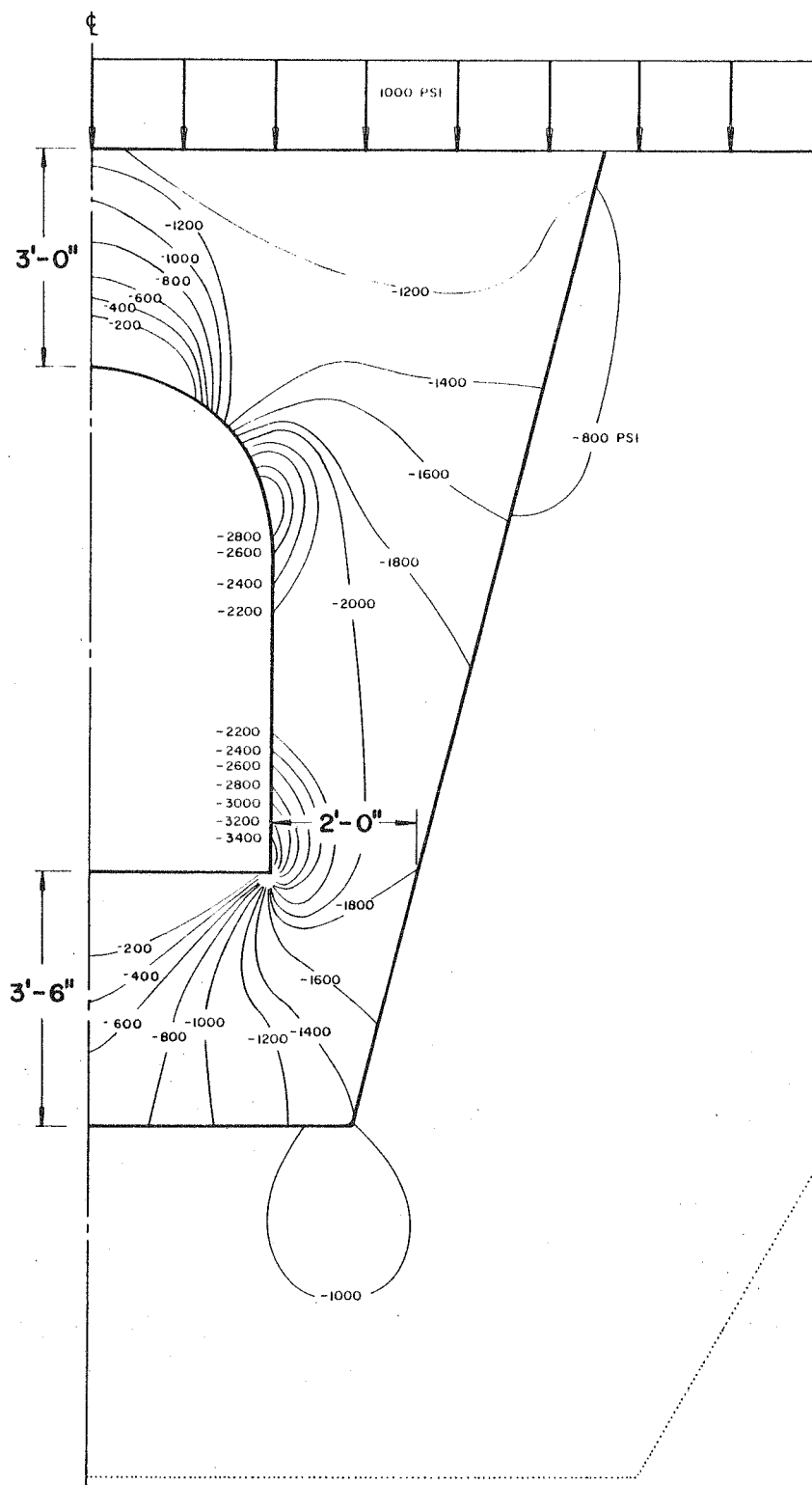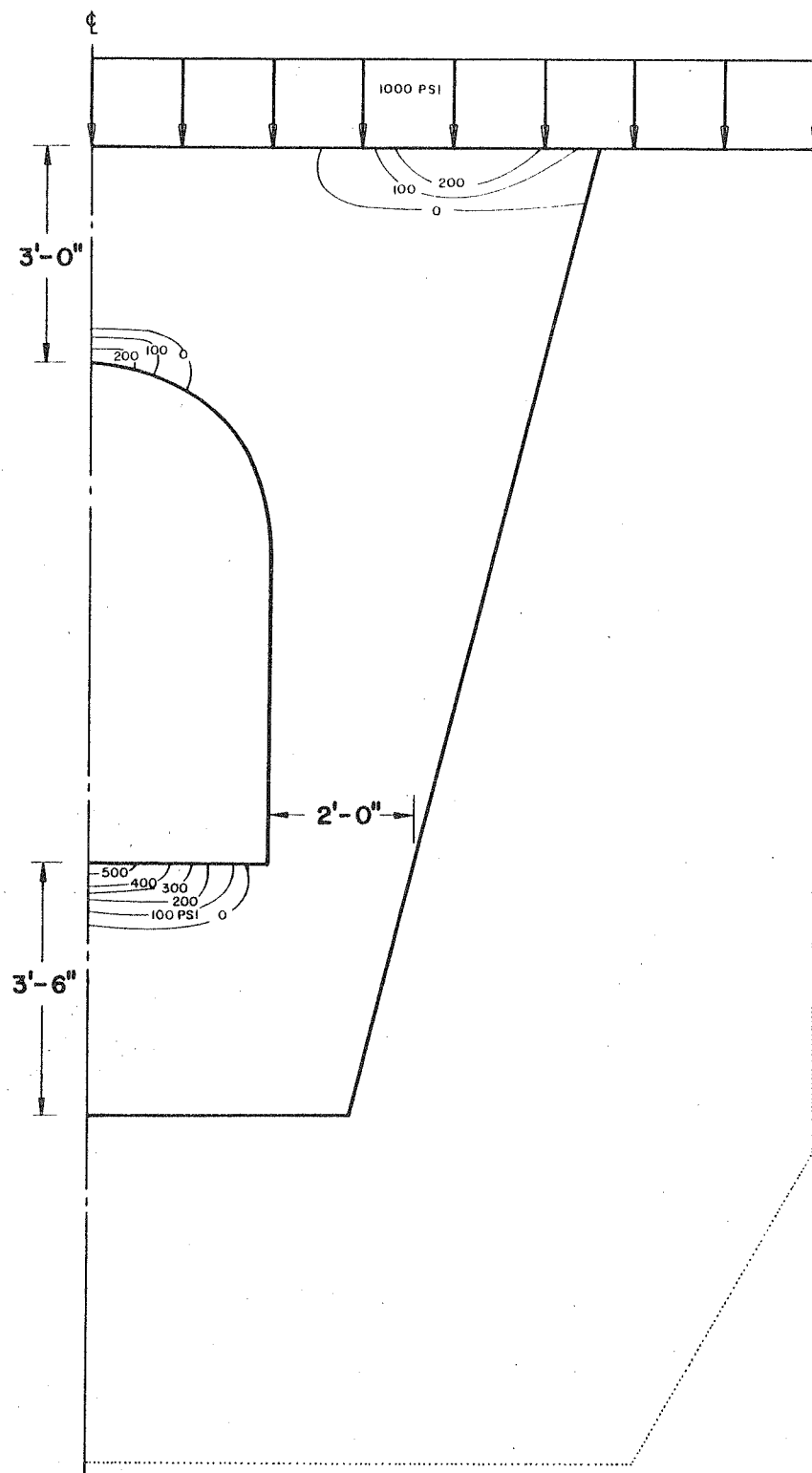
FIGURE 25 – CASE 6
COMPRESSIVE PRINCIPAL STRESSES

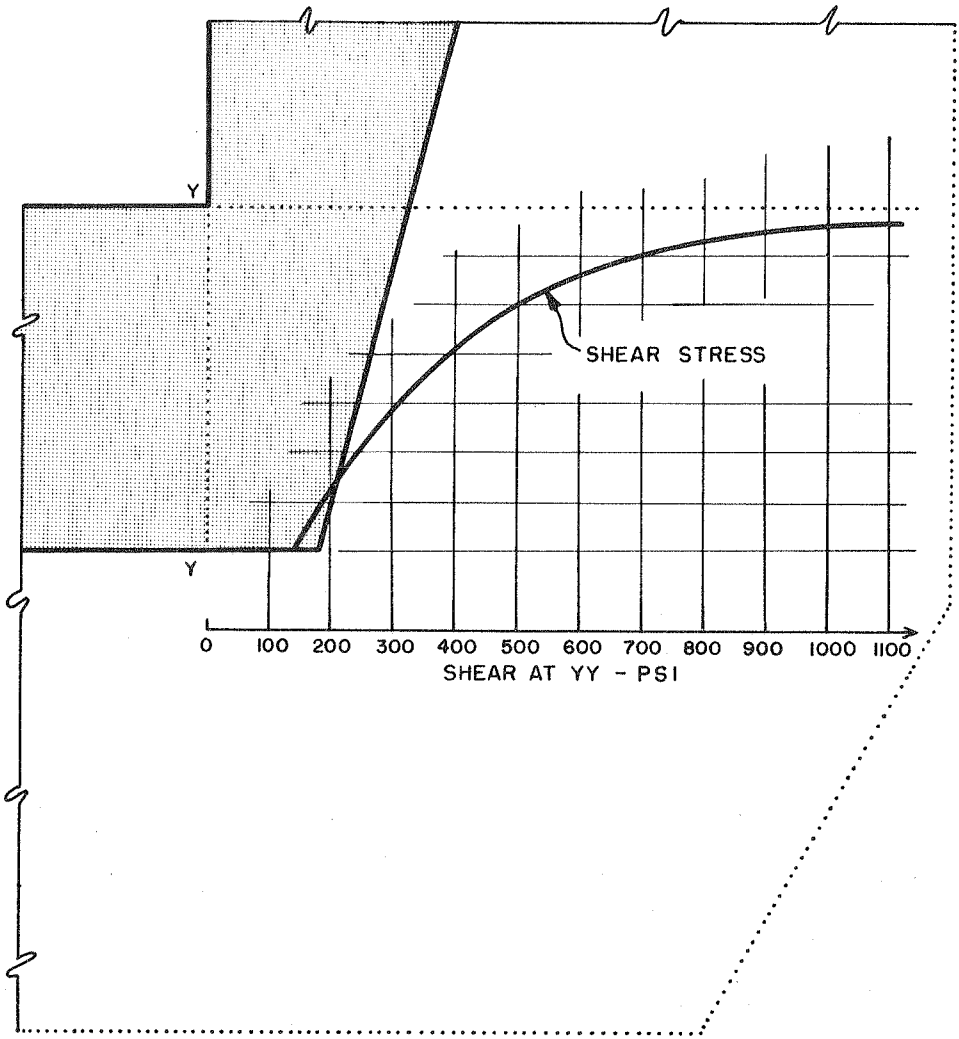FIGURE 26 - CASE 6
TENSILE PRINCIPAL STRESSES
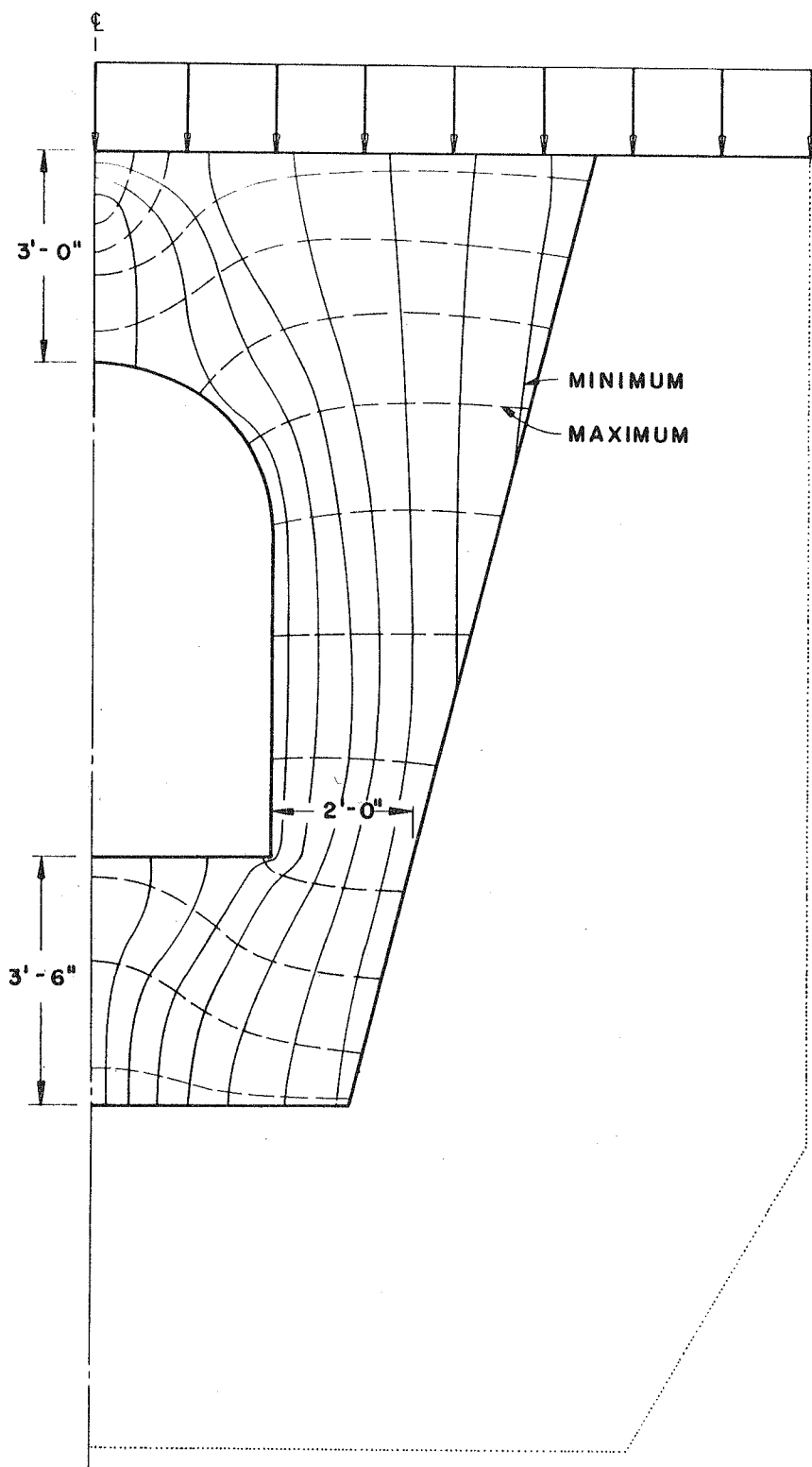
FIGURE 27 - CASE 6 - SHEAR STRESS AT BASE
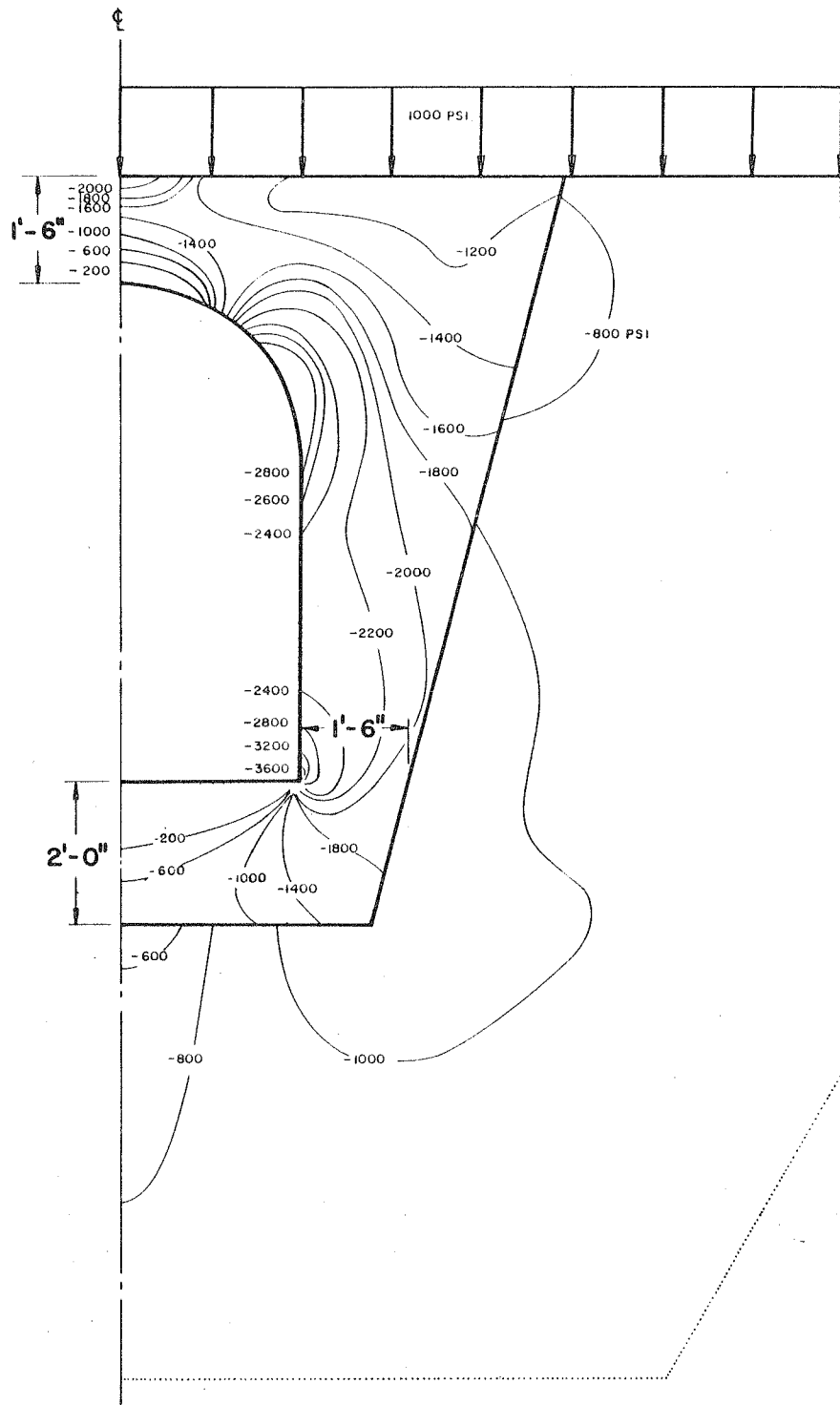
FIGURE 28 - CASE 6
DIRECTION OF PRINCIPAL STRESSES
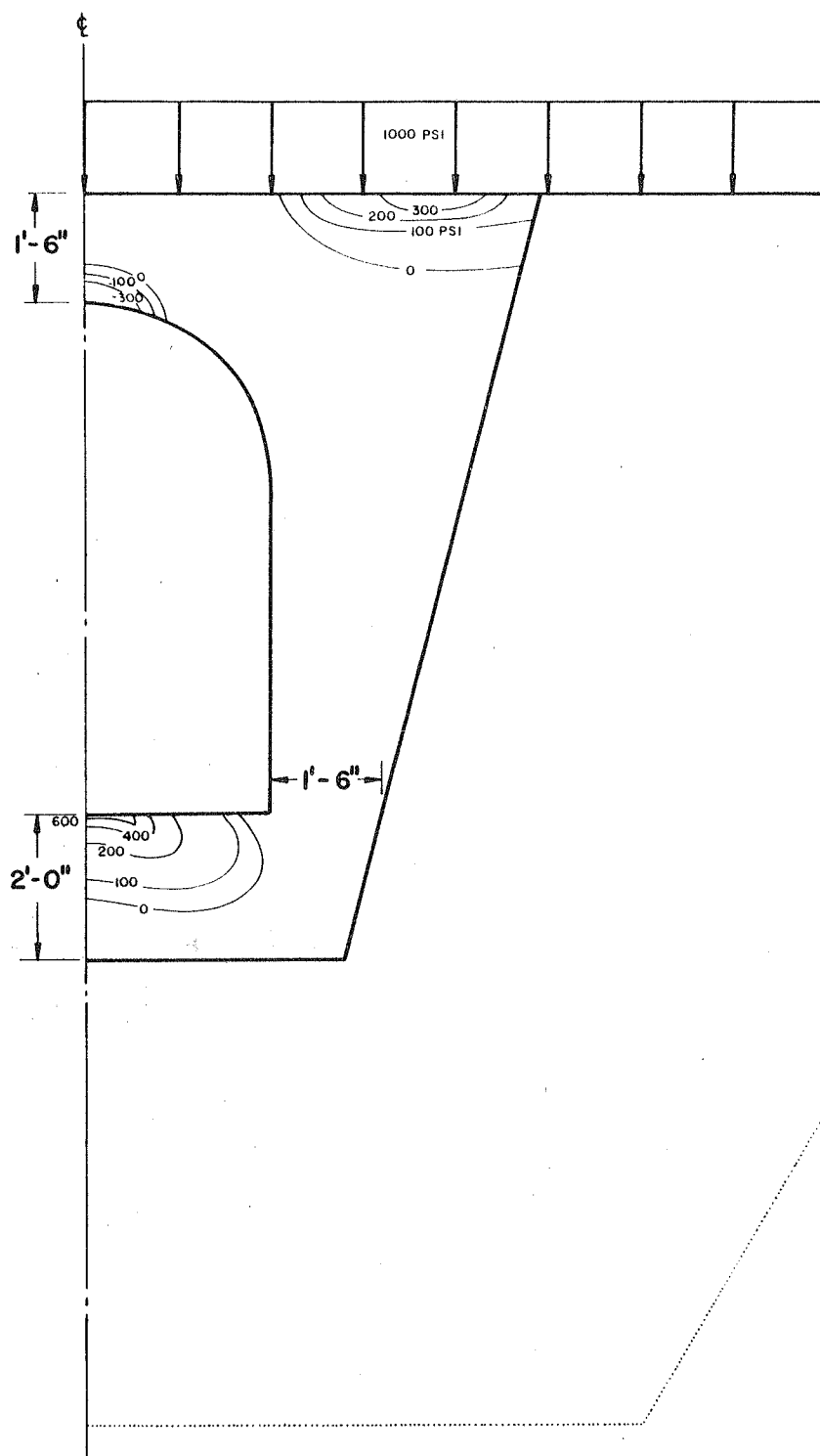
FIGURE 29 - CASE 7
COMPRESSIVE PRINCIPAL STRESSES

FIGURE 30 - CASE 7
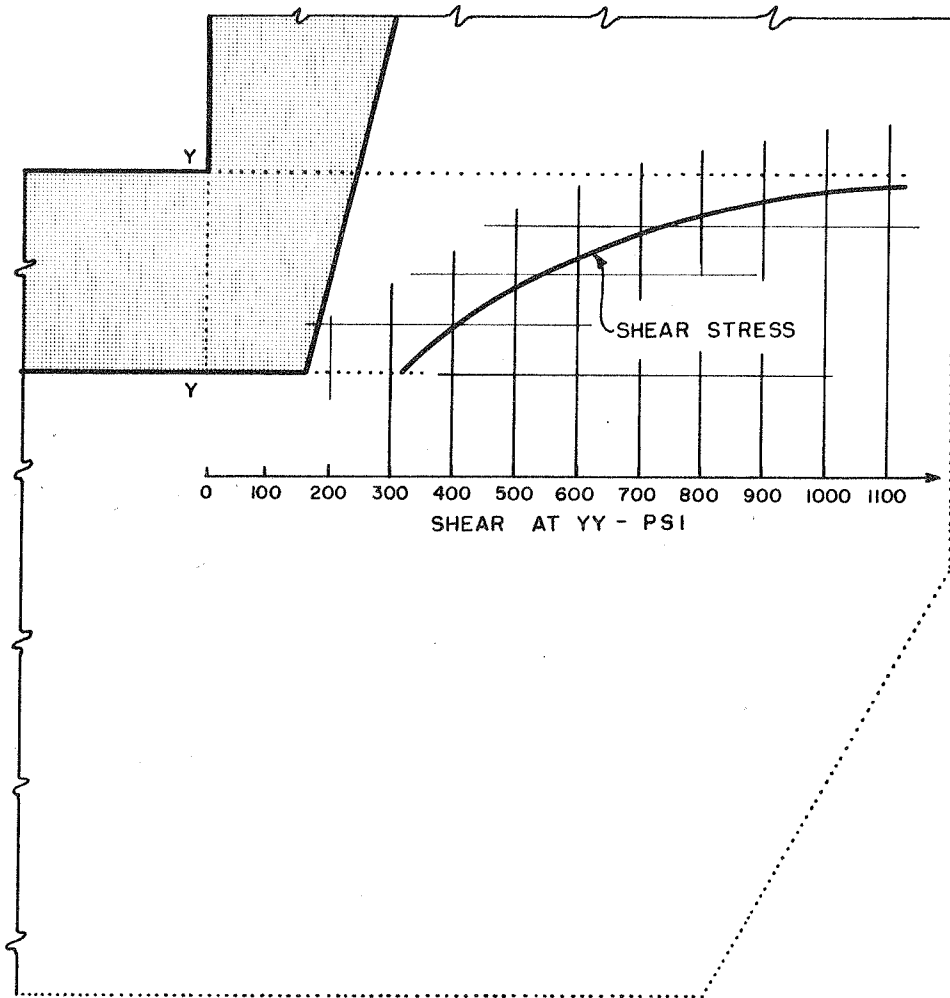TENSILE PRINCIPAL STRESSES

61

SHEAR AT YY - PSI

FIGURE 31 - CASE 7 - SHEAR STRESS AT BASE

resulted in higher stresses all around, the greatest change being the increase in compressive stress at the spring line of the arch. Maximum tensile stresses in crown and invert are both of the same order of magnitude, the stress concentration factor being 0.6, higher than in any of the cases yet discussed.

Case 9

Case 9 also represents a widened gallery to be used as an instrument chamber, with generally thinner side, top, and bottom dimensions. Thus Case 9 most nearly resembles Case 7 with the addition of the widened central portion. However, as shown in Figures 35 and 36, the maximum stress concentration factor at the crown has increased from 2.8 to 4.4 and the maximum tensile stress concentration factor at the crown has increased from 0.3 to 1.0 (more than threefold). The maximum tensile stress at the invert has increased slightly from 0.6 to 0.7. The tensile regions have increased in size and occupy all of the invert and about half of the crown of the arch. In general, as shown in Figure 37, shear stresses throughout the base of thinner-walled galleries are much larger than those shown for thick-walled sections. Directions of principal stresses shown in Figure 38 are quite similar to those shown previously for Figure 28.

Gutter Effect - Case 10

In the cases discussed to now, the gutter which exists at one side of the invert in the actual structure has been omitted. The next two cases were designed to explore the change in stress induced by the gutter. Case 10 represents the thin-walled section of Case 7 with the addition of the gutter. Actually, since symmetry was assumed to shorten the work of the computation, the analysis provided results for a symmetrical section having two gutters, as shown in Figure 9. These stress results,
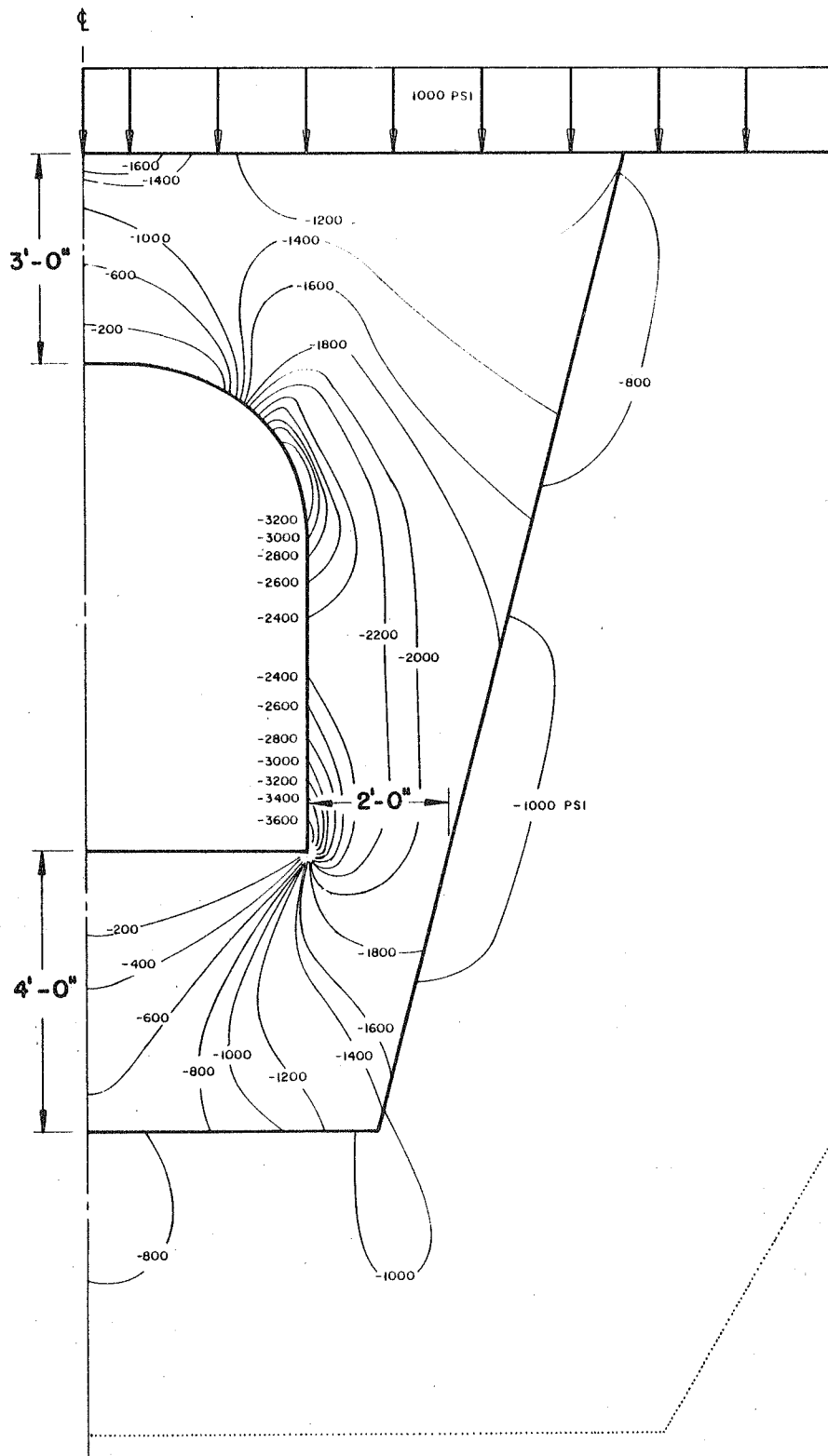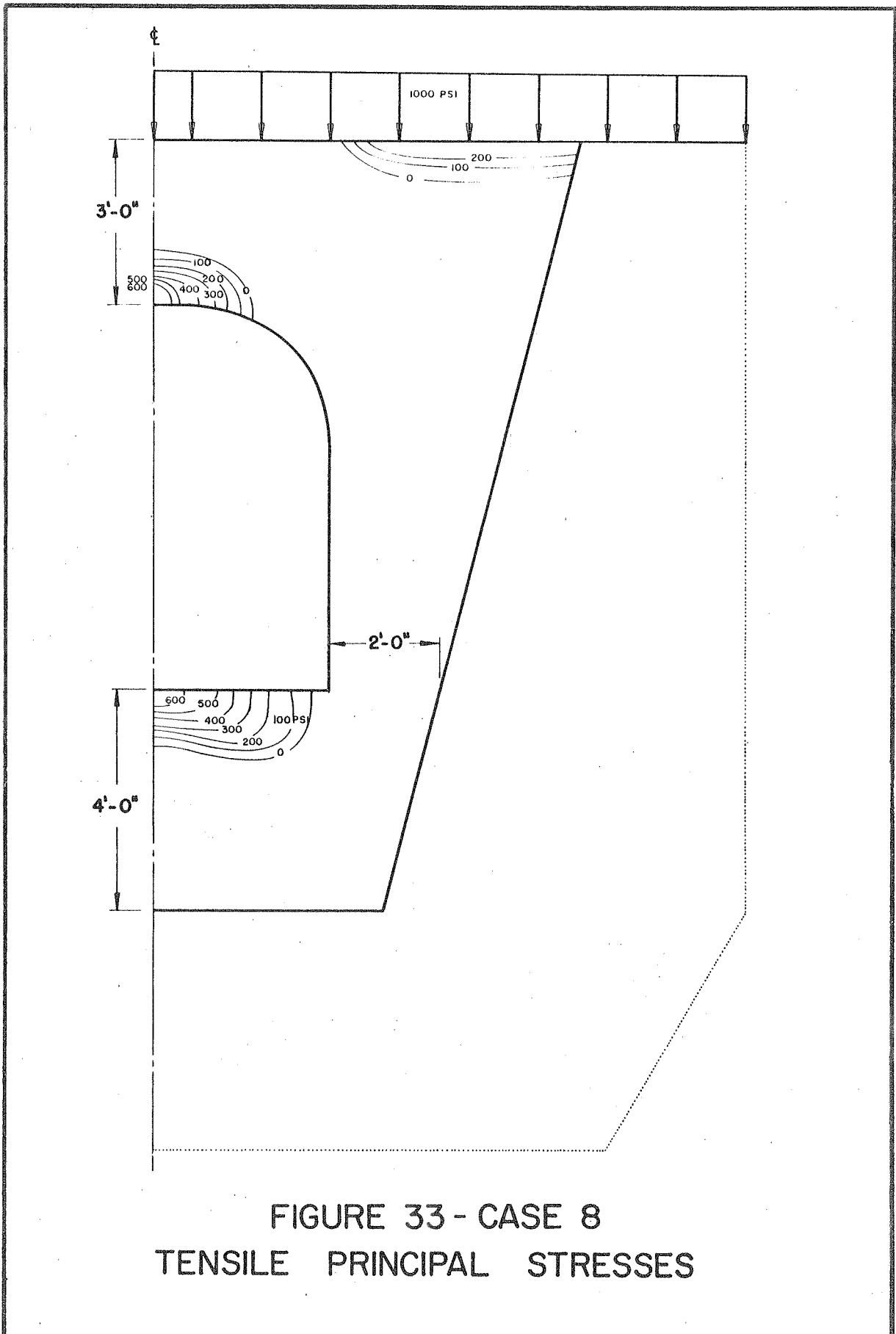
FIGURE 32 - CASE 8
COMPRESSIVE PRINCIPAL STRESSES

FIGURE 33 - CASE 8
TENSILE PRINCIPAL STRESSES

SHEAR STRESS

SHEAR AT YY – PSI
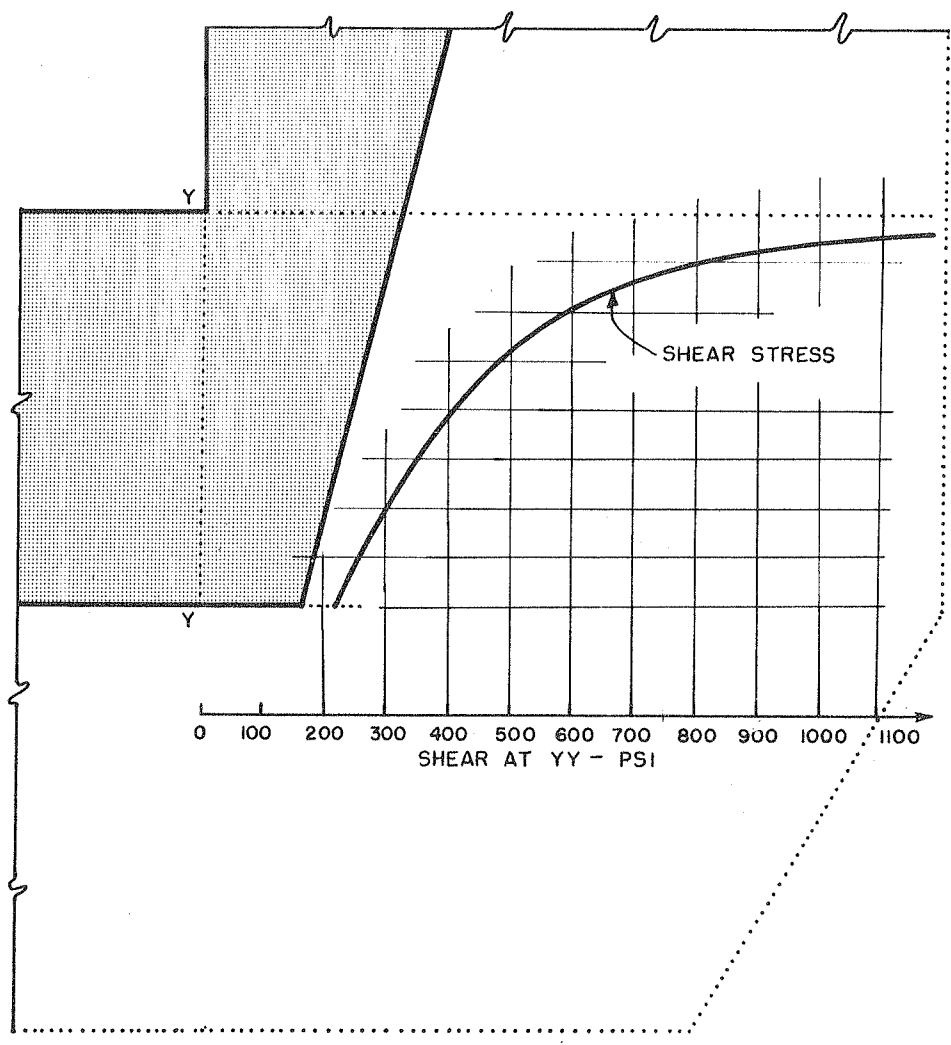
Y

Y

0 100 200 300 400 500 600 700 800 900 1000 1100

FIGURE 34 - CASE 8 - SHEAR STRESS AT BASE

FIGURE 35-CASE 9
COMPRESSIVE PRINCIPAL STRESSES
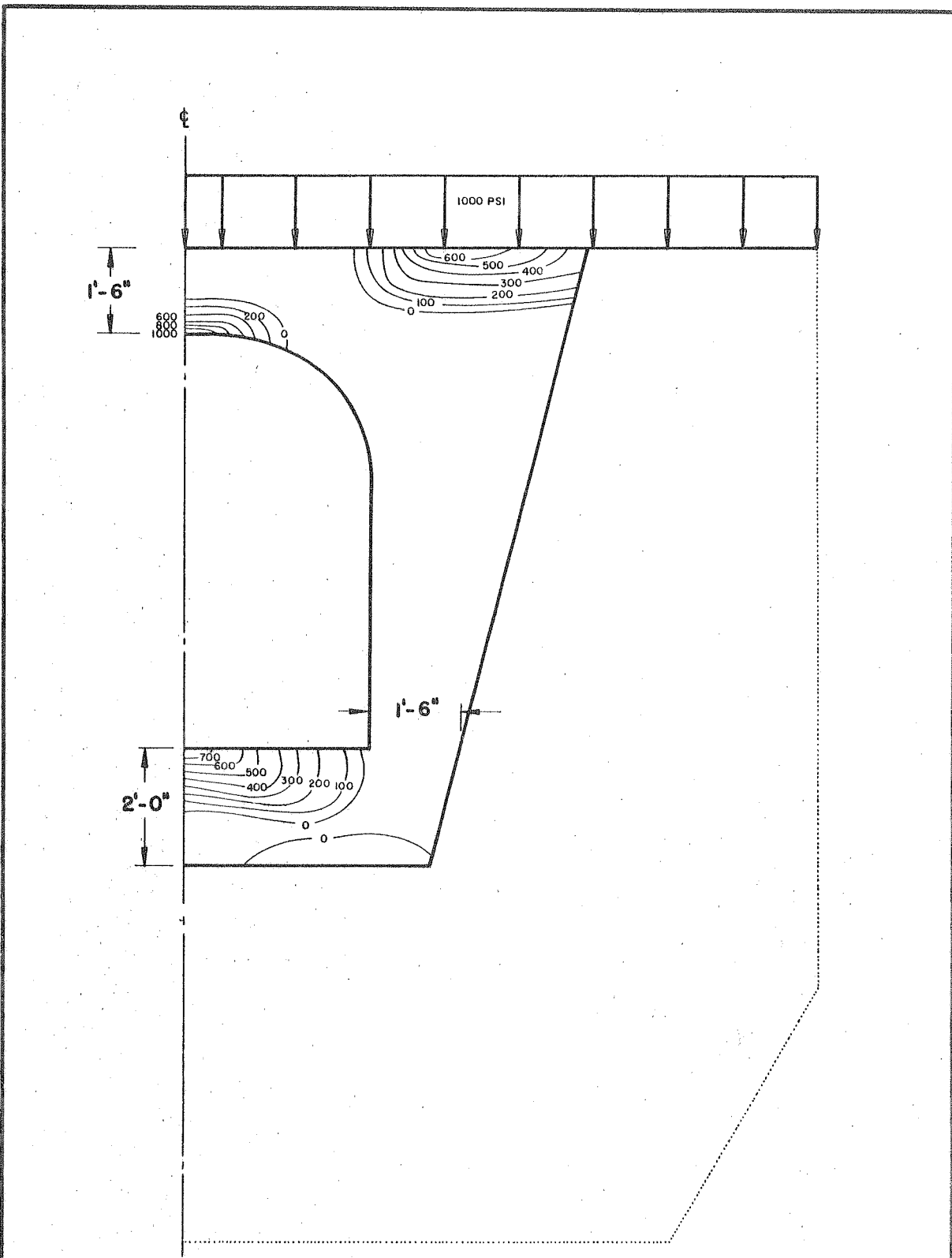
FIGURE 36 – CASE 9
TENSILE PRINCIPAL STRESSES

SHEAR AT YY — PSI
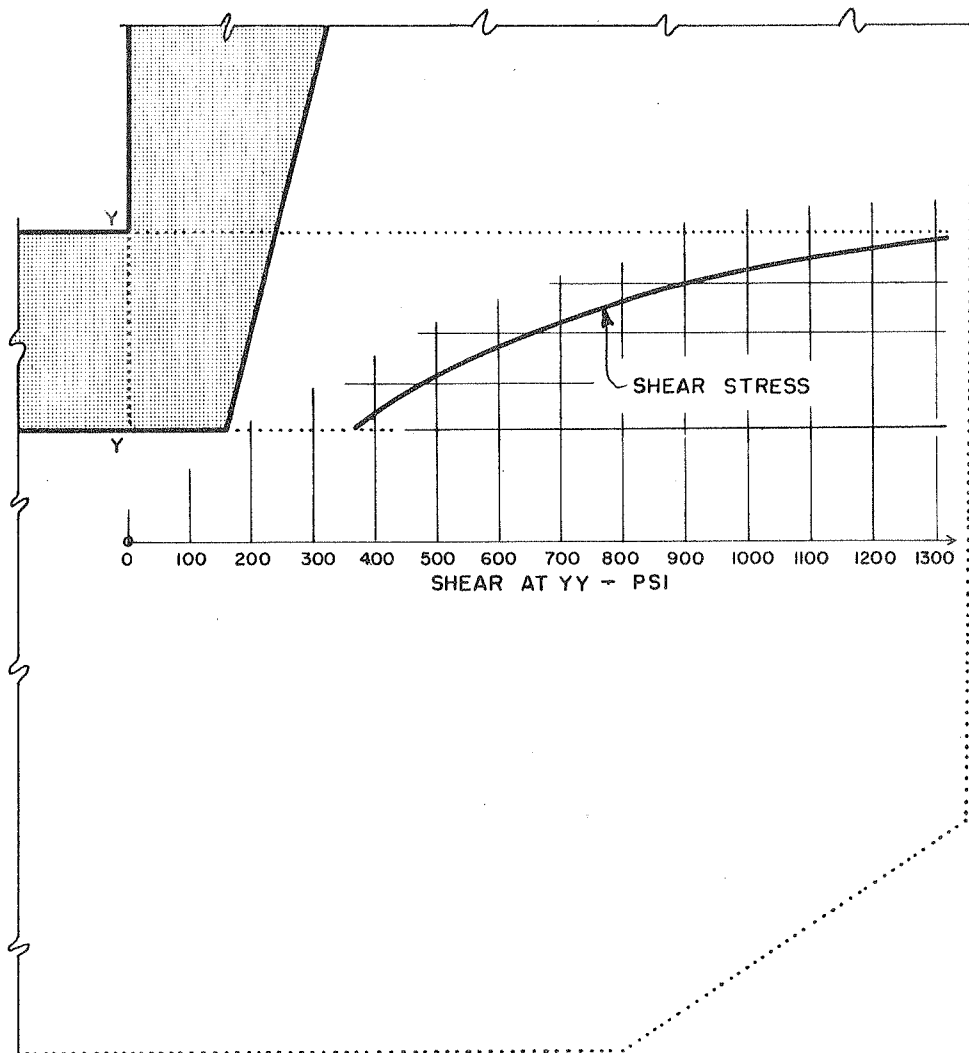
SHEAR STRESS

FIGURE 37 - CASE 9 - SHEAR STRESS AT BASE
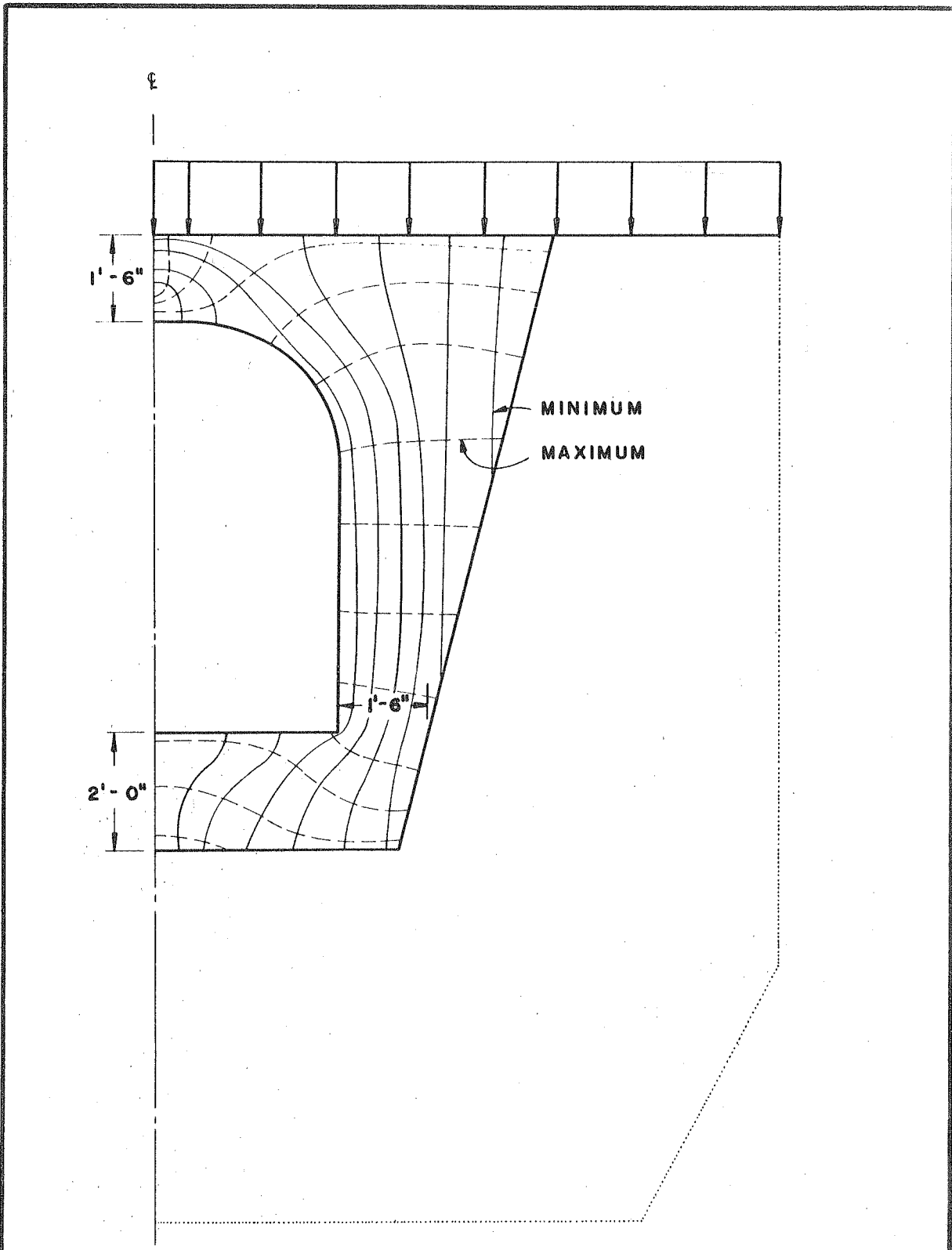
FIGURE 38 - CASE 9
DIRECTION OF PRINCIPAL STRESSES

however, combined with those for Case 7 show a nearly continuous stress distribution, as will be discussed later, hence it is believed that the assumption of symmetry introduced negligible error.

The compressive stress distribution for Case 10 is shown in Figure 40. The changes from Case 7 (Figure 29) caused by the introduction of the gutter are quite interesting. The fillet effect at the base of the wall causes a significant reduction of the stress concentration in this zone, from 3.6 to 3.0. At the same time, however, the concentration at the springing of the arch increased from 2.8 to 3.4. Tensile stress concentrations at the crown of the arch are unchanged, but the invert tensile stresses are reduced roughly by half.

Case 11

Case 11 is the same as Case 6 with the addition of the gutter. This case represents the ultimate development of the thicker sections for the heavy loads. The compressive stresses (shown in Figure 42) are the same as in Case 6 (Figure 25) at the spring line, but have been reduced significantly at the base, from a factor of 3.4 to 2.8, by the fillet effect of the gutter. Maximum tensile stresses (Figure 43) in crown and invert have been greatly reduced from Case 6 (Figure 26) by the gutter, as have the base shearing stresses, shown in Figure 44.

Stress Concentration Factors

In discussing the stresses found in the 11 separate cases analyzed, maximum tensile and compressive stresses have been cited in terms of stress concentration factors, which are the ratios of the computed maximum stress to the superposed stress of 1000 psi. It will be noted that while there were differences in magnitude of these factors for the individual cases, the regions of highest compressive and tensile stress were in
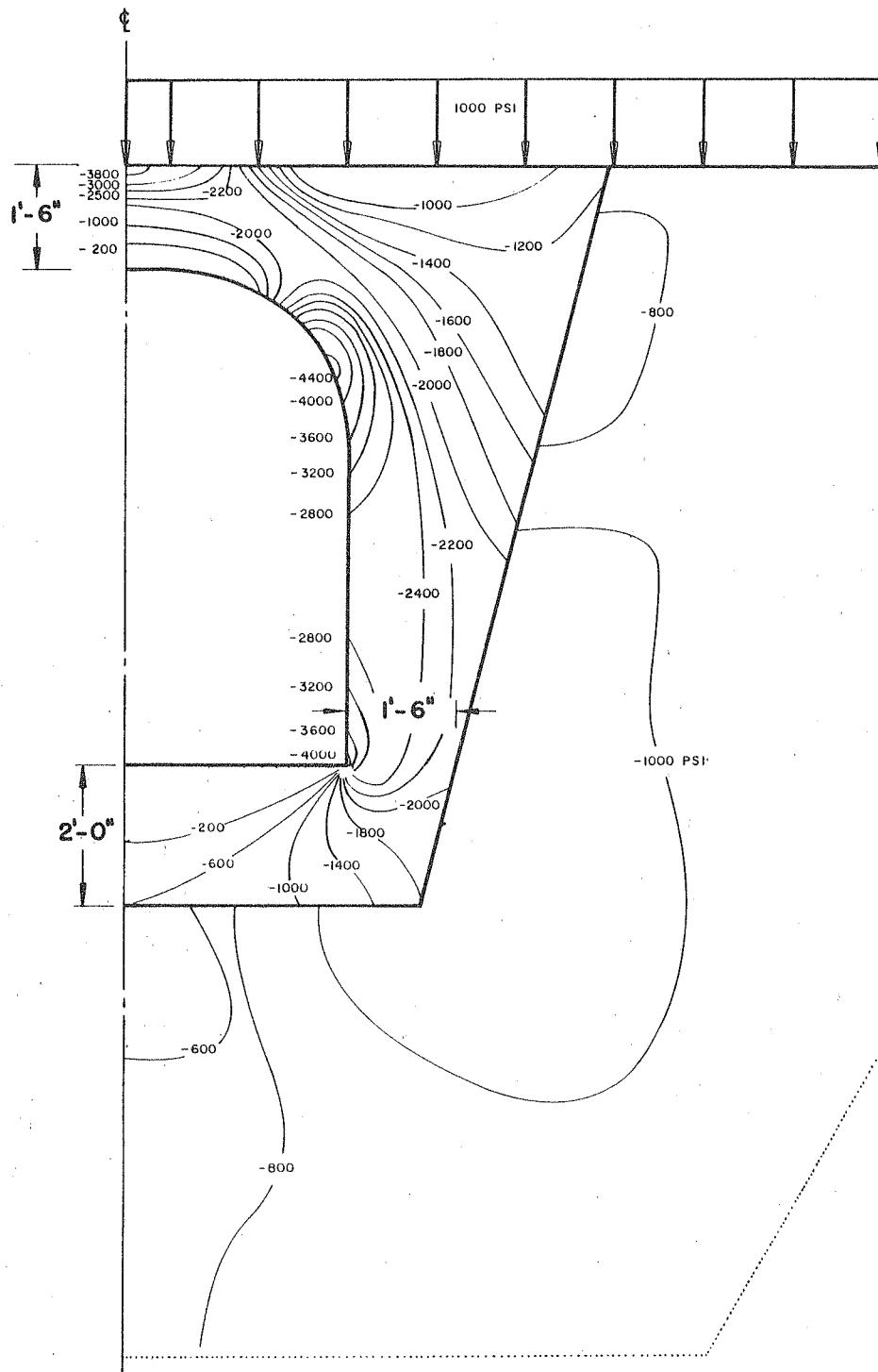
FIGURE 39 - CASE 10
COMPRESSIVE PRINCIPAL STRESSES
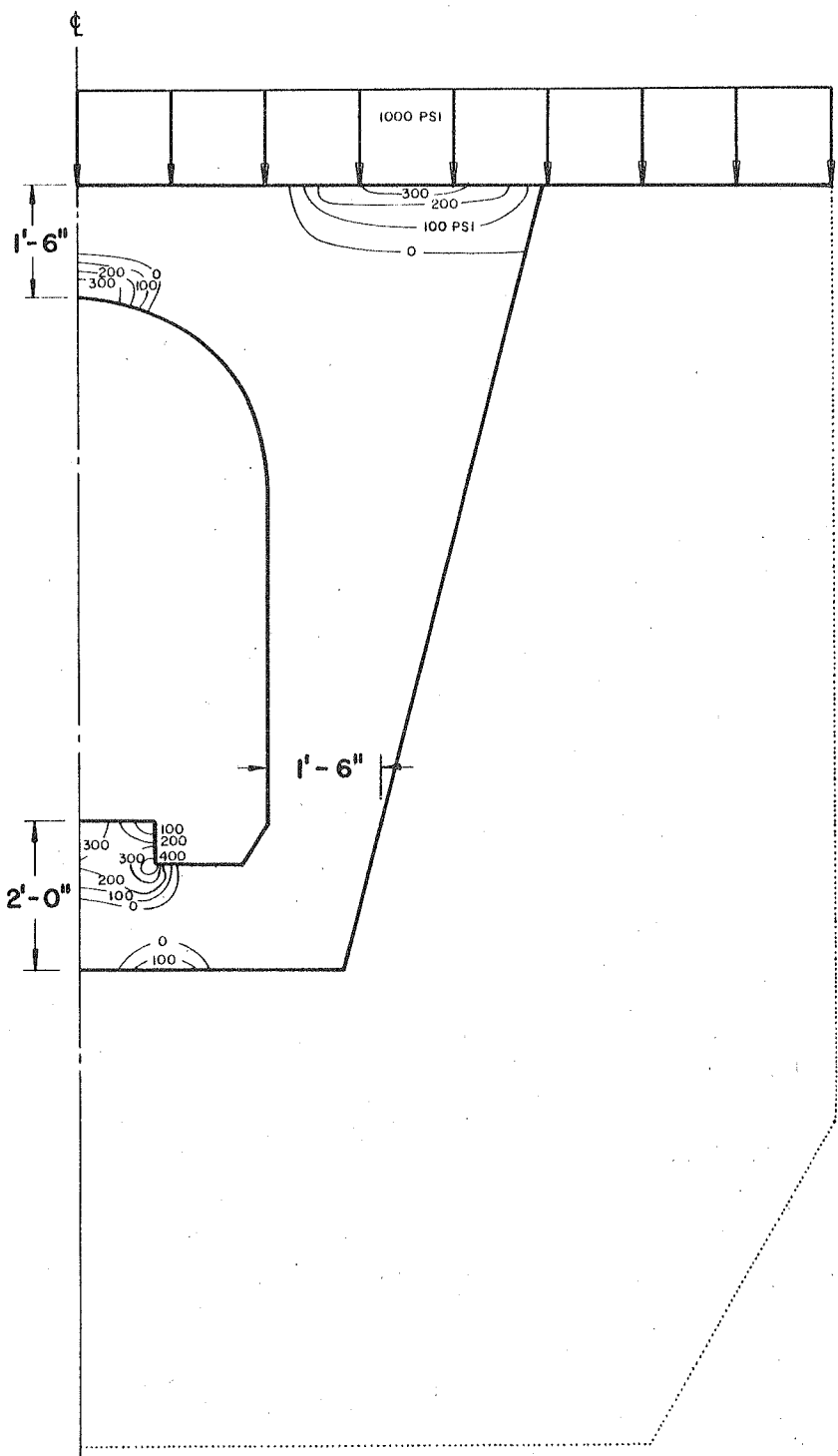
FIGURE 40 - CASE 10
TENSILE PRINCIPAL STRESSES
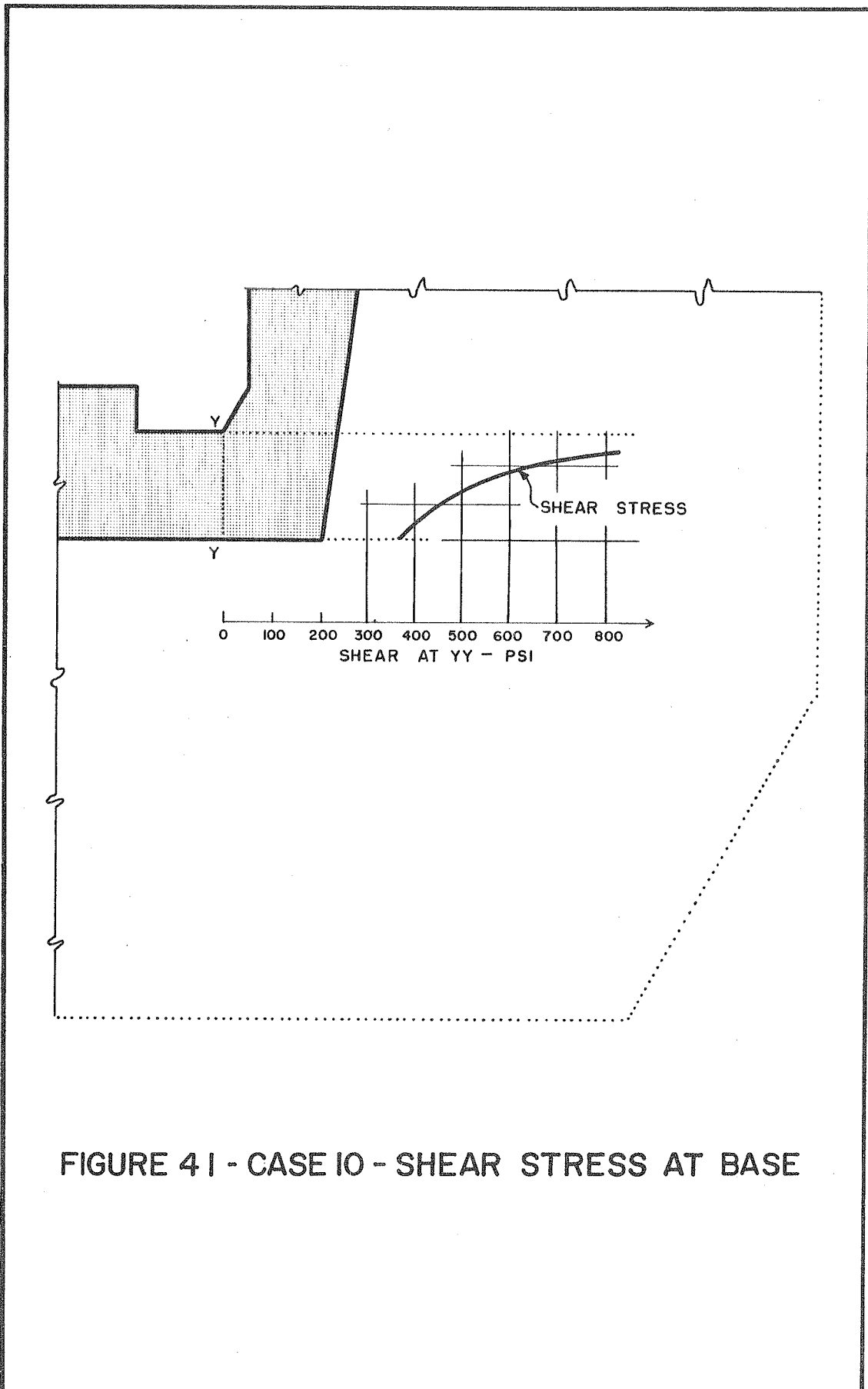
FIGURE 4 I - CASE IO - SHEAR STRESS AT BASE
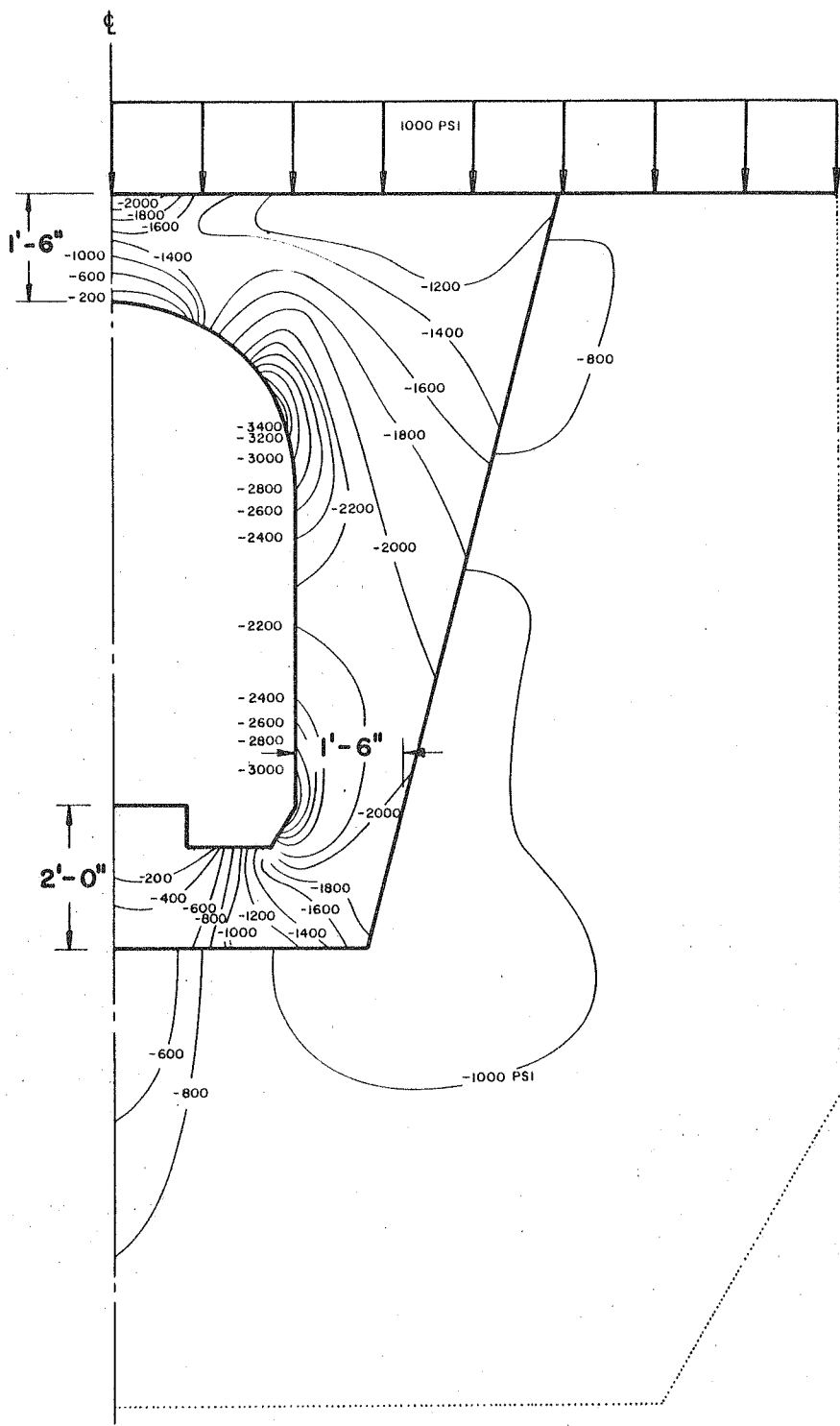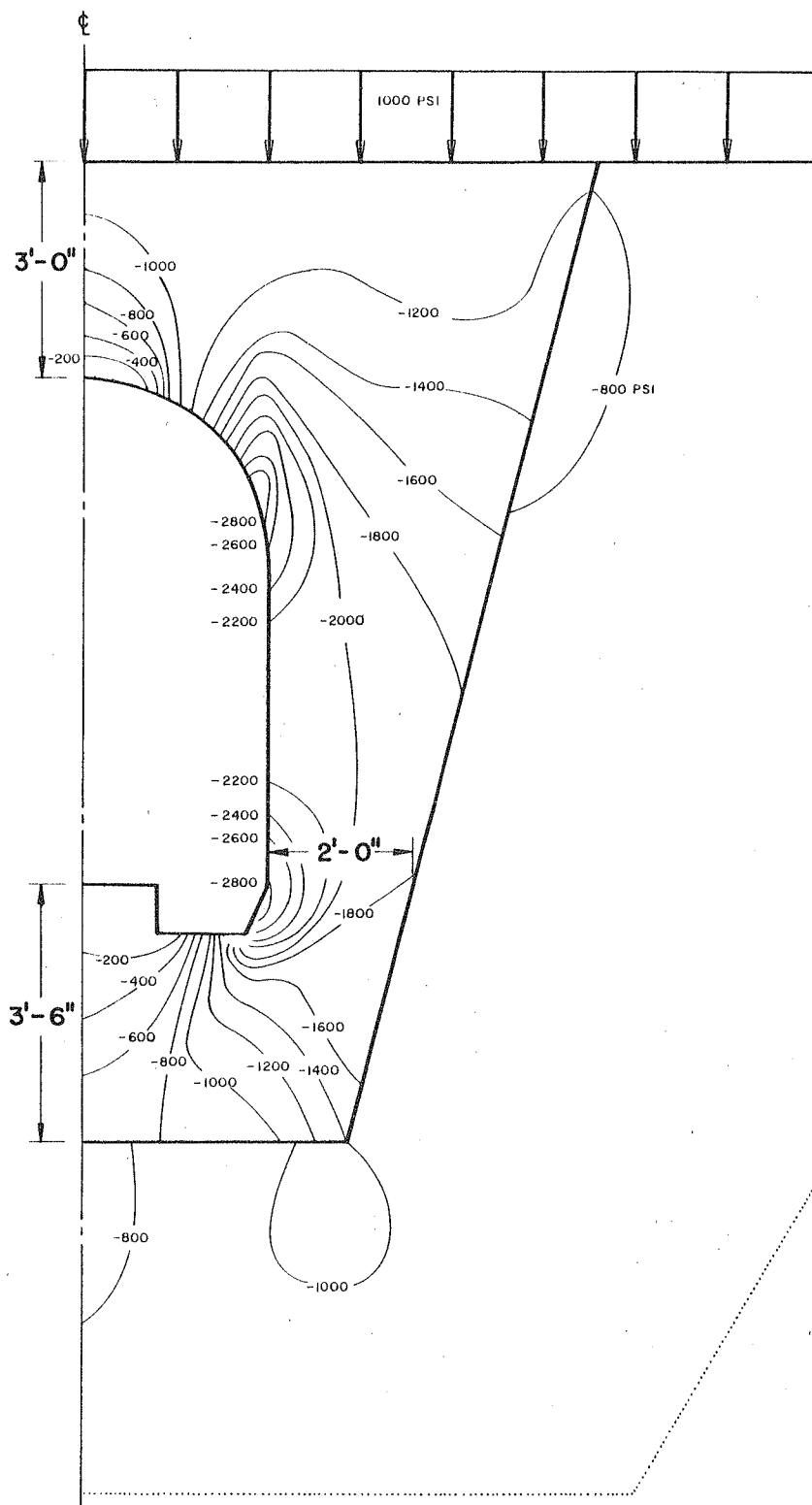
FIGURE 42 - CASE II
COMPRESSIVE PRINCIPAL STRESSES
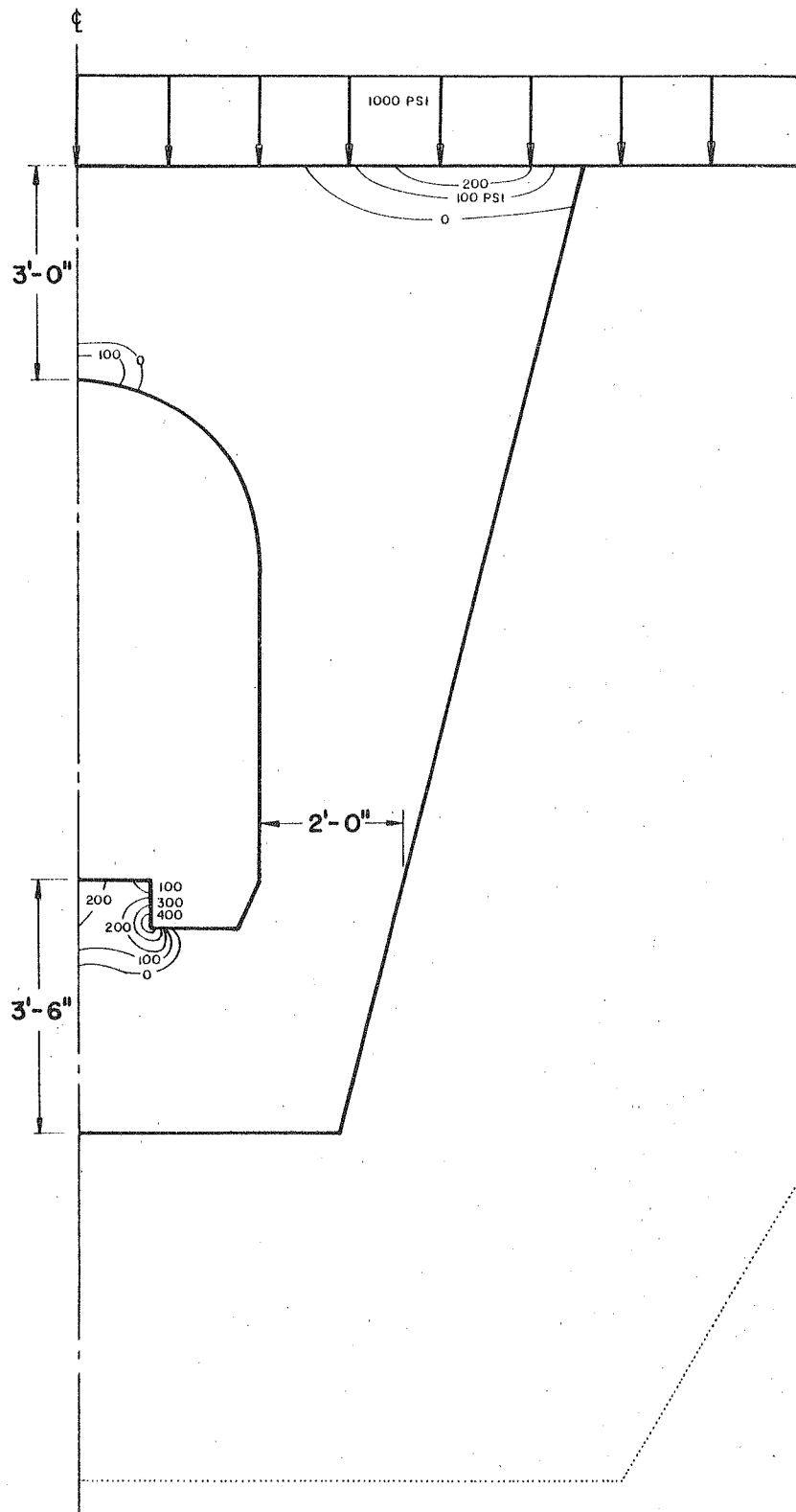
FIGURE 43 - CASE II
TENSILE PRINCIPAL STRESSES

SHEAR STRESS

SHEAR AT YY – PSI
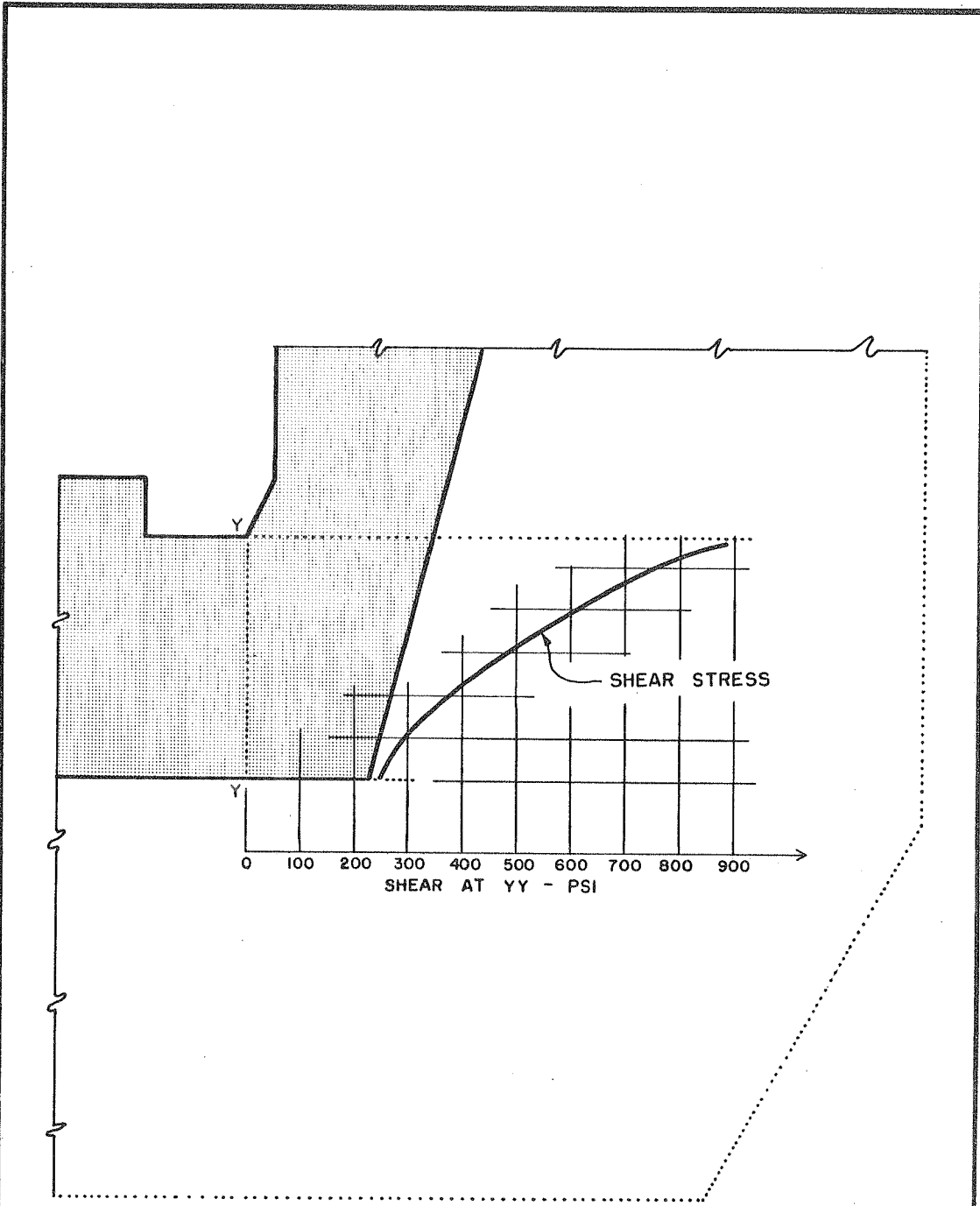
FIGURE 44 - CASE II - SHEAR STRESS AT BASE

roughly the same position for each configuration studied. Maximum compressive stresses were found at the spring line of the arch, and at the side of the gallery near the base. Maximum tensile stresses were found at the crown of the arch, and at the center of the invert, or floor of the gallery. Hence, for direct comparison of the effect of configuration and dimension on maximum stresses, Table 2 has been assembled giving the stress concentration factors for all cases studied.

TABLE 2 - Stress Concentration Factors

Case	Figure	Dimension - Ft-in			Concentration Factors			
		Crown A	Invert B	Side C	Compression		Tension	
					Spring	Base	Crown	Invert
1[a,b]	II	3-5	4-0	2-10	--	--	--	--
2[b]	II	3-5	4-0	2-10	2.6	3.2	.09	.4
3	II	3-5	4-0	2-10	2.6	3.2	.1	.4
4	II	3-0	4-0	2-10	2.6	3.2	.2	.4
5	II	3-5	3-6	2-10	2.6	3.2	.1	.4
6	II	3-0	3-6	2-0	2.8	3.4	.2	.5
7	II	1-6	2-0	1-6	2.8	3.6	.3	.6
8	III	3-0	4-0	2-0	3.2	3.6	.6	.6
9	III	1-6	2-0	1-6	4.4	4.0	1.0	.7
10	IV	1-6	2-0	1-6	3.4	3.0	.3	.3[c]
11	IV	3-0	3-6	2-0	2.8	2.8	.1	.2[c]

[a] Coarse mesh analysis

[b] Poisson's ratio for rock and concrete equal

[c] Concentration Factor of .4 found in gutter

Stresses at Base of Gallery with Gutter

Figure 45 has been prepared to show the distribution of the stress at the base of a thick-walled gallery for the unsymmetrical case of the gutter on one side only. This has been done by combining the results for Case 11 (with gutter) with the results from Case 6 (without gutter). The top sketch shows the principal compressive stresses and the bottom shows the principal tensile stresses. Each drawing has been made separately on either side of the center line with no attempt to smooth the stresses across the center line. However, examination of the drawing shows that the compressive principal stress pattern is nearly continuous across the center line. For the principal tensile stresses, there is some difference in detail in the continuity of the maximum stresses, and the outline of the complete tensile stress region is somewhat discontinuous. However, it is expected that very little difficulty would be experienced by the designer in using these diagrams for the determination of required tensile reinforcement.

Similarly, results for Case 7 have been combined in Figure 46 with results for Case 10 to show the stresses for the thin-walled non-symmetrical gallery with gutter. For this thinner section, the tensile stress patterns are more nearly continuous and the compressive stress pattern is the more discontinuous of the two. However, the stress patterns are continuous enough to indicate that no significant stress differences would be obtained if a complete analysis were made for the unsymmetrical case.

CASE 6

CASE II

PRINCIPAL COMPRESSIVE STRESSES

PRINCIPAL TENSILE STRESSES

2'-0"

3'-6"
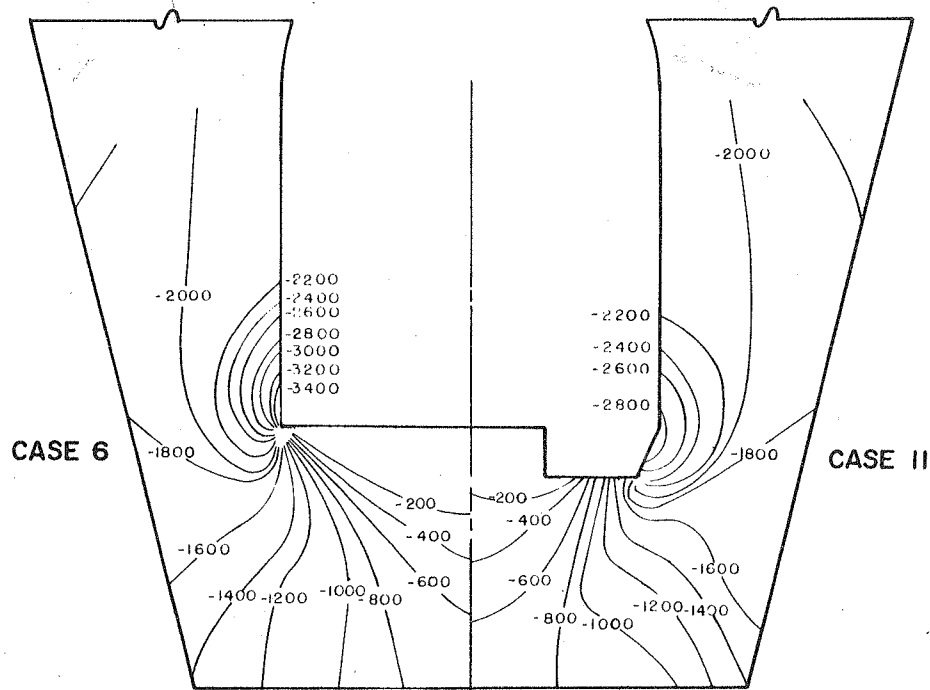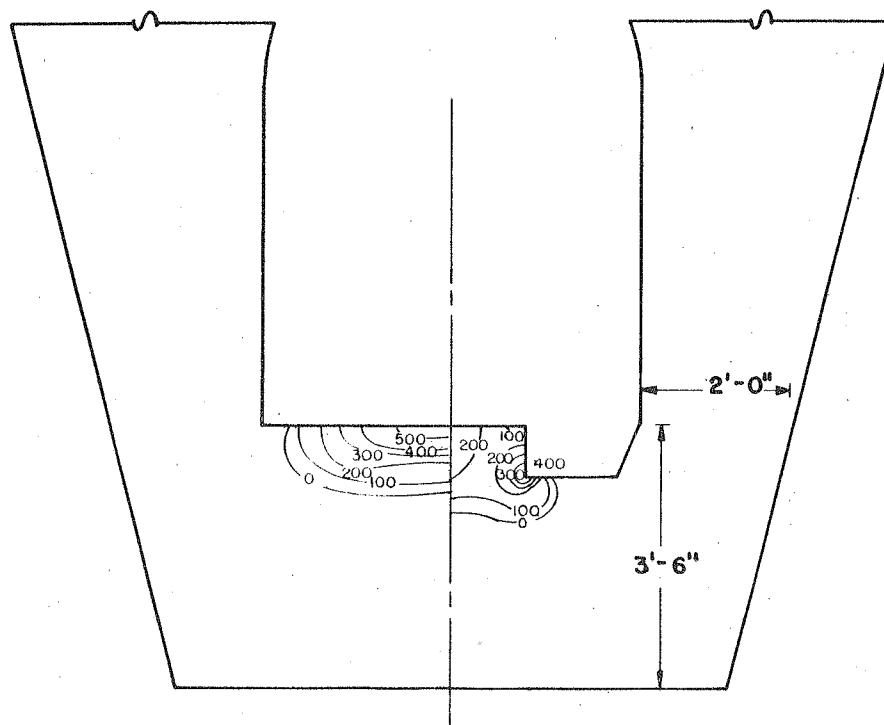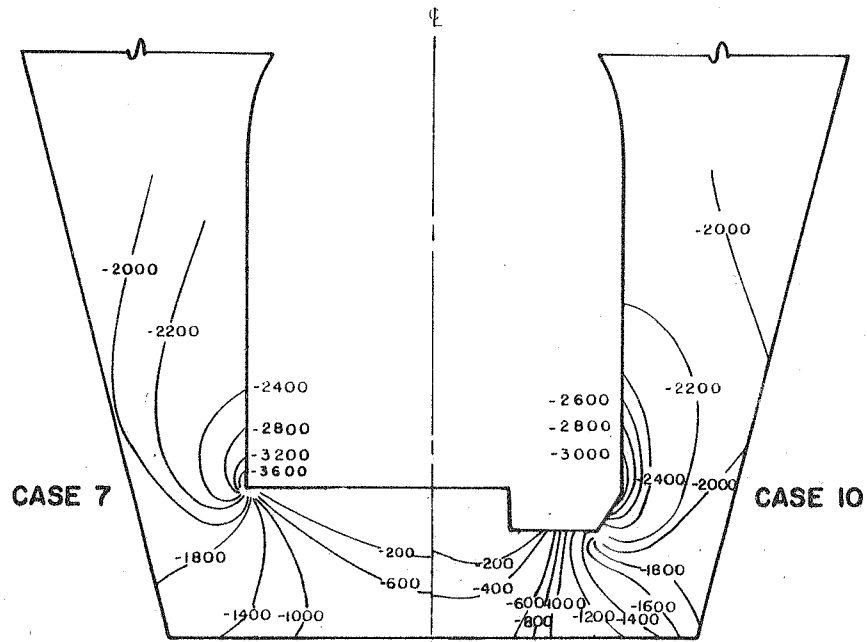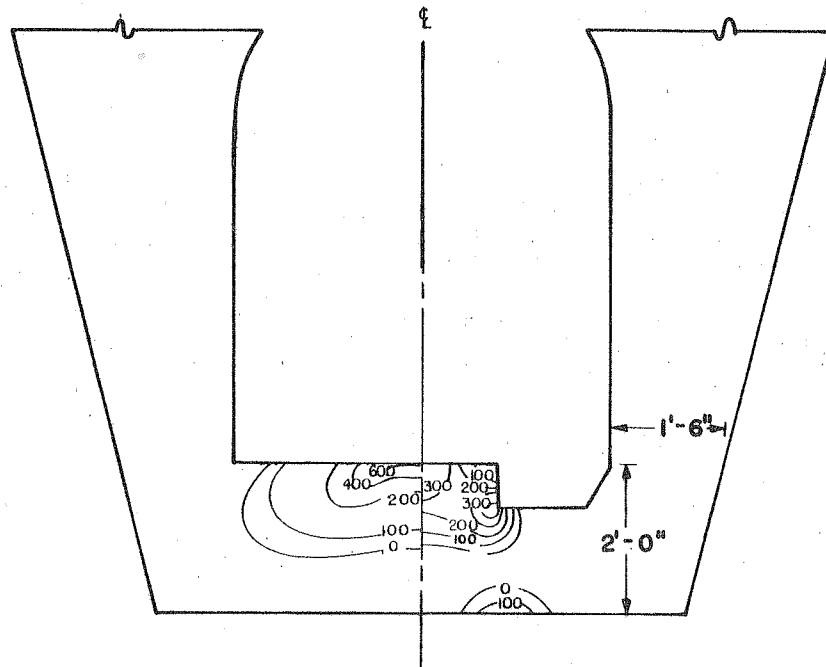
FIGURE 45 – EFFECT OF GUTTER ON STRESSES
THICK – WALLED GALLERY

CASE 7

CASE 10

PRINCIPAL COMPRESSIVE STRESSES

PRINCIPAL TENSILE STRESSES

FIGURE 46 - EFFECT OF GUTTER ON STRESSES
THIN-WALLED GALLERY

Statics Check

In order to provide an indication of the overall accuracy obtained in the computations, a static equilibrium check was made for each individual case studied. Since the system considered in each case represents a small portion of a semi-infinite body, the check was made for a free body bounded by the centerline, the upper surface, the vertical boundary of the analysis, and a line drawn horizontally in the concrete midway between the invert floor and the base of the grout gallery, as shown in Figure 47. For Case 1, the forces acting are the external load applied on the upper surface $\int w\,dx$, and the sum of the vertical stress on the lower boundary $\int \sigma_y\,dx$. For all other cases, some shear acts on the right hand boundary, and a force $\int \tau_{xy}\,dy$ had to be included in the computation. The equation of statics to be satisfied in these cases was:

$$\sum V = \int w\,dx + \int \sigma_y\,dx + \int \tau_{xy}\,dy = 0$$

The results of the statics check are summarized in Table 3. This shows that the average error was less than 2 1/2 percent, and that the maximum error was just under 3 percent.

In evaluating the accuracy of the analysis, it should be recognized that the analysis procedure successively relaxes constraining forces at the nodal points until equilibrium of nodal forces is fully achieved. Thus, if the statics check were applied to the nodal point forces, a complete check would be obtained. The slight discrepancies noted are associated with the process of determining the stresses in the system, which are established by first computing a uniform stress for each element and then "averaging" these discrete stress values in the construction of the stress contours.

FIG. 47 - FREEBODY FOR STATICS CHECK

TABLE 3 - Statics Check of Computed Stresses

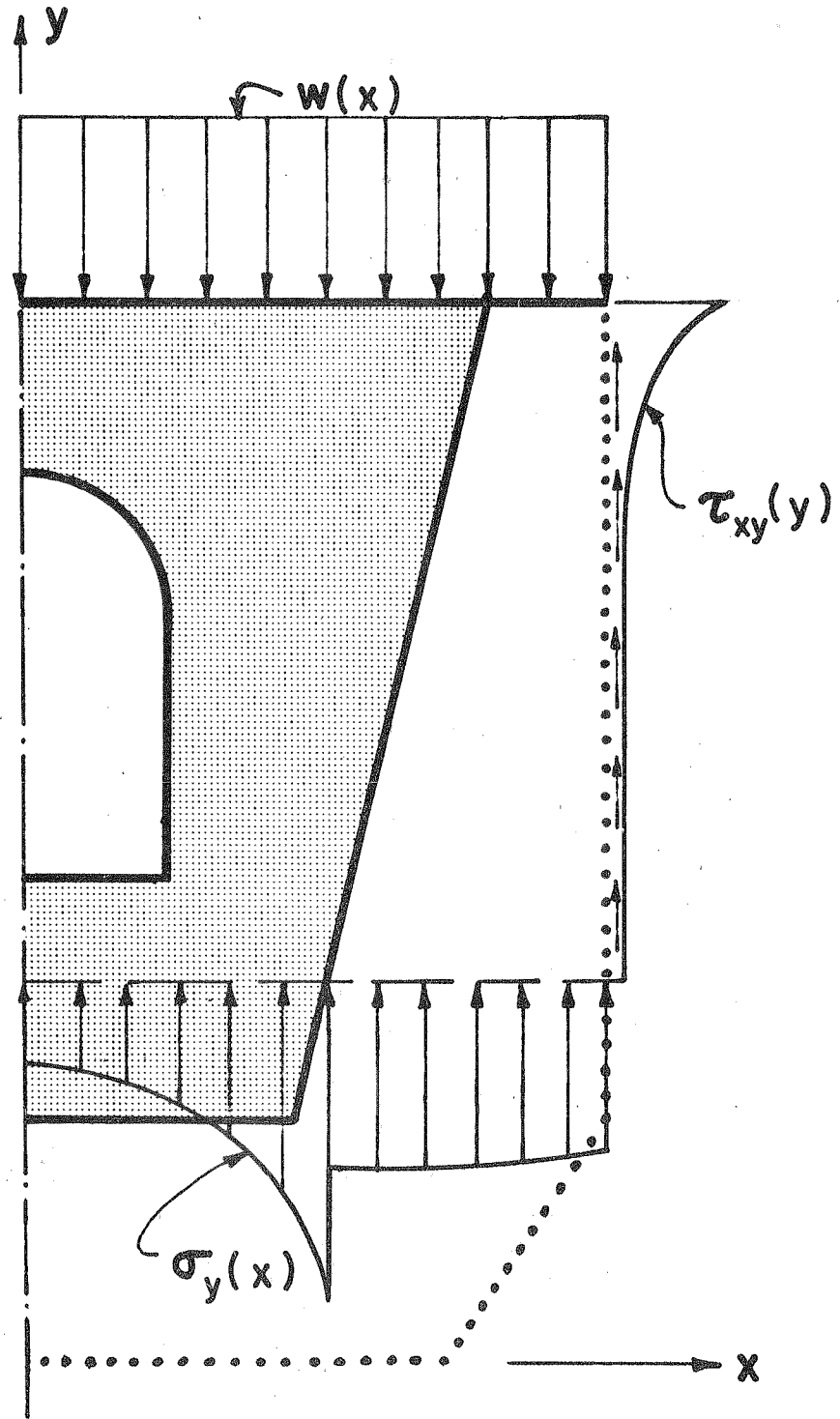| Case	Dimensions			Applied Load LB	$\int \sigma_y \, dx + \int \tau_{xy} \, dy$	Difference	Percent Error
	A	B	C				
1	3-5	4-0	2-10	270,000	263,327	6,673	2.47
2	3-5	4-0	2-10	120,000	123,011	3,011	2.51
3	3-5	4-0	2-10	120,000	122,561	2,561	2.13
4	3-0	4-0	2-10	120,000	122,507	2,507	2.09
5	3-5	3-6	2-10	120,000	123,556	3,556	2.96
6	3-0	3-6	2-0	120,000	122,535	2,535	2.11
7	1-6	2-0	1-6	120,000	123,070	3,070	2.56
8	3-0	4-0	2-0	127,800	129,940	2,140	1.67
9	1-6	2-0	1-6	127,200	130,611	3,411	2.68
10	1-6	2-0	1-6	120,000	117,307	2,693	2.24
11	3-0	3-6	2-0	120,000	123,168	3,168	2.64
Average							2.37

CONCLUSIONS

Method of Analysis

One of the most important conclusions to be drawn from the investigation
reported herein is with regard to the effectiveness and practicality of the
finite element method of analysis. The complex systems which have been solved
demonstrate that the method can be used in determining stresses and deflec-
tions in completely arbitrary plane stress or plane strain problems. Vari-
ations of material properties, complicated boundary configurations, difficult
loading conditions all are handled automatically by the single standardized
procedure. It is not necessary to treat the grout gallery as an isolated
system subjected to some assumed force distribution along the concrete-rock
interface. Instead, the combined system, including the grout gallery and
the supporting rock, is treated in a single analysis with boundaries assumed
at a great enough distance that they have negligible influence on the gallery
stresses. The triangular element pattern may be laid out so as to accommodate
any arbitrary configuration easily, and the element sizes may be selected
to give the desired amount of detail regarding the stress distribution in
each region of the structure.

Grout Gallery

As described under "Scope", it was not the purpose of this investigation
to draw conclusions as to the optimum dimensions of the grout gallery for
any specified loading conditions. However, the analyses described here in-
dicate that a grout gallery of considerably slimmer dimensions than those
first proposed can carry heavy superimposed loads safely, and where light
loads are anticipated, a nominally-dimensioned grout gallery was found to
give very reasonable stresses. Increasing the width of the gallery to
form an instrument chamber caused only a minor increase in stresses, and

required no radical change of dimension. The unsymmetrical case of the grout gallery with gutter was analyzed approximately by joining two halves of two symmetrical analyses: with and without the gutter. By this expedient, a larger number of finite elements and nodal points could be used in each individual analysis, thus increasing the detail obtained at the regions of concentration of stress. Results indicate that the gutter does not lead to significant stress increases, in fact, the maximum stress values are actually reduced in these analyses.

ACKNOWLEDGMENTS

The authors of this report wish to thank a number of individuals who made substantial contributions to the work described in this report. Mr. Edward L. Wilson was responsible for the development of the digital computer program used in the analyses. Mr. James L. Tocher was responsible for the actual layouts and analyses of the several types of grout galleries, aided by Mr. Shigeki T. Yamahara.

The California Department of Water Resources, through Mr. James V. Williamson, selected the configurations of the grout gallery to be studied, and helped to establish the properties of concrete and rock used in the analyses.

The IBM-704 digital computer used in the analyses was operated by the University of California Computer Center.